International Scientific-Technical and Production Journal

The Paton WELDING JOURNAL

February
2008
2

English translation of the monthly «Avtomaticheskaya Svarka» (Automatic Welding) journal published in Russian since 1948

Founders: *E.O. Paton Electric Welding Institute of the NAS of Ukraine*
International Association «Welding»

Publisher: *International Association «Welding»*

Address:
E.O. Paton Electric Welding Institute,
International Association «Welding»,
11, Bozhenko str., 03680, Kyiv, Ukraine
Tel.: (38044) 287 67 57
Fax: (38044) 528 04 86
E-mail: journal@paton.kiev.ua
http://www.nas.gov.ua/pwj

State Registration Certificate
KV 4790 of 09.01.2001

Subscriptions:
$324, 12 issues per year,
postage and packaging included.
Back issues available.

CONTENTS

ANALYSIS OF RISK OF HOT CRACK FORMATION IN BRAZE-WELDED TITANIUM-ALUMINIUM JOINTS ON BASIS OF MATHEMATICAL MODELING

V.I. MAKHNENKO and **A.S. MILENIN**
E.O. Paton Electric Welding Institute, NASU, Kiev, Ukraine

On basis of the results of mathematical modeling of heat deformation processes in laser braze-welding of titanium-aluminium joints, analysis of risk of hot crack formation in aluminium part of permanent joints has been carried out.

Keywords: mathematical modeling, braze-welding, titanium, aluminium, heat deformation, risk of hot crack formation

Use of dissimilar materials for manufacturing welded assemblies in state-of-the-art structures allows achieving unique combination of such useful properties as minimal weight and high strength, corrosion resistance, and long service life of an item. That's why dissimilar materials are used on ever growing scale in aerospace, ship building, automotive, and other industries, which is enabled by development of welding technologies and first of all beam methods of welding [1–4].

In particular, in the design of passenger air liners of the A380 series, produced by the «Airbus» concern, dissimilar titanium-aluminium guides of seats («seat tracks») have been suggested [5]. This welded structure represents a flange beam of complex profile, which consists of titanium (Ti6Al4V alloy) and aluminium (AA6056 alloy) parts interconnected by longitudinal seams produced by laser welding [6]. Chemical composition of the Ti6Al4V alloy is as follows: 5.3–6.9 Al; 3.5–5.3 V; 0.05 N; 0.1 C; 0.0125 H; 0.3 Fe; and the AA6056 alloy: 0.7–1.3 Si; 0.5 Fe; 0.5–1.1 Cu; 0.4–1.0 Mn; 0.6–1.2 Mg; 0.25 Cr; 0.1–0.7 Zn.

Welding of titanium with aluminium is a complex of complicated and mutually connected physical-chemical processes, which may exert significant influence on operation properties of a welded assembly. In particular, because of low mutual solubility of titanium and aluminium in case of their mixing in liquid phases it is practically impossible to avoid formation of brittle intermetallic compounds [7], which may make a welded joint unfit for efficient application.

Using significant difference in melting points of the considered titanium and aluminium alloys, process of their connection may be successfully fulfilled according to the scheme of braze-welding without melting of titanium, provided molten aluminium pool is available [8]. However, during solidification of the melted aluminium edge of a welded assembly formation of hot cracks is possible (which is peculiar to the aluminium alloys, in particular, of the Al–Mg–Si system), and this should be taken into account when optimizing the welding cycle [9].

For the purpose of analyzing risk of formation of hot cracks in aluminium part of a dissimilar (titanium-aluminium) joint depending upon technological parameters of the welding processes in case of laser braze-welding of seat tracks of the A380 series passenger air liners a mathematical model was developed and implemented.

In [6] scheme of the processes of producing braze-welded butt titanium-aluminium joints is shown, which was developed in Institute of Applied Beam Technologies (BIAS), Bremen, Germany. An item being welded is in a force rigging, which ensures its uniform pressing to the support table and action of the axial force. Welding is performed by two laser heat sources simultaneously from two sides of the item. For this purpose a carriage with installed on it chambers, which ensure availability of argon in the area of high heating temperatures, moves with connected to it light guides over surface of the aluminium shelf. The carriage is also provided with a system for focusing laser beam, in addition it creates additional pressing of the item being welded in the area of the heat sources action.

Geometric parameters of the dissimilar seat tracks are as follows:

beam length, mm	1000
thickness of aluminium part of the beam web, mm	2.0
thickness of titanium part of the beam web, mm	1.8
thickness of aluminium beam flange, mm	3.2
height of aluminium part of the beam web, mm	8.0
height of titanium part of the beam web, mm	42.6

Several technological parameters of the welding process are presented below:

speed of the source movement along seat track joint, mm / s	4.33
power of each of the sources, kW	1.75
welding spot diameter, mm	5.0
force of pressure on the «carriage», N	754
distributed pressure force, N / mm	4.41
axial force, N	376
efficiency of the laser heat action:	
on surface of aluminium	0.17
on surface of titanium	0.30

As far as a welded seat track has elongated shape, it is expedient to consider this process within the framework of a 2D mathematical model.

Formation of a seam (melting of aluminium edge, spreading of molten aluminium over solid titanium, formation of the surface physical contact) occurs within short time and insignificantly affects its heat strain state during cooling; that's why for simplifica-

tion of the calculation geometry of the seam in the developed model was determined experimentally and it was considered initially preset.

Scheme of a braze-welded joint and its macrosection are presented in Figure 1.

Preliminary investigations directed at choice of the welding process optimal conditions, showed that satisfactory braze-welded contact (good spreading of molten aluminium, stable over the item length shape of the seam, absence of the titanium edge melting) occurs in case of variation of the power of each laser source within the 1.5–2.0 kW range and speed of the source movement of 2.33–5.66 mm / s, whereby geometric parameters of the seam were registered (width and height of the bead, length of the wetting line), which were later used in the mathematical model for correct description of the temperatures and heat strain state kinetics. In Figure 2 dependence of the weld width upon brought to the welding heat sources energy, obtained from the results of processing of respective experimental data, is shown.

First stage of the investigation was modeling of the temperature field kinetics in the specimen being welded. For this purpose bidimensional equation of heat conductivity was numerically solved:

$$C(x, y, T)\frac{\partial T(x, y, t)}{\partial t} = \frac{\partial}{\partial x}\left(\lambda(x, y, T)\frac{\partial T(x, y, t)}{\partial x}\right) + \frac{\partial}{\partial y}\left(\lambda(x, y, T)\frac{\partial T(x, y, t)}{\partial y}\right), \quad (1)$$

where $C(x, y, T)$ is the heat capacity per unit volume of the material, J / (mm^3·°C); $T(x, y, t)$ is the temperature at the instant of time t in point (x, y) of the rectangular coordinate system, °C; $\lambda(x, y, T)$ is the metal heat conductivity in point (x, y) with temperature T, J / (mm·s·°C).

Initial and boundary conditions of the heat conductivity problem (1) were assumed as follows:

$$-\lambda(x, y, T)\frac{\partial T(x, y, t)}{\partial n}\Big|_{x, y \in J} = \alpha_{em}(T(x, y, t) - T_{env}), \quad (2)$$

$$T(x, y, 0) = \begin{cases} T_L^{Al}, & \text{if } (x, y) \in F, \\ T_{env}, & \text{if } (x, y) \notin F, \end{cases} \quad (3)$$

where n is the normal to surface; $\alpha_{em} \cong 2\cdot10^{-5}$ W / (mm^2·°C) is the heat emission coefficient in case of the item metal contact with ambient atmosphere; $T_L^{Al} = 640$ °C is the melting point of the used aluminium alloy; T_{env} is the temperature of the environment, °C; F is the weld zone, limited by curve $ABB'A'C'C$ (see Figure 1); J is the boundary of the welded joint metal contact with ambient atmosphere.

Temperature dependences of properties of the considered alloys, which are used in the mathematical model, are given in Tables 1 and 2.

Obtained in this way kinetics of the bidimensional temperature field allowed calculating changes of the heat strain state of the specimen (over the whole technological process).

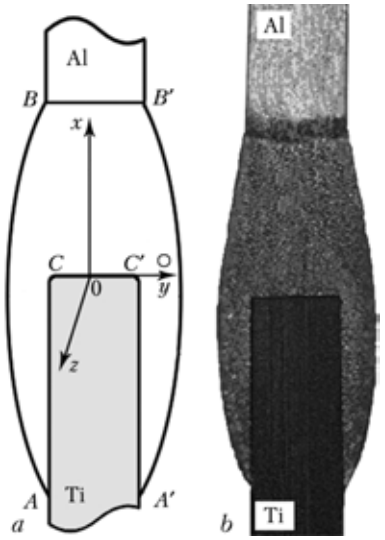

Figure 1. Scheme (*a*) and macrosection (*b*) of braze-welded dissimilar joint; circle shows area of investigation of degree of hot cracking risk

Mathematical model of the stress-strain state development is based on principle of presenting increments of components of tensor of deformations ε_{ij} in the form of the sum of increments of elastic ε_{ij}^e and plastic ε_{ij}^p deformations:

$$d\varepsilon_{ij} = d\varepsilon_{ij}^e + d\varepsilon_{ij}^p. \quad (4)$$

Proceeding from (4), on basis of Hooke's law and law of plastic flow, connection between strains and stresses may be expressed in the following way [11, 12]:

$$\begin{cases} d\varepsilon_{yy} = d\left(\dfrac{\sigma_{xx} - \sigma}{2G} + K\sigma + \varphi\right) + (\sigma_{xx} - \sigma)d\Lambda, \\ d\varepsilon_{yy} = d\left(\dfrac{\sigma_{yy} - \sigma}{2G} + K\sigma + \varphi\right) + (\sigma_{yy} - \sigma)d\Lambda, \\ d\varepsilon_{xy} = d\left(\dfrac{\sigma_{xy}}{2G}\right) + \sigma_{xy}d\Lambda, \end{cases} \quad (5)$$

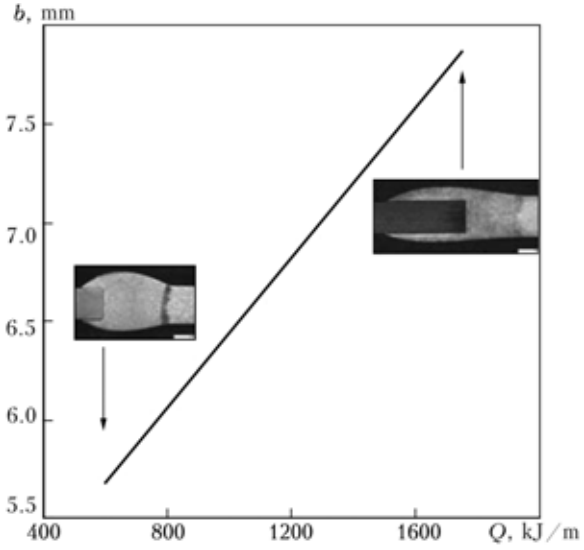

Figure 2. Dependence of weld width b upon heat input Q brought to laser source of heating; macrosections of braze-welded joints are obtained at the q respective values

Table 1. Thermophysical and mechanical properties of Ti6Al4V titanium alloy used in mathematical model [10]

T, °C	λ, J / (cm^3·°Ñ)	$\tilde{N}$, J / (cm^3·°Ñ)	σ_t, MPa	$Å$, GPa	$\alpha\cdot10^5$, °Ñ$^{-1}$
20	0.059	2.48	1060	119	0.71
100	0.072	2.50	870	115	0.80
200	0.086	2.57	720	110	0.89
300	0.100	2.70	630	104	0.92
400	0.114	2.83	570	97	0.94
500	0.128	3.01	460	91	0.96
600	0.142	3.23	350	85	0.97
700	0.156	3.54	230	80	0.98

Note. Here and in Table 2 following designations are used: σ_t — yield strength; E — Young's modulus; α — coefficient of linear expansion; the rest see in text.

Table 2. Thermophysical and mechanical properties of AA6056 aluminium alloy used in mathematical model [13]

T, °C	λ, J / (cm^3·°Ñ)	$\tilde{N}$, J / (cm^3·°Ñ)	σ_t, MPa	$Å$, GPa	$\alpha\cdot10^4$, °Ñ$^{-1}$
20	1.1	2.50	220	98	0.23
100	1.2	2.60	213	95	0.23
200	1.4	2.70	200	90	0.24
300	1.5	2.80	188	80	0.25
400	1.6	2.90	140	70	0.26
500	1.8	2.95	100	60	0.27
600	2.0	3.00	20	50	0.28
700	5.0	3.00	20	40	0.28

where σ_{xx}, σ_{yy} and σ_{xy} are the stress tensor components; $\sigma = 1 / 3(\sigma_{xx} + \sigma_{yy} + \sigma_{zz})$; G is the shear modulus; K is the volume compression factor; φ is the relative elongation function; Λ is the scalar function, value of which depends upon stress-strain state in each point of the item.

Component $d\varepsilon_{zz}$ was determined from the viewpoint of the beam theory as linear function of x and y, taking into account curvature of the welded beam axis and moments of applied external forces.

Numerical investigation of the heat-strained state of the item being welded was carried out by the method of finite elements.

Hot cracks occur within the brittleness temperature range (BTR) and are caused by the heat strain processes, occurring in the weld metal area and heat-affected zone. In the considered case simultaneous fulfillment of the following conditions may serve as a criterion for formation of this kind of defects:

- plastic strains, accumulated during cooling of aluminium portion of the specimen within BTR, exceed certain characteristic critical values, at which risk of hot cracking is sufficiently high;
- normal components of tensor of stresses in the investigated area are positive;
- geometric area of fulfillment of first two conditions is sufficiently high for development of a macrodefect (respective linear size of the area should exceed 1 mm).

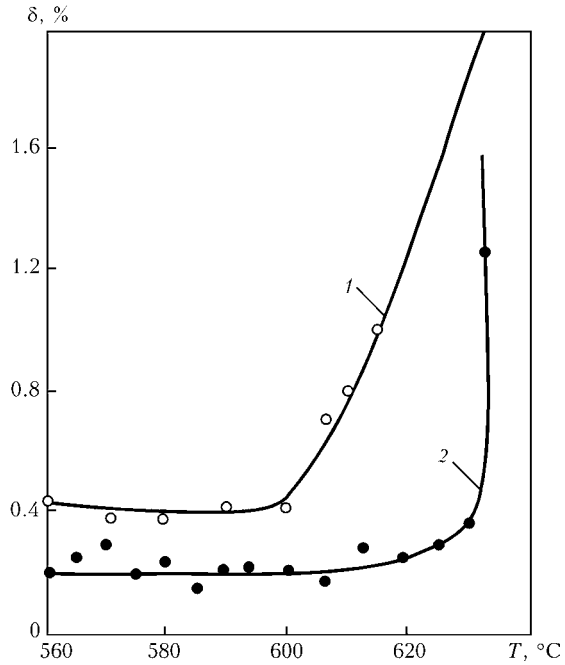

Figure 3. Change of deformations δ in case of failure within BTR of Al–Mg–Si system aluminium alloy of equiaxial (*1*) and columnar (*2*) solidification structure [10]

In Figure 3 dependence of deformations upon temperature, at which failure of aluminium alloys occurred, is shown that allows determining their critical values within BTR. For conservative evaluation such value is assumed to be 0.2 % within the whole BTR of 560–640 °C.

As showed results of numeric investigation of the heat strain processes, risk of hot crack formation is the highest in the areas, which are close to the dissimilar contact of titanium and aluminium. That's why for analysis of influence of technological parameters on risk of hot cracking, characteristic area T was selected located near titanium edge (see Figure 1, *a*). In this area increase of plastic strains in cooling within BTR of a welded item at various values of power of the laser source of welding heating and speed of the focal spot movement along the welded butt was investigated.

One may see from Figures 4 and 5 that plastic strains ε_{zz}^p accumulated within BTR exceed the allowable critical value. As far as normal stresses σ_{zz} in the considered area are positive, one may draw conclusion that there is a certain risk of formation of cross hot cracks. Appearance of longitudinal hot cracks is improbable.

Influence of technological welding parameters within allowable range of variation on accumulation of plastic strains within BTR is low, which is explained by rather narrow BTR and high rate of aluminium cooling because of its high heat conductivity.

Because of fulfillment of two conditions of the hot cracking criterion an important characteristic is size of the area of plastic strains within BTR at different technological parameters of the process. As showed calcula-

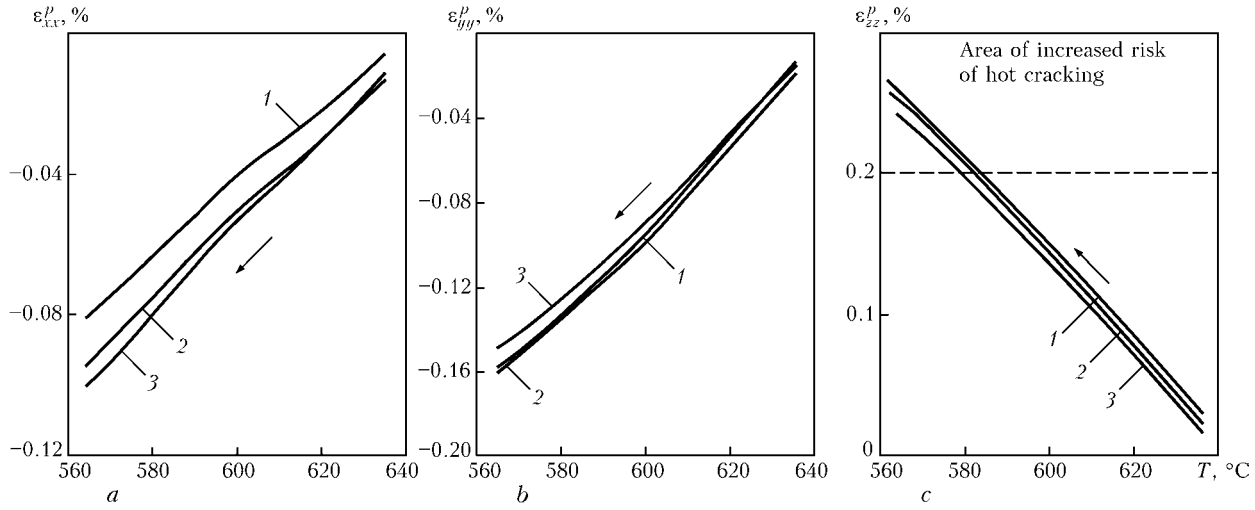

Figure 4. Kinetics of accumulation of plastic strains ε^p_{xx} (*a*), ε^p_{yy} (*b*) and ε^p_{zz} (*c*) within BTR at speed of source movement v = 4.33 mm / s and different values of power of each laser heat source: *1* — q = 2.0; *2* — 1.75; *3* — 1.5 kW

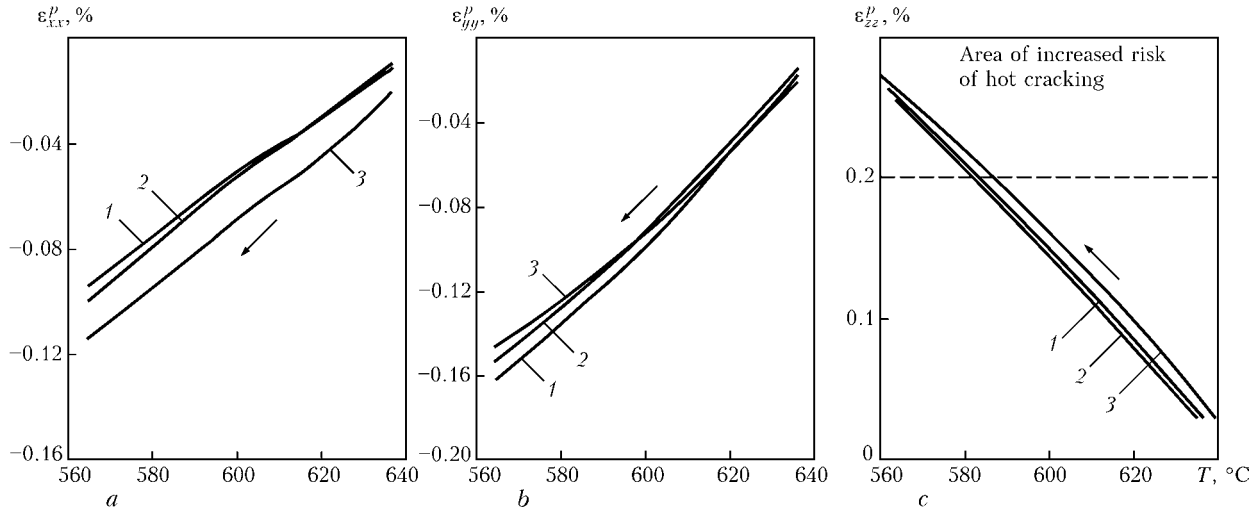

Figure 5. Kinetics of accumulation of plastic strains ε^p_{xx} (*a*), ε^p_{yy} (*b*) and ε^p_{zz} (*c*) within BTR at power of each laser source of heating q = = 1.75 and different values of speed of its movement: *1* — v = 4.33; *2* — 5.0; *3* — 2.33 mm / s

tion within the mathematic model framework, characteristic linear dimension of the risk area does not exceed 0.4–0.6 mm and varies insignificantly in case of the welding mode change. It follows from this that at a selected range of allowable values of speed of the welding heating sources and their power, and taking into account corresponding to these technological parameters geometric dimensions (mentioned above) of a structure being welded, formation of hot cracks in aluminium portion of the item is improbable, which is confirmed by results of the investigations. However, even a relatively small change of the weld geometry (for example, increase of the wetting line length or of the weld height) may cause significant increment of plastic strains accumulated within BTR, and occurrence of hot cracks in the area of a dissimilar contact.

Authors are grateful to Dr. T. Pretorius and his colleagues from BIAS for their cooperation in fulfillment of the experimental works.

1. Wagner, F., Zerner, I., Kreimeyer, M. et al. (2001) Characterization and properties of dissimilar metal combinations of Fe / Al-sheet materials. In: *Proc. of ICALEO* (Orlando, Florida, USA, Sept. 2001), 365–374.
2. Darwish, S.M. (2004) Analysis of weld-binded dissimilar materials. *Int. J. of Adhesion & Adhesives*, **24**, 347–354.
3. Mishra, R.S., Ma, Z.Y. (2005) Friction stir welding and processing. *Mater. Sci. and Eng.*, **50**, 1–78.
4. Sepold, G., Grupp, M. (2001) Laser materials processing — Quo Vadis? *Laser Assisted Net Shape Eng.*, **3**, 133–134.
5. Kreimer, M., Vollertsen, F. (2005) Processing titanium–aluminum hybrid joints for aircraft applications. In: *Proc. of 3rd Int. WLT-Conf. on Lasers in Manufacturing* (Munikh, June, 2005), 238–243.
6. Makhnenko, V.I., Milenin, A.S., Semyonov, A.P. (2007) Mathematical modeling of thermal-deformation processes in braze-welding of butt joints of the titanium–aluminium type. *The Paton Welding J.*, **11**, 2–5.
7. Ryabov, V.R. (1983) *Welding of aluminium and its alloys with other metals*. Kiev: Naukova Dumka.
8. Sabokar, V.K., Zamkov, V.N., Kireev, L.S. (1998) Specifics of argon-arc and diffusion welding of titanium with aluminium. *Avtomatich. Svarka*, **1**, 14–17.
9. Cicala, E., Duffet, G., Andrzejewski, H. et al. (2005) Hot cracking in Al–Mg–Si alloy laser welding — operating parameters and their effects. *Mat. Sci. and Eng. A*, **395**, 1–9.
10. Prokhorov, N.N. (1976) *Physical processes in metals during welding*. Vol. 2, Moscow: Metallurgiya.
11. Makhnenko, V.I., Velikoivanenko, E.A., Pochinok, V.E. et al. (1999) Numerical methods of the predictions of welding stresses and distortions. In: *Welding and Surfacing Rev.*, Vol. 13, Part 1. Amsterdam: Harwood AP.
12. Makhnenko, V.I., Pochinok, V.E. (2006) *Strength calculation of welded joints with crack-like imperfections*. Kiev: PWI.
13. Boyer, R., Welsch, G., Collings, E.W. (1994) *Materials properties handbook. Titanium alloys*. Miami: ASM Int.

SENSITIVITY TO CRACKING AND STRUCTURAL CHANGES IN EBW OF SINGLE CRYSTALS OF HEAT-RESISTANT NICKEL ALLOYS

K.A. YUSHCHENKO[1], B.A. ZADERY[1], A.V. ZVYAGINTSEVA[1], S.S. KOTENKO[1], E.P. POLISHCHUK[1], V.S. SAVCHENKO[1], I.S. GAKH[1] and O.P. KARASEVSKAYA[2]

[1]E.O. Paton Electric Welding Institute, NASU, Kiev, Ukraine

[2]G.V. Kurdyumov Institute for Metal Physics, NASU, Kiev, Ukraine

Transverse cracks in the weld metal were found to be the main defects of the EB-welded joints in single crystals of heat-resistant nickel alloys. Sensitivity to formation of such cracks in EBW of single-crystal nickel superalloy JS-26 depends, primarily, upon the welding speed, preheating and structural state of the initial metal. A probable cause of cracking of the weld metal is its structural heterogeneity, which results from peculiarities of the thermal-deformation cycle of welding, as well as from the initial structural state of metal. The range of the welding speeds, where the cracks are not formed, was determined. Increase in the welding speed leads to growth of the quantity of the cracks, and preheating shifts the critical welding speed towards higher values.

Keywords: electron beam welding, nickel alloys, single crystals, weld, crack resistance, temperature-time conditions, welding speed, preheating, X-ray diffractometry, violation of single-crystal structure, dislocation structure, local zones of stresses

Continuous demand for extending life and improving performance of aircraft and marine gas turbine engines, stationary gas turbine plants, gas pumping stations and various-purpose jet engines is met by increasing their temperature parameters. In turn, this requires development and application of alloys with increased heat-resistant properties, including with single-crystal or crystallographic-oriented structure. Complex alloying of such materials, leading to stability of strengthening phases and low diffusivity of alloying elements at increased temperatures, and practical absence of high-angle grain boundaries are the factors that, on the one hand, provide the optimal set of mechanical properties and maximal service life of parts, and, on the other hand, determine their insufficient workability, and in this case ---- weldability. According to the data of studies [1, 2], weldability of heat-resistant nickel alloys implies the possibility of producing permanent joints with a minimal degradation of structure and mechanical properties of the materials being joined. High level of mechanical properties of the alloys at increased temperatures, wide brittle temperature range, low safety factor for deformability in this range, and decreased thermal conductivity promote formation of substantial welding stresses, and determine low relaxation ability of metal, thus leading to formation of cracks during welding [3]. Therefore, one of the main indicators of weldability of such alloys is sensitivity to cracking. In view of the above-said, many superalloys, especially casting ones, are considered hard-to-weld or unweldable by traditional fusion welding methods.

At the same time, the actual data on quantitative evaluation of the sensitivity to cracking in fusion welding of single-crystal heat-resistant nickel-base alloys with a strengthening γ'-phase content of over 50 %, as well as data on the causes of this cracking, are very scanty [4, 5], whereas data on single-crystal or structurally oriented alloys are not available at all. As shown in studies [6–10], the possibility exists of producing welded joints with a sufficiently perfect single-crystal structure by fusion welding of single-crystal heat-resistant nickel alloys, provided the certain process parameters are kept to and crystallographic orientation of samples is maintained.

Experimental procedures. High-strength strain-hardening heat-resistant alloy JS-26, which is used for manufacture of gas turbine blades, was chosen as a material for experiments. The alloy has the following chemical composition, wt. %: Ni ---- base, 0.13–0.18 C, 4.3–5.6 Cr, 8.0–10.0 Co, 0.8–1.4 Mo, 10.9–12.5 W, 1.4–1.8 Nb, 5.5–6.2 Al, 0.8–1.2 V, 0.8–1.2 Ti, 0.015 B, 0.025 Ce, 0.005 Y, 0.005 La, 0.015 P, 0.25 Mn, 1.0 Fe.

The samples measuring 50 × 50 × 2 mm for the welding experiments were cut from single-crystal billets 5–8 mm thick, which were produced by the method of high-rate directed solidification. The cut location was subjected to grinding prior to welding. To relieve residual stresses due to grinding, and considering that alloy JS-26 has a non-equilibrium structure, the samples before welding were heat-treated at a temperature of 1265 °C for 1 h.

The sensitivity to cracking was evaluated by using an upgraded (small-sized samples) circular patch test [11–13]. The samples prior to welding were rigidly fixed on a welding table. Circular welds 3–5 mm wide (depending upon the welding speed) were made on a sample 40 mm diameter (Figure 1). Welding was performed both with preheating of the weld edges to a

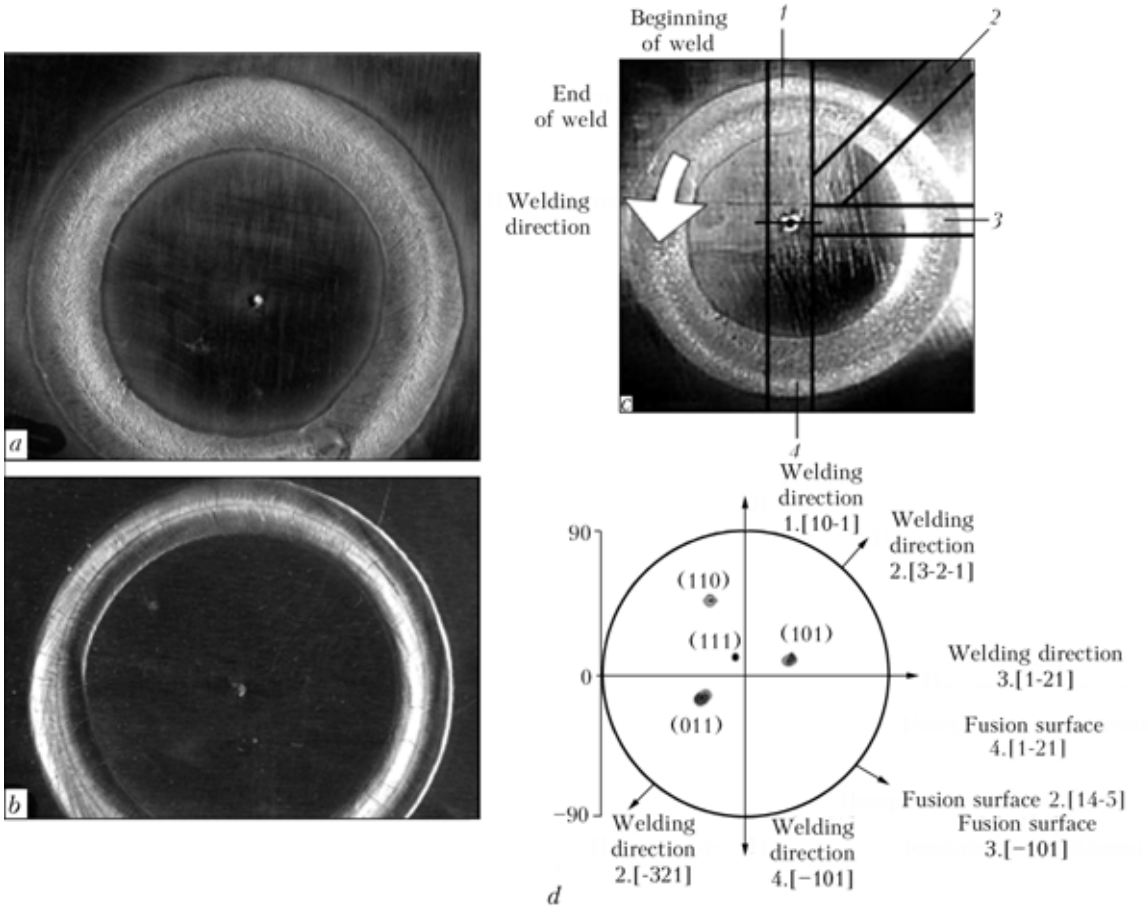

Figure 1. Appearance of circumferential welds at welding speed of 10 (*a*) and 60 (*b*) m / h, schematic of cutting of samples for experiments (*c*), and stereographic orientation of circular patch tests (*d*): *1–4* — sample numbers

temperature of 200–450 °C and without preheating. The welding speed was varied within a range of 5–80 m / h. The welding parameters were chosen on the basis of formation of certain geometry of the welds. Preheating was used to provide a uniform temperature field, decrease the solidification rate and reduce the temperature gradient at the solidification front of the weld pool. Criterion of the sensitivity to cracking was the quantity of visible cracks along the length of a circumferential weld. The beam fade-in and fade-out regions were neglected.

Metallographic and X-ray structure examinations were performed on sections of the surface of a welded joint 5 mm wide, which were cut from a circular patch test (Figure 1, *c*) and made according to the standard procedures.

Distribution of the intensity of scattered X-ray radiation near the sites of the reciprocal lattice was studied by the X-ray diffractometry method. This was done by the orientation X-ray procedure [14–16] using the standard diffractometer DRON-3M with a monochromatic CuK_β-radiation and special sample holder, which provide the four-circle equatorial experimental geometry and X-ray reflections without any special oriented arrangement of single-crystal samples. The phase composition of the alloy was determined from distribution of the intensity of X-ray reflections along diffraction vector **G** (**q** = **G** / |*G*|) – ($I_{\mathbf{q}\parallel}$) («θ – 2θ» are the X-ray patterns), their shape, half-width $d_{\mathbf{q}\parallel}$ and position of the maximum. Distributions of the intensity in a plane normal to vector **G** (**q** = **G** / |*G*|) – ($I_{\mathbf{q}\perp}$), their shape and half-width $\delta_{\mathbf{q}\perp}$ were used to study the sub-structure of single crystals. Distributions $I_{\mathbf{q}\perp}$ were determined over the entire azimuthal plane, this differing the used orientation diffractometry method from similar investigations using different variants of the «rocking curve» [15–17], where distribution $I_{\mathbf{q}\perp}$ is studied in one of the azimuthal directions. According to the theory of scattering of X-rays by non-ideal crystals [18], $I_{\mathbf{q}\perp}$ and $\delta_{\mathbf{q}\perp}$ are determined by the density, type, position and homogeneity of distribution of dislocations in a material, and depend upon the direction in the azimuthal plane.

Crystallographic orientation of the samples was determined from pole figures {220} and {111} by the standard backward filming procedure. Distributions $I_{\mathbf{q}\perp}$ and $I_{\mathbf{q}\parallel}$ were studied from reflections {220}, {110} and {331}. At the same time, the irradiated region was varied from 0.5 to 2.0 mm^2, depending upon the character of the experiment, which made it possible to estimate the experimental data at the mesoscopic structural level.

Crack resistance. Transverse cracks are the main defects of the welded joints in single crystals of alloy JS-26 (Figure 2). These cracks initiate in the weld metal, propagate to the fusion line, and decay in the HAZ region, often involving a marked plastic deformation. The cracks mostly have a branching intermit-

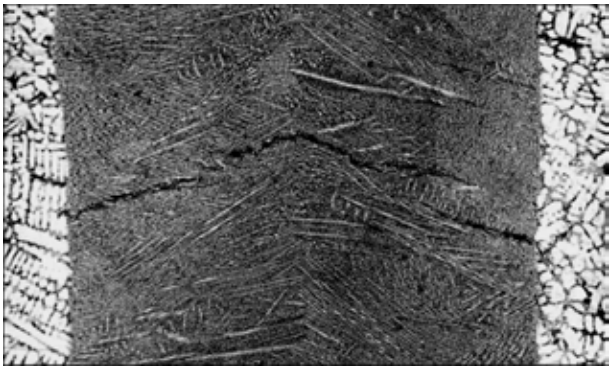

Figure 2. Transverse crack in weld metal on alloy JS-26 (×30)

tent character. Sometimes they do not propagate to the fusion line and take half or smaller part of the weld.

Analysis of the experimental data shows that the sensitivity to cracking in EBW of alloy JS-26 is determined by the temperature-time welding parameters, and, first of all, by the welding speed, preheating temperature and cooling rate. The cracks are formed primarily at the presence of high temperature gradients and cooling rates as a result of a high welding speed, high specific thermal power of the heat source, and enhanced heat removal.

The sensitivity to cracking was found to depend upon the welding speed and preheating of the weld edges (Figure 3). For metal 1–3 mm thick, the transverse cracks are formed at a welding speed above 15 m / h. The sensitivity to cracking grows with increase in the welding speed (Figure 3). The maximum of cracks is observed in the welds made at a speed of 60–80 m / h. And this is accompanied by increase in the crack opening degree. Increase in the specific thermal power at a constant welding speed leads to the same results. Preheating of samples to 350–450 °C shifts the critical welding speed to a range of higher values (to 25 m / h), whereas an enhanced cooling, on the contrary, brings it close to 5 m / h. These dependencies can be explained by a change in temperature gradient at a stage of heating, solidification and cooling, this, in turn, leading to changes in the rate of plastic deformation and level of welding stresses,

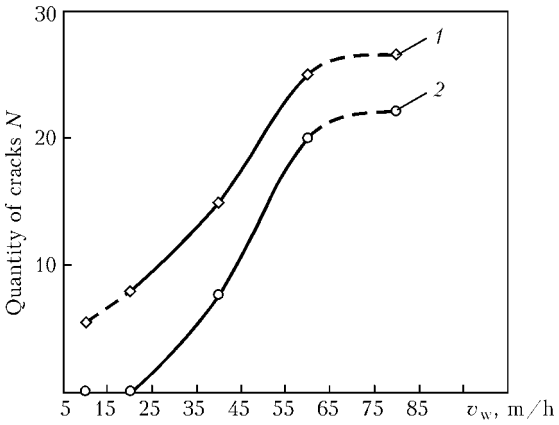

Figure 3. Dependence of sensitivity to cracking of alloy JS-26 in EBW of patch test samples upon the welding speed without (*1*) and with (*2*) preheating at $T_{preheat}$ > 350–450 °C

as well as character of structural and phase γ–γ′ transformations, and extent of their completeness.

Metallographic examinations. The initial metal is characterised by a developed, strictly oriented coarse-dendrite structure (Figure 4, *a*, *c*), consisting of the γ + γ′-phases and complex carbides. The grain boundaries are absent. The content of the γ′-phase is about 63 %. The structure of metal of the samples cut from different circumferential regions of a patch test differed only in a varying orientation of dendrites relative to the fusion line. HAZ is sufficiently narrow, equals about 0.3–0.1 mm, and is hard to distinguish for the joints made at welding speeds of 10 and 60 m / h, respectively.

Metal of the welds made at a speed of 10 m / h is characterised by smaller sizes of dendrites and dendrite spacings, compared with the base metal. Individual closed boundaries can be seen, like those after conventional chemical etching, and especially after surface oxidation of sections (Figure 4, *b*).

The structure of metal of the welds made at a speed of 60 m / h (Figure 4, *d*) is characterised by thinner, strictly oriented dendrites growing from the fusion line to the weld centre. The grain boundaries in the welds are hardly distinguishable. Transverse avalanche wavy cracks can be seen in microsections of the welds, as well as on the surface of the welded joints. Colonies of unidirectional dendrites, which were not fully formed into grains, were revealed by the method of deep oxidation of the sections.

Results of metallographic examinations show that a clearly defined inheritance of the initial crystallographic orientation by the weld metal took place in all variants of the welded joints considered (Figure 4, *c*).

X-ray examinations. It can be concluded from examination of pole figures (see Figure 1, *d*) that the patch tests were made on samples of the identical crystallographic orientation <335> close to <111>. Hence, the fusion surfaces are planes of zone <111> (<335>, to be more exact), which make angles of 25 to 45° to the preferential growth directions (<100>, <111>) of fcc metals. Therefore, the fusion planes are strongly diverted from the preferential growth direction on the perimeter of the circumferential weld. So, it is impossible to distinguish the weld regions with the most favourable orientation of the fusion surface, i.e. effect of the orientation factor can be ignored in analysis of the mechanism of formation of the structural state. Thus, it might be expected that structure of the weld metal will be similar in different samples of the same patch test. The data of microstructural analysis, type and quantity of the cracks, and results of X-ray examinations of different samples of the same patch test proved the conclusion of a practical identity of the structure along the length of the circumferential welds made at the same welding speed.

Results of X-ray examinations are indicative of the fact that the base metal is a single crystal containing γ + γ′-phases (Figure 5). Lattice parameters of the γ +

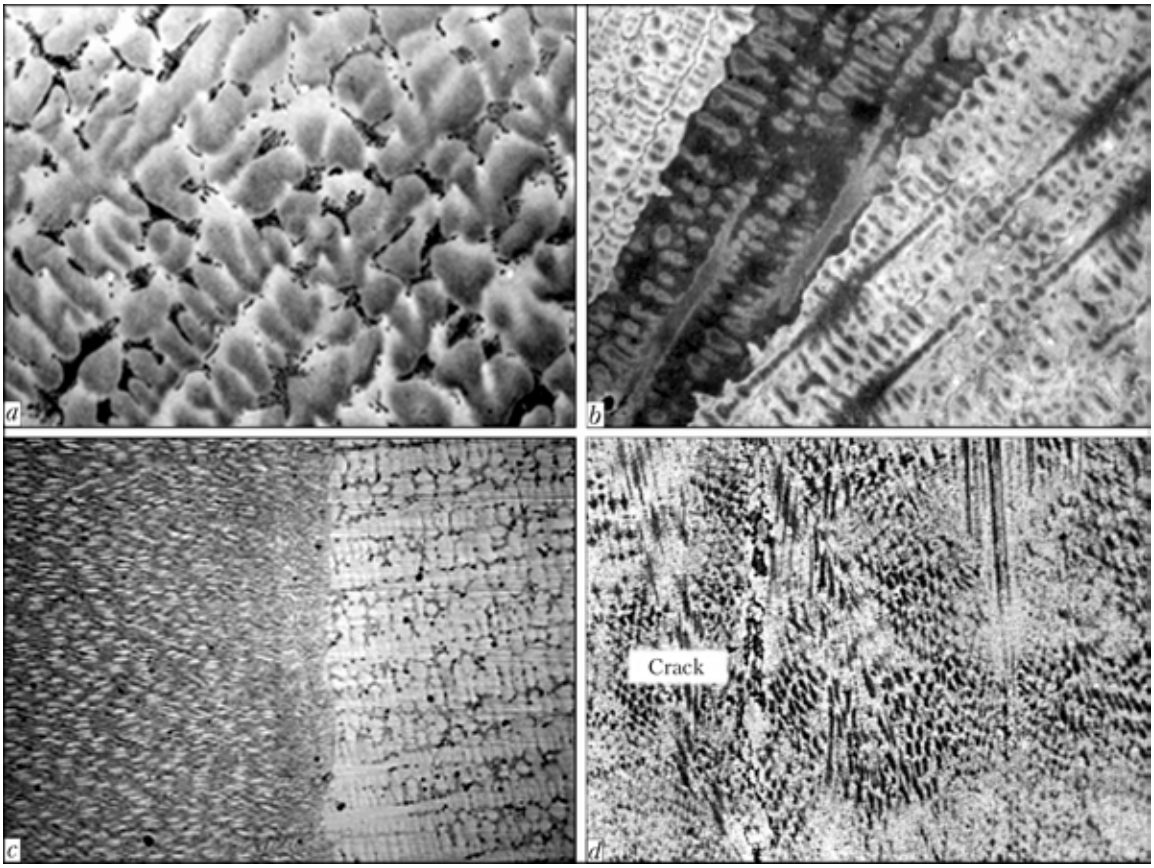

Figure 4. Microstructure of welded joints in single crystals of alloy JS-26: *a* — base metal (×100); *b* — weld (×200), v_w = 10 m / h; *c* — weld to base metal transition region (×25), v_w = 10 m / h; *d* — weld (×200), v_w = 60 m / h

+ γ'-phases can be considered coinciding at the experimental accuracy ($2\theta \sim 0.01°$), this corresponding to their mismatch parameter of less than 0.01 %. Positions of maxima of the intensities of distributions $I_{\mathbf{q}\perp}$ for the $\gamma + \gamma'$-phases (line (220)) and γ'-phase (line (110)) are in the same device coordinates, which reflects coincidence of their crystallographic orientations (Figure 5, *a*, *d*). It can be noted, at the same time, that the γ'-phase has a somewhat higher angular scattering of reflections of a low intensity, compared with the γ-phase (Figure 5, *b*, *e*).

It should be noted that the base metal has an X-ray peculiarity, which has not been observed before in other single-crystal materials, such as one-phase crystals and heat-resistant nickel-base blades. The peculiarity consists in the presence of an elongated region of diffused multiple-degree scattering of X-rays, extended about the preferential direction. It follows from study [18] that the diffused multiple-degree scattering of X-rays is possible because of fluctuation heterogeneities of crystal, covering its entire volume. Apparently, it is the non-uniform state of the two-phase system formed in growing of billets, or in welding of samples (the base metal was studied as part of the welded joint), that is the cause of diffused scattering.

Figure 6 shows pole figures {220} and distributions $I_{\mathbf{q}\perp}$ of reflection (022), which were obtained in different zones of a welded joint made at a speed of 10 m / h. As follows from examination of the pole figures, the base metal (Figure 6, *a*) and HAZ metal (Figure 6, *c*) maintained the single-crystalline structure of the initial material.

Distributions $I_{\mathbf{q}\perp}$ in the HAZ metal and fusion zone have a preferential broadening in one crystallographic direction (about [11–2]), which may be related to an increased density of like-sign dislocations of the primary, most loaded systems, and their uniform distribution at a mesoscopic structural level. The direction of preferential broadening of a reflex persists in distributions $I_{\mathbf{q}\perp}$, and the intensity spots separated from the main reflection by high-angle boundaries are formed in the weld regions located near the fusion zone (initial solidification regions) (Figure 6, *e*). The pole figure at the weld centre corresponds to a material consisting of individual grains (Figure 6, *g*), although the general crystallographic orientation persists.

Violation of the single-crystal structure in the weld is of a specific character and takes place in all the samples. The specific character of formation of the granular structure consists in the fact that formation and separation of grains from the single crystal, as well as their re-orientation, occur not chaotically, but in a certain direction [112], which coincides with the position of high-angle diffused broadening in the initial material. If the high-angle diffused broadening in the initial single crystal resulted from the non-compensated elastic energy present in it, it is highly probable that it was this fact that determined formation and direction of re-orientation of separate grains in the weld. Therefore, if structure of the base material

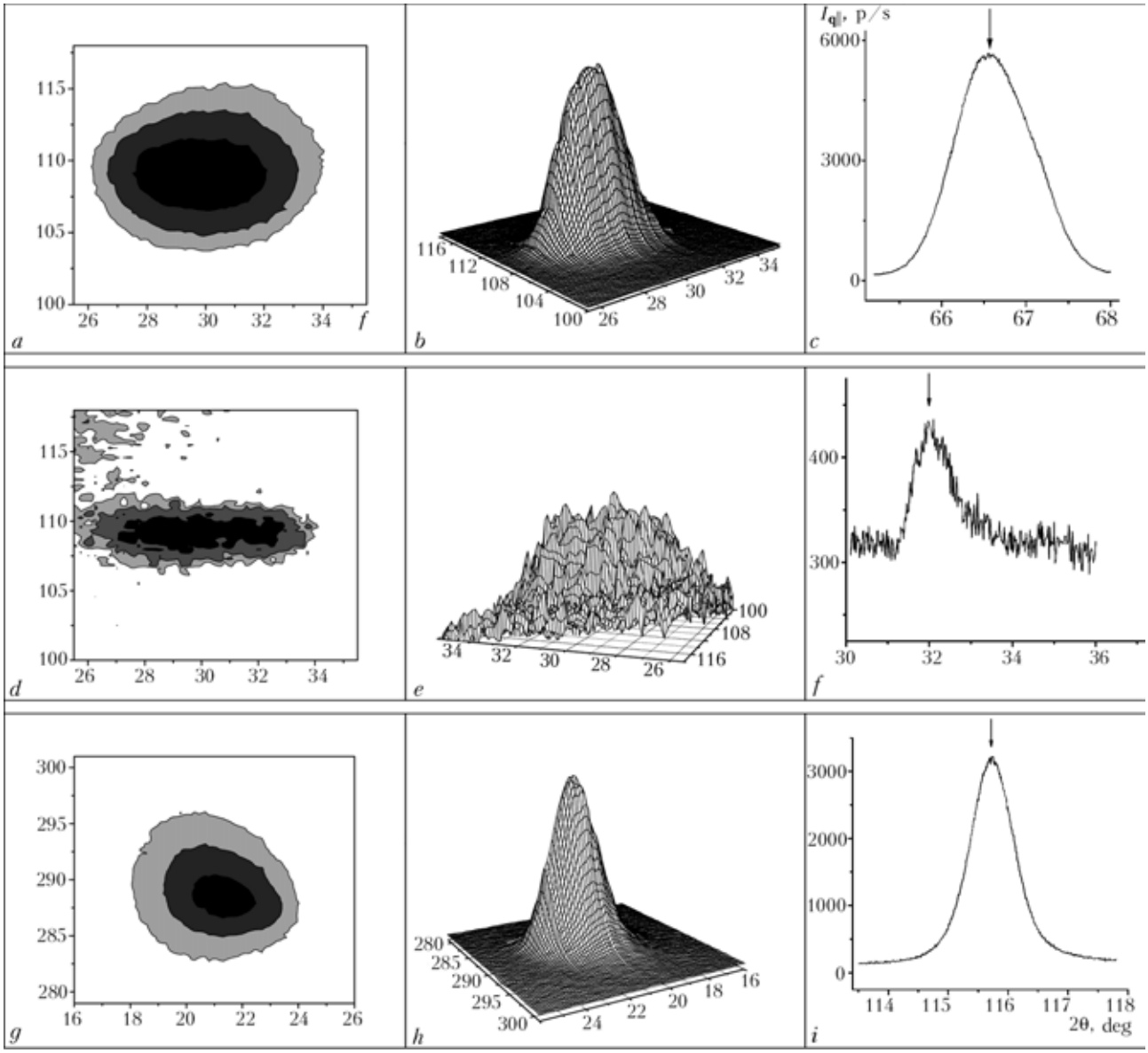

Figure 5. Intensity distributions $I_{q\perp}$ (*a*, *b*, *d*, *e*, *g*, *h*) in device coordinates, and $I_{q\parallel}$ (*c*, *f*, *i*) in base metal (specimen # 4) for lines of the γ + γ′-phase (220) (*a*–*c*), (331) (*g*–*i*) and γ′-phase (110) (*d*–*f*)

is in a non-equilibrium state, structure with an increased dislocation density will be formed in the weld.

Pole figures {220} and distributions $I_{q\perp}$ for reflection (022) of different zones of the welded joint made at a speed of 60 m / h are shown in Figure 7. As follows from their examination, positions of the main X-ray reflexes corresponding to a single-crystal orientation of the irradiation region persist for all the zones of the welded joint (base metal, HAZ, fusion zone, weld). The intensity of reflexes, which do not correspond to the single-crystal orientation of the irradiation region, increases in the HAZ metal and fusion zone, these reflexes being located in the region of high-angle diffused broadening of the base material, like in the case of a low welding speed. Fine intensive reflexes, not related to the dominant orientation of the irradiation region, as well as located near the specific diffused region of an increased intensity, can be seen at the weld centre.

Distributions $I_{q\perp}$ (Figure 7, *d*) in the HAZ metal (probably in the fusion zone as well), like in the case of a low welding speed, undergo a preferential broadening in one crystallographic direction, which also can be related to increase in the dislocation density in the primary, most loaded systems and their homogeneous distribution at the mesoscopic structural level. Like in the case of a low welding speed, formation of the intensity regions separated from the main reflex by high-angle boundaries can be seen in the X-ray patterns of distribution $I_{q\perp}$. Distribution $I_{q\perp}$ in the fusion zone and weld near the fusion zone is characterised by emergence of the second direction of substantial broadening of reflexes (Figure 7, *f*, *g*), which is associated with formation of the secondary dislocation systems. Broadening of distributions $I_{q\perp}$ at the weld centre increases along this direction. According to the orientation factor determining the total impact of different dislocation systems on broadening of reflexes in the azimuthal plane, increase in the quantity

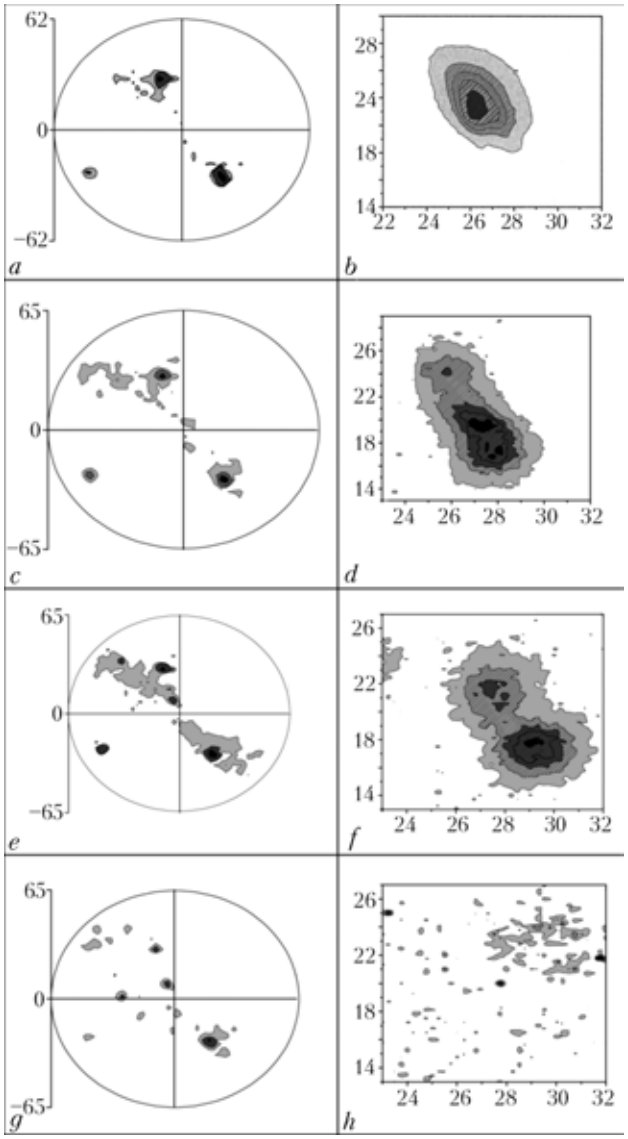

Figure 6. Pole figures {220} and distribution $I_{\mathbf{q}\perp}$ of reflection (022) in different zones of welded joint (v_w = 10 m / h); *a*, *b* — base metal; *c*, *d* — HAZ metal; *e*, *f* — weld near fusion line; *g*, *h* — weld centre

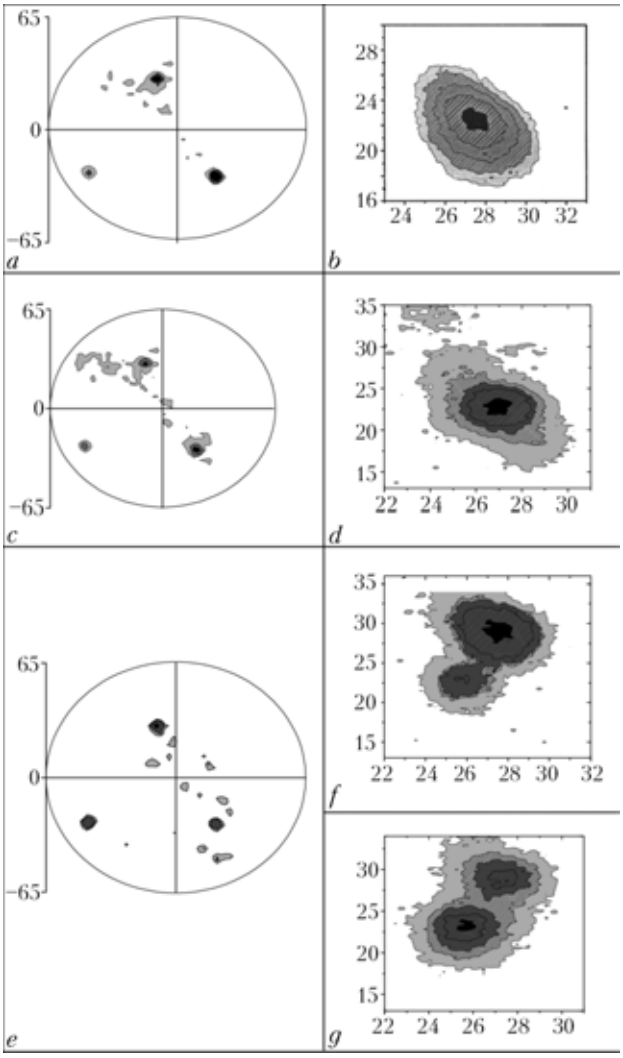

Figure 7. Pole figures {220} and distribution $I_{\mathbf{q}\perp}$ of reflection (022) in different zones of welded joint (v_w = 60 m / h); *a*, *b* — base metal; *c*, *d* — HAZ metal; *f* — fusion line, weld; *e*, *g* — weld centre

of the dislocation systems in the case of their uniform distribution should lead to isotropic broadening in the azimuthal plane. In the welds made at a welding speed of 60 m / h, distributions $I_{\mathbf{q}\perp}$ are characterised by anisotropy of broadening in the azimuthal plane. Anisotropy of broadening of distributions $I_{\mathbf{q}\perp}$ is caused by a non-uniform distribution of dislocations at the mesoscopic level. Increase in the density of the secondary dislocation systems leads to formation of the zones of local stresses in the non-uniform dislocation ensembles. Development of heterogeneous disorientations leads to acceleration of deformation and fracture of the material [19–24]. Disorientations become particularly complicated with accumulation in the crystal of the redundant dislocations with different Burgers vectors. This is accompanied by formation of high stress fluctuation fields, which may be a cause of cracking. Cracking under conditions of high stress fluctuations is promoted by a low ductility of the alloy, and a relatively low temperature of structure formation in the weld at increased welding speeds, where the relaxation processes have not time to be completed.

The position of maximum of distributions $I_{\mathbf{q}\parallel}$, {331} and {420}, for the joints made at a speed of 10 and 60 m / h is almost constant both for the HAZ and weld metals. Separation of distributions $I_{\mathbf{q}\parallel}$ {331} {422} {420} («θ – 2θ» curves) into the γ- and γ′-phase is not observed in the experiment with CuK_β-radiation. Processing of the $I_{\mathbf{q}\parallel}$ curves by the Fourier-analysis method and curves plotted on the basis of a standard does not lead to a separation of $I_{\mathbf{q}\parallel}$ either. The γ + γ′ mismatch parameter in the irradiation region remains at the same level as in the initial material. Decrease in the width of distributions $I_{\mathbf{q}\parallel}$, despite broadening of $I_{\mathbf{q}\perp}$ observed at the weld centre, is caused most probably by decrease in the simultaneously reflecting area, which is associated with refining of dendrites and formation of stray grains.

Results and discussions. The observed violation of the single-crystal structure in the weld on alloy JS-26 can be caused by two processes: firstly, by loss of stability of directed solidification at the solidifica-

tion front of the weld pool, and, secondly, by formation of a heterogeneous dislocation structure during cooling and accompanying formation of the zones of heterogeneous disorientations with a high dislocation density and localisation of stresses.

In directed solidification of multi-component alloys, an important criterion of structure formation is the **G** / V ratio, where **G** is the temperature gradient, and V is the solidification front velocity. The **G** / V ratio has a critical value for each alloy, and determines the sensitivity of a system to a directed structure formation.

The effect of **G** / V on structure formation should be considered together with crystallographic direction of the preferential growth of crystals and orientation at the weld pool solidification front. In this case, the higher the mismatch between the direction of the maximal heat removal and that of the preferential growth, the higher should be the values of **G** / V to provide an acceptable perfection of single-crystal structure in the welded joint. In a case where the deviation from the preferential growth direction is insignificant, and the welding direction coincides with the axes of high symmetry of the single crystal welded, the positive result is achieved in welding at the low values of **G** / V.

In welding at low speeds, solidification of the weld pool occurs at low rates as well. However, the marked deviation of the shape of a solidification macrofront of the molten pool metal from the flat one, and substantial (25–45°) disorientation between the direction of preferential solidification and real direction of growth of the weld metal crystalline grains lead to formation of regions in the central part of the weld metal that have a crystallographic orientation differing from the initial one. On the other hand, a longer time of dwelling of different zones of the welded joint at high temperatures leads to formation of the dislocation ensembles in the welded joints, which are homogeneous at the mesoscopic level. In this case, the homogeneous distribution of dislocations causes formation of the sub-granular structure in the weld, which has low disorientation angles between individual grains of the sub-structure, and, hence, provides a more perfect single-crystal structure of the joint.

At high welding speeds, macroshape of the solidification front of the weld pool is closer to the flat one, which should favour a more complete inheritance of the crystallographic orientation of the fusion surface, from which the weld metal crystalline grains grow. In this case, however, temperature gradient **G** and the level of temporary stresses increase, the time of dwelling of the welded joint zones at high temperatures reduces, and, finally, the processes of relaxation of welding and structural stresses decelerate. This involves the anisotropic distribution of dislocations and formation of the zones of local stresses, which can be accompanied by decrease in the perfection of single-crystal structure and cracking for the low-ductility material with a coherent bond of the phase components, formed in the sub-solidus region.

We relate the observed low-angle diffused broadening in the base metal to a substantial elastic energy of crystal, caused by fluctuation heterogeneities covering the entire volume. In this connection, it can be suggested that the state of the material prior to welding plays an important role in its ability to retain a single-crystal structure and resist cracking during welding. If the material prior to welding is in a non-equilibrium state (has a substantial elastic energy) or contains an increased dislocation density, e.g. as a result of its operation, machining, etc., the structural imperfection of metal will only grow during welding. It may reach a critical value and, combined with a high level of welding stresses, may cause cracking.

Most probably, low workability (high sensitivity to cracking during welding) of heat-resistant nickel alloys can be explained by the presence of a high amount of the γ'-phase in their composition, which determines the high values of yield strength and relaxation resistance of the alloy over a wide range of temperatures [25], thus causing increase in values and rate of welding stresses. Under the effect of welding heating, the γ'-phase may dissolve partially or fully [26], whereas in cooling it again precipitates from solid solution to cause interface volumetric stresses. The total effect of welding and volumetric stresses is one of the main causes of a high sensitivity of nickel alloys to cracking during fusion welding [27–30]. Such cracks are formed as a result of localisation of plastic deformation in the process of stress relaxation, which is caused by decrease in the relaxation resistance of the weld and HAZ metal. It is for this reason that increase in the welding speed, accompanied by increase in the level and rate of growth of temporary welding stresses, leads to increase in the quantity of cracks in the welded joint.

Homogenising annealing or overageing of the initial material prior to welding [31] of strain-hardening nickel alloys, providing an alloy with coarser precipitates of the γ'-phase, bring values of strength properties and ductility of the base metal closer to those of the HAZ metal, which creates more favourable conditions for relaxation of welding stresses in a larger volume of the material joined.

Allowing for the above-said and the fact that the density of dislocations in the weld metal produced at a high (60 m / h) welding speed grows, compared with the initial single crystal, 15–20 times at a substantial non-uniformity of their distribution, and 6–8 times at a sufficient uniformity of their distribution for the weld produced at a low (10 m / h) welding speed, the role of the welding speed and conditions in formation of cracks in the JS-26 alloy welds becomes understandable.

CONCLUSIONS

1. Multi-component heat-resistant nickel superalloys of the JS-26 type are characterised by low workability

and, first of all, by low weldability, the main indicator of which is the sensitivity to cracking during welding. The basic technological factors that determine importance of this indicator include: structural perfection of initial single crystal, and temperature-time conditions of formation of a welded joint, caused by the welding speed, preheating and heat removal conditions.

2. Characteristic defects of the EB-welded joints in JS-26 alloy single crystals are transverse cracks, which form in the weld metal and decay near the fusion zone or in HAZ. In welding of 1–3 mm thick samples of the patch test type, the cracks can be avoided at a welding speed of up to 10–15 m / h. Preheating to 450 °C allows the welding speed to be increased to 20–25 m / h.

3. With the majority of the variants of welding parameters and conditions under consideration, metal of the welded joint retains the initial crystallographic orientation of single crystal.

4. Violation of the temperature-time and crystallographic conditions of directed solidification in weld formation, which are determined mostly by the welding speed and preheating temperature, cause decrease in perfection of the single-crystal structure of the weld metal, and lead to formation of grains with a different crystallographic orientation.

5. Welding at increased speeds leads to a substantial increase in the density of dislocations, their nonuniform distribution and associated formation of the local zones of stresses, which can be one of the main causes of cracking of the weld.

6. Dislocation density in the weld metal made at a speed of 60 m / h (low-temperature mechanism of structure formation) grows, compared with the initial single crystal, 15–20 times, and 6–8 times at a speed of 10 m / h (high-temperature mechanism of structure formation).

7. Lattice parameters of the $\gamma + \gamma'$-phases remain almost unchanged, within the measurement error, in all regions of the welded joint, independently of the welding speed.

1. Yushchenko, K.A. (2004) Weldability and advanced processes for materials welding. *The Paton Welding J.*, **9**, 39–44.
2. Yushchenko, K.A., Derlomenko, V.V. (2005) Analysis of modern views on weldability. *Ibid.*, **1**, 5–9.
3. (1995) *Superalloys II*. Ed. by I.G. Sims et al. Moscow: Metallurgiya.
4. Ejdelshtein, V.E., Yakushin, B.F., Steblov, V.I. (1996) High-temperature deformation and formation of near-weld cracks in welding of alloy of Nimonic type. *Avtomatich. Svarka*, **11**, 40–44.
5. Sorokin, L.I. (1997) About hot cracking in welding of high-strength alloys. *Svarochn. Proizvodstvo*, **7**, 9–11.
6. David, S.A., Babu, S.S., Vitek, J.M. (2003) Solidification and microstructure. *J. of Metals*, **6**, 14–20.
7. Barabash, O.M., Babu, S.S., David, S.A. et al. (2003) Deformation in the heat-affected zone during spot welding of a nickel-base single crystal. *J. Appl. Phys.*, 94(**1**), 738–742.
8. Park, J.-W., Babu, S.S., Vitek, J.M. et al. (2003) Stray grain formation in single crystal Ni-base superalloy welds. *Ibid.*, 94(**6**), 4203–4209.
9. Yushchenko, K.A., Karasevskaya, O.P., Kotenko, S.S. et al. (2005) Inheritance of structure-oriented state of metallic materials by welded joints. *The Paton Welding J.*, **9**, 2–9.
10. Pollock, T.M., Murphy, W.H. (1996) The breakdown of single-crystal solidification in high refractory nickel-base alloys. *Metal. Mater. Transact. A*, **27**, 1081–1094.
11. Borland, J.C., Rogerson, J.H. (1962) Examination of the patch test for assessing hot cracking tendencies of weld metal. *British Welding J.*, 9(**8**), 494–499.
12. Rundel, G.R., Nehrenberg, A.E. (1966) Weld metal cracking of Invar in circular patch test. *Welding J.*, 45(**4**), 156–160.
13. Zessmenn, G.G. (1964) Welding evaluation of experimental columbium alloys. *Ibid.*, 43(**3**), 103–115.
14. Fewster, P.F. (2000) Insight into polycrystalline materials with ultrahigh resolution and reciprocal space mapping. Commission on power diffraction. *Microstructure of Materials*, 24(**12**), 17.
15. Karasevskaya, O.P. (1999) Orientation X-ray experimental method of phase analysis. *Metallofizika i Nov. Tekhnologii*, 21(**8**), 34.
16. Ungar, T., Mughrabi, H., Ronnpagel, D. et al. (1984) X-ray line-broadening study of the dislocation cell structure in deformed [001]-orientated copper single crystals. *Acta Met.*, **32**, 333.
17. Wilkens, M., Ungar, T., Mughrabi, H. (1987) X-ray rockin-curve broadening of tensile-deformed [001]-orientated copper single crystals. *Phys. Status Solidi A*, **104**, 157–170.
18. Krivoglaz, M.A. (1996) *X-ray and neutron diffraction in nonideal crystals*. Berlin: Springer.
19. Mughrabi, H. (1983) Dislocation wall in deformed metal crystals. *Acta Met.*, **31**, 1367–1379.
20. Panin, V.E., Likhachev, V.A., Grinyaev, Yu.V. (1985) *Structural levels of deformation of solids*. Novosibirsk: Nauka.
21. Likhachev, V.A., Panin, V.E., Vladimirov, V.I. et al. (1989) *Cooperative deformation processes and localization of deformation*. Kiev: Naukova Dumka.
22. Malygin, G.A. (1995) Self-arrangement of dislocations and localization of sliding in plastically deformed crystals. *Fizika Tv. Tela*, Vol. 37, 3–42.
23. Sarafanov, G.F. (1998) On the theory of formation of heterogeneous dislocation structures. *Fizika Metallov i Metallovedenie*, **85**, 46–53.
24. Koneva, N.A., Kozlov, E.V. (1990) Physical nature of plastic deformation staging. *Izvestiya Vuzov. Fizika*, **2**, 89–106.
25. Maslenko, S.B. (1983) *Heat-resistant steels and alloys*. Moscow: Metallurgiya.
26. Yushchenko, K.A., Savchenko, V.S., Zvyagintseva, A.V. (2004) Effect of heat treatment and degree of alloying on structural changes in nickel alloys. *The Paton Welding J.*, **7**, 12–14.
27. Lippold, J.C., Kotecki, D.I. (2005) *Welding metallurgy and weldability of stainless steels*. Willey Interscience.
28. Savchenko, V.S., Markashova, L.I., Yushchenko, K.A. (1994) Effect of weld composition and fine structure on processes of thermoplastic deformation and under-bead crack formation in welding of austenitic steels. *Avtomatich. Svarka*, **4**, 6–10.
29. Savchenko, V.S., Yushchenko, K.A. (1997) Mechanism of formation and methods of elimination of under-bead microcracks in multilayer welds with stable-austenitic structure. In: *Proc. of Materials Solutions'97 Conf. on Joining and Repair of Gas Turbine Components* (Indianopolis, Indiana, 15–17 Sept., 1997), 17–22.
30. Yushchenko, K.A., Savchenko, V.S., Chervyakov, N.O. et al. (2004) Character of formation of hot cracks in welding cast heat-resistant nickel alloys. *The Paton Welding J.*, **8**, 34–38.
31. Gessinger, G.Kh. (1988) *Powder metallurgy of heat-resistant alloys*. Chelyabinsk: Metallurgiya.

MECHANICAL PROPERTIES OF WELD METAL AND COLD CRACKING RESISTANCE OF TEE-JOINTS ON 13KhGMRB STEEL

V.D. POZNYAKOV
E.O. Paton Electric Welding Institute, NASU, Kiev, Ukraine

Effect of deposited metal composition on mechanical properties of single-pass fillet welds in T-joints on high-strength alloyed steel 13KhGMRB and resistance of these joints to delayed fracture depending upon hydrogen concentration, welding heat input and shielding atmosphere composition have been evaluated. It is shown that the highest resistance of such joints to cold cracking is observed in CO_2 welding using 1.6–2.0 mm low-alloy wire Sv-08G2S, with preheating to 60 °C and limited diffusible hydrogen content (up to 3.5 ml / 100 g) of the welds.

Keywords: arc welding, shielding gases, high-strength steel, tee joints, mechanical properties, cold cracks, cooling rate, preheating, diffusible hydrogen

Tee joints with fillet welds are a considerable part (about 70 %) of welded joints in structures made of high-strength alloyed steel sheets ($\sigma_{0.2}$ = 590–690 MPa) up to 20 mm thick. In most of the cases they should have mechanical properties on the level of those of base metal. Cold cracks in the weld metal (WM) and heat-affected zone (HAZ) are frequent and dangerous defects of such joints [1].

Recommendations on selection of welding consumables, welding modes and preheating temperature for performance of fillet welds are usually based on the results of testing butt joints. It is known, however, that the conditions of structure formation, as well as mechanical properties in fillet and butt welds, differ essentially in a number of cases. This is, primarily, related to the fact that unlike butt joints, heat removal in tee joints occurs not in two, but in three directions, and the cooling rate of such joints will be increased in such welding modes, respectively [2].

This study is devoted to evaluation of the mechanical properties and delayed fracture resistance of tee joints of high-strength steel with single-pass fillet welds made by welding wires of different alloying.

Investigations were conducted on rolled sheets of 13KhGMRB steel 12 and 20 mm thick of the following composition, wt.%: 0.128–0.132 C; 0.20–0.22 Si; 0.87–0.91 Mn; 1.4–1.5 Cr; 0.12–0.14 Ni; 0.42–0.45 Mo; S ≤ 0.022; P ≤ 0.020, 0.0011–0.0015 B. In as-delivered condition (after quenching and subsequent tempering) the steel has the following mechanical properties: $\sigma_{0.2} \geq 588$ MPa; $\sigma_t \geq \geq 686$ MPa; $\delta_5 \geq 14$ %; $KCU^{-70} \geq 29$ J / cm^2. Solid wires of 1.6 mm diameter of Sv-08G2S, Sv-10KhG2SMA and Sv-08KhN2G2SMYu grades were used as basic welding consumables (Table 1). In some cases wires of 1.2 and 2.0 mm diameter were used during investigations.

Mechanical properties and impact toughness of the metal of the studied welds were evaluated by the results of testing standard samples made from tee and special butt joints shown in Figure 1 [1]. The design of these joints allows simulation of the conditions of making fillet welds. For this purpose the edges of the plates being joined were cut at an angle of 45° to a chamfer size equal to the legs of the studied welds (k = 8 mm). Cylindrical samples of 3 mm diameter (type 1 to GOST 6996–66) were made from fillet welds of tee joints, and samples of 10 × 5 × 55 mm size (type VII) were cut out of butt joints. Mechanized welding of the above samples was performed in CO_2 in the following mode: I_w = 290–300 A, U_a = 32–34 V, v_w = 13–14 m / h. WM composition is given in Table 2.

As a result of active stirring of the molten electrode and base metals, the welds made with Sv-08G2S wire are further alloyed with such elements as chromium and molybdenum. This leads to their strength values rising from $\sigma_{0.2}$ = 375–405 MPa and σ_t = 500–532 MPa (values characteristic for the deposited metal) up to $\sigma_{0.2}$ = 634–693 MPa, σ_t = 781–802 MPa (level of steel 13KhGMRB), and ductility decreasing from δ_5 = = 24.2–26.3 to 16.3–16.7 %. Values of impact toughness of such welds (KCU^{-70} = 33–46 J / cm^2) fully meet the requirements made of the base metal and are comparable with cold resistance of welds made with

Table 1. Composition (wt.%) of welding wires

Wire grade	C	Si	Mn	Cr	Ni	Mo	Al	S	P
Sv-08G2S	0.080	0.79	1.71	–	–	–	–	0.022	0.025
Sv-10KhG2SMA	0.084	0.73	1.95	0.95	–	0.49	–	0.021	0.023
Sv-08KhN2G2SMYu	0.078	0.58	1.66	0.87	2.3	0.47	0.086	0.024	0.022

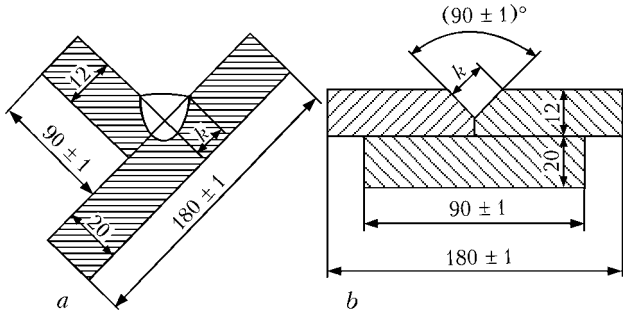

Figure 1. Schematic of tee (*a*) and butt joints with a backing (*b*) on steel 13KhGMRB

wires Sv-10KhG2SMA (KCU^{-70} = 30–41 J / cm^2) and Sv-08KhN2G2SMYu (KCU^{-70} = 44–49 J / cm^2). In view of this fact, Sv-08G2S wire can be recommended for welding high-strength alloyed steels with $\sigma_{0.2} \leq$ ≤ 620 MPa when making single-pass fillet welds with up to 8 mm leg. As the strength properties of such welds are lower than those made with welding wires Sv-10KhG2SMA and Sv-08KhN2G2SMYu ($\sigma_{0.2}$ = = 748–776 MPa, σ_t = 852–870 MPa and $\sigma_{0.2}$ = 890–910 MPa, σ_t = 1000–1020 MPa, respectively), it may be assumed that they will differ by a higher cold cracking resistance.

Cold cracking resistance of joints with fillet welds was evaluated by the results of testing special technological samples from steel 13KhGMRB, the prototype for which was the Tekken sample. In this case tee samples in rigid restraint with flange *1* of thickness δ_1 = 20 mm and web *2* with δ_2 = 12 mm were used (Figure 2, *a*). Design dimensions of the sample were selected so as to simulate the most unfavourable conditions of making single-pass fillet welds: considerable difference in thickness between the web and the flange ($\delta_2 / \delta_1 = 0.6$). The samples were assembled and joined from both sides by connecting welds *3* with the leg of 15–15 mm so that a gap of 2 mm width remained between the web and flange in the location of tested weld *4*. Tested weld of the length of 75–76 mm was made in the specified mode by mechanized gas-shielded welding. At the start and end of this weld, sections 2–3 mm long were left unwelded up to the connecting welds. Sample cooling rate was controlled by variation of their preheating temperature. Thermal cycle of sample heating and cooling was recorded in their central part (from the flange side) in the HAZ section heated up to 1150–1250 °C. Temperature was measured by chromel-alumel thermocouples of 0.5 mm diameter, the data being recorded in H 117 / 1 oscillograph.

Cracks in welded joints were detected by two methods ---- recording acoustic emission signals [3] after sample cooling to a temperature below 100 °C

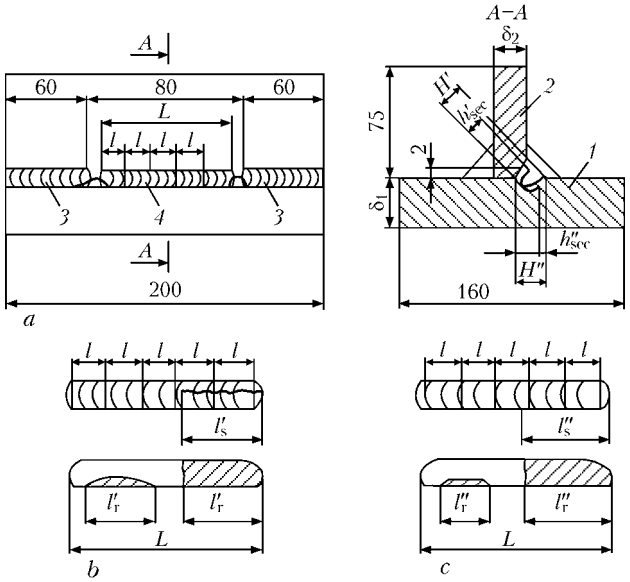

Figure 2. Schematic of a tee sample for evaluation of cold cracking resistance of fillet welds (*a*), and schematic for determination of the extent of cracks in a tee sample on the surface (WM_s), in the section (WM_{sec}) and root (WM_r) of the weld, as well as on the surface (HAZ_s), section (HAZ_{sec}) and root (HAZ_r) of the flange HAZ (*c*) (for other designations see the text)

and investigation of the surface of macro- and microsections cut out of the control section of welded joints in the direction transverse relative to weld axis 10 days after completion of welding.

As shown by investigations, cracks most often developed in tee welded joints from the flange side and propagated either along the weld, or along the HAZ. Therefore, at their analysis presence of cracks in WM and HAZ was recorded separately. Their extent was recorded in percent to the total length of the reference weld in its root part (WM_r, HAZ_r), mid-section (WM_{sec}, HAZ_{sec}) and on the surface (WM_s, HAZ_s) (Figure 2, *b*, *c*):

$$WM_r = \frac{\sum l_r}{L} \cdot 100\ \%; \quad WM_{sec} = \frac{\sum h'_{sec}}{H'} \cdot 100\ \%;$$

$$WM_s = \frac{\sum l_s'}{L} \cdot 100\ \%,$$

$$HAZ_r = \frac{\sum l_r''}{L} \cdot 100\ \%; \quad HAZ_{sec} = \frac{\sum h''_{sec}}{H''} \cdot 100\ \%;$$

$$HAZ_s = \frac{\sum l_s''}{L} \cdot 100\ \%,$$

where L is the length of the tested weld, mm; $\sum l'_s$, $\sum l'_r$ is the sum of crack length on WM surface and in the weld root, respectively, mm; $\sum h'_{sec}$ is the sum

Table 2. Composition (wt.%) of WM in welded joints on 13KhGMRB steel

Wire grade	C	Si	Mn	Cr	Ni	Mo	Al	S	P
Sv-08G2S	0.092	0.42	1.30	0.58	–	0.18	–	0.023	0.022
Sv-10KhG2SMA	0.090	0.57	1.25	0.84	–	0.34	–	0.021	0.023
Sv-08KhN2G2SMYu	0.094	0.38	1.49	1.13	1.97	0.41	0.018	0.023	0.024

Table 3. Modes of welding fillet joints with k = 8 mm

Shielding gas	Wire diameter, mm	I_w, À	U_a, V	v_w, m / h	Q_w, kJ / cm
CO_2	1.2	180–190	26–28	9.0	15.2
	1.6	280–300	30–32	14.6	17.7
	2.0	330–350	32–34	16.0	18.3
Ar + 22 % CO_2	1.6	280–300	28–30	14.6	17.5

of crack length in the weld section, mm; $\sum l''_s$, $\sum l''_r$ is the sum of crack length on the surface and in HAZ root, mm; $\sum h''_{sec}$ is the sum of crack length in the section of flange HAZ, mm; H' is the weld height, mm; H'' is the weld leg on the flange, mm; h'_{sec}, h''_{sec} is the crack length along the height of the weld and HAZ, respectively, mm.

The publications contain quite a lot of data on the adverse influence of hydrogen on cold cracking resistance of welded joints from high-strength steels [4–10]. However, the authors of this work [11] obtained data, which indicate that diffusible hydrogen has a secondary influence on the intensity of cracking of fillet joints of higher strength low-alloyed steels. In this connection, it appeared to be rational to study to what extent the hydrogen factor influences the process of cracking of tee joints on the studied high-strength steel.

Change of hydrogen concentration in the deposited metal was controlled by special preparation of carbon dioxide gas. Minimum concentration of diffusible hydrogen in the metal of the studied welds was equal to 3.1 ml / 100 g (analysis of its content was conducted by the chromatographic method [12]) and it was achieved after soaking the cylinders with carbon dioxide gas for 48 h in the position with the valve facing downwards with subsequent bleeding of moisturized gas. A stable higher concentration of hydrogen in WM ($[H]_{dif}$ = 18 ml / 100 g) was ensured by passing carbon dioxide gas through a tank with water.

Welding wires Sv-08G2S, Sv-10KhG2SMA and Sv-08KhN2G2SMYu of 1.6 mm diameter were used for evaluation of the influence of the composition of hydrogen-saturated WM on cold cracking resistance of tee joints of 13KhGMRB steel. Sample welding was performed in CO_2 in the modes given in Table 3.

As shown by investigations, cold cracks were observed in all the samples welded without preheating (Figure 3). In technological samples welded without preheating by Sv-08KhN2G2SMYu and Sv-10KhG2SMA wires at $[H]_{dif}$ = 18 ml / 100 g, the acoustic emission signals, indicating crack initiation, were recorded at the welded joint temperature of about 100 °C, i.e. directly after mounting the sensors on samples. 25–30 min after the end of welding cracks appeared on the weld surface. In samples which were welded under similar conditions, but using Sv-08G2S wire, the first acoustic emission signals were recorded somewhat later ---- 20–22 min after the end of welding. Development of the formed crack was less intensive. For a long time it propagated in the welded joint and only after 20 h it was found on the sample surface. In order to eliminate cracking in the samples with such a concentration of diffusible hydrogen, it was necessary to preheat them up to the temperature of 120 °C in case of application of Sv-08G2S and Sv-10KhG2SMA wires and up to 180 °C in welding with Sv-08KhN2G2SMYu wire.

Lowering of diffusible hydrogen content in the metal of fillet welds to 3.1 ml / 100 g would allow an essential increase of cold cracking resistance of tee joints on 13KhGMRB steel. Here the first acoustic emission signals in all the cases were recorded only after complete cooling of the samples. Cracks in the samples, as a rule, propagated for several days and came to the weld surface only in welding by Sv-08KhN2G2SMYu wire. Their formation can be completely eliminated only at sample preheating up to 60 °C.

Analysis of the obtained results showed that at increase of hydrogen concentration from 3.1 up to 18 ml / 100 g in WM produced in CO_2 with Sv-08G2S and Sv-10KhG2SMA wires the critical preheating temperature, at which no cracks are present in the weld root, increases by 60 °C by average, whereas when Sv-08KhN2G2SMYu wire is used under the same conditions it rises by 120 °C. Therefore, with increase of the degree of fillet weld metal alloying and cooling rate of tee joints on high-strength steel, the adverse influence of hydrogen is enhanced. Note the fact that when alloyed wires of grades Sv-08KhN2G2SMYu and Sv-10KhG2SMA are used, i.e. in those cases when WM strength is essentially higher than that of the base metal, cracks initiated and propagated only along the weld. In the case, if in welding with Sv-08G2S wire these values in WM and base metal are comparable, cracks formed in the HAZ. It is obvious that this is associated with the features of formation of the stress-strain state in such joints and different diffusion mobility of hydrogen in WM [13].

Considering the established dependence of hydrogen influence on cold cracking resistance of tee joints of 13KhGMRB steel in further studies aimed at evaluation of the influence of welding heat input Q_w and shielding medium on this process, the level of $[H]_{dif}$ concentration in the deposited metal was limited to 3.0–3.5 ml / 100 g. Wire of Sv-08G2S grade was accepted as the basic welding consumable during performance of such work, as it, in our opinion, is the most acceptable for welding single-pass fillet welds with up to 8 mm leg.

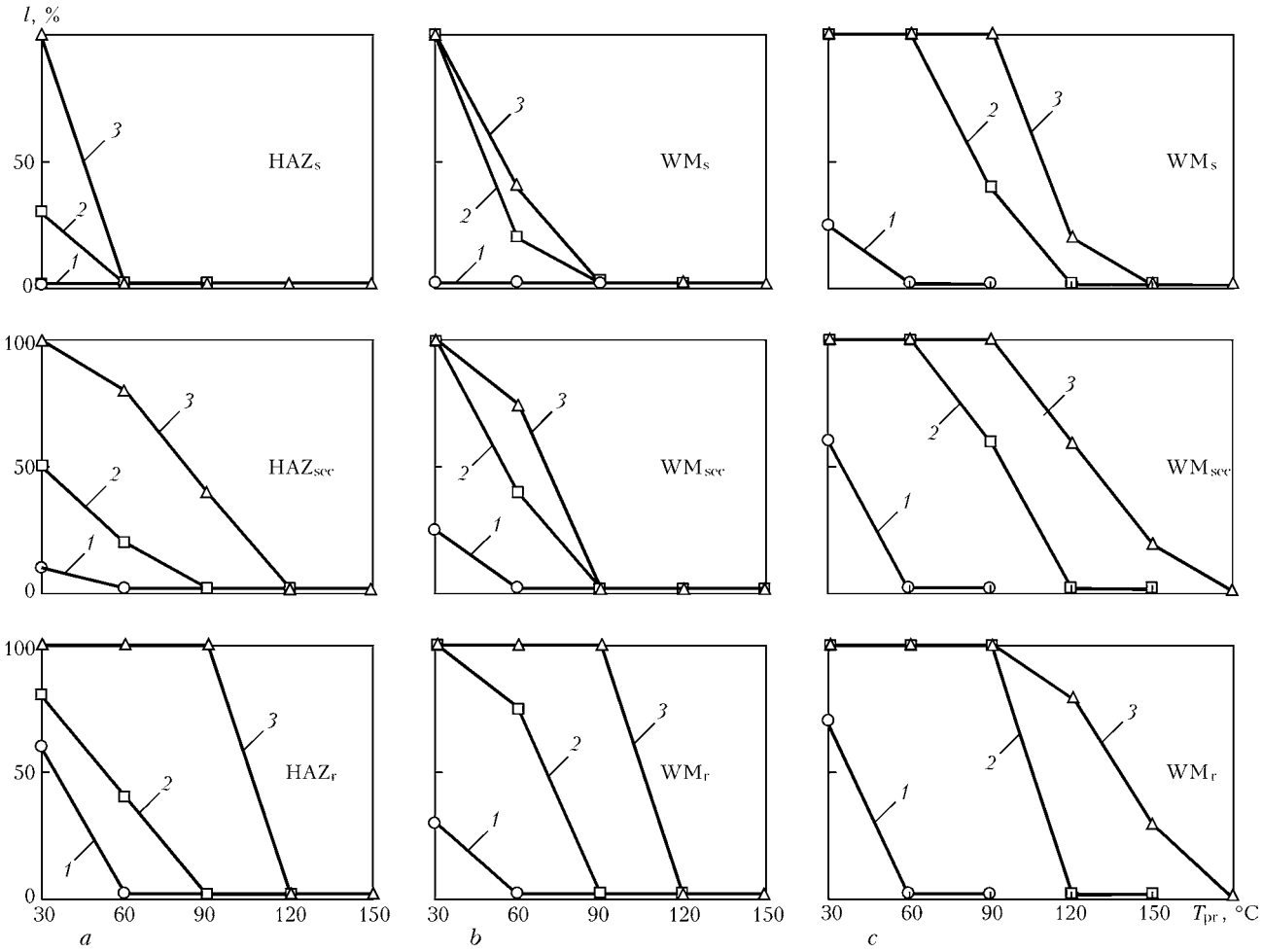

Figure 3. Dependence of the extent of crack l on preheating temperature T_{pr} of tee samples welded in CO_2 with wires Sv-08G2S (*a*), Sv-10KhG2SMA (*b*) and Sv-08KhN2G2SMYu (*c*) at different concentrations of diffusible hydrogen in the deposited metal: *1* — $[H]_{dif}$ = = 3; *2* — 10; *3* — 18 ml / 100 g

Wires of 1.2, 1.6 and 2.0 mm diameter are used in welding the joints with fillet welds. Depending on that Q_w can change from 15.2 up to 18.3 kJ / cm. Wire diameter is usually selected depending on gas shielding, thickness of metal being welded, and other conditions. In this case, welding wire diameter was selected, allowing for the need to change the welding heat input, which affects the cold cracking resistance of tee joints. Weld leg was practically unchanged during such studies. However, with increase of Q_w base metal penetration depth increased and cooling conditions of welded joint HAZ changed.

In CO_2 welding of tee joints with welding wire of 1.2 mm diameter (Q_w = 15.2 kJ / cm) the joint HAZ in the samples is cooled quite intensively. Even at preheating up to 100 °C the cooling time of the metal heated above point A_{c3}, increases only slightly (from 7 up to 9 s) in the temperature range from 800 to 500 °C ($\tau_{8/5}$), while the cooling rate in the temperature range from 600 to 500 °C ($w_{6/5}$) decreases from 28 to 20 °C / s (Figure 4, *a*, *b*). It would seem that a slight increase of the heat input in welding, when wire of 2.0 mm diameter is used, allows an essential slowing down of the process of welded joint cooling. Even in welding without preheating, $\tau_{8/5}$ values in-

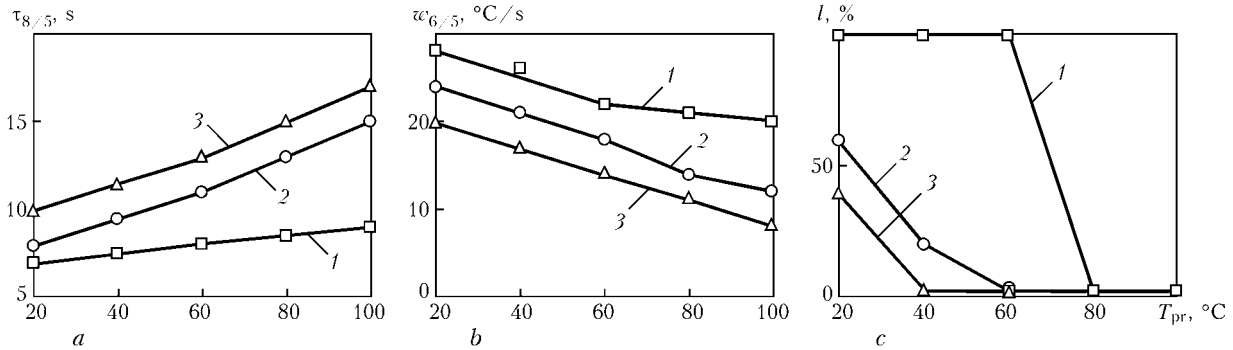

Figure 4. Preheating influence on time of cooling from 800 to 500 °C (*a*), rate of cooling from 600 to 500 °C (*b*) and crack length in the weld root (*c*) of technological samples welded using Sv-08G2S wire of 1.2 (*1*), 1.6 (*2*) and 2.0 (*3*) mm diameter in CO_2

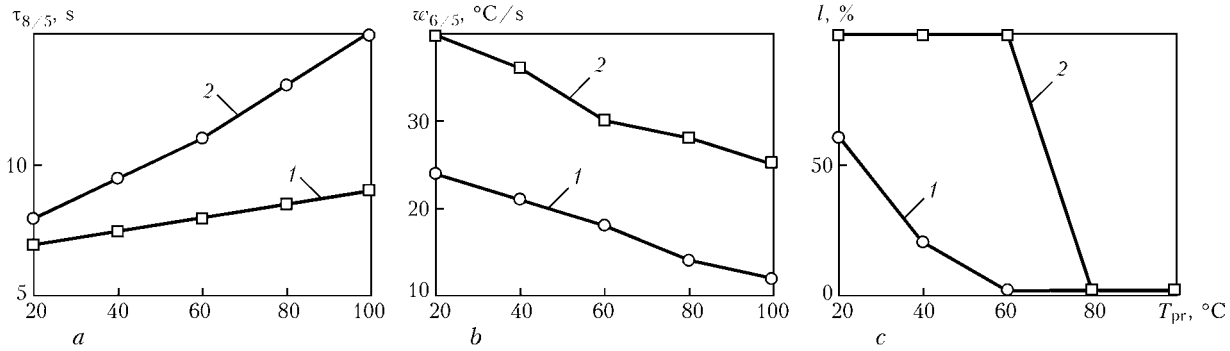

Figure 5. Preheating influence on time of cooling from 800 to 500 °C (*a*), rate of cooling from 600 to 500 °C (*b*) and crack length in the weld root (*c*) of technological samples welded using Sv-08G2S wire in CO_2 (*1*) and argon-based mixtures (*2*)

crease up to 10 s, and at sample heating up to the temperature of 100 °C ---- by another 7 s. Apparently, the noted regularities in the change of the cooling conditions of welded joints made by wires of different diameters, are related not only to increase of heat input in welding with 2.0 mm diameter wire, but also to increase of current density. From Figure 4, *c* it is seen that slowing down of the cooling rate, observed in welding with greater diameter wires, promotes an essential increase of cold cracking resistance of welded joints. Even a slight preheating up to 40 and 60 °C allows completely eliminating cracking in the samples. When 1.2 mm wires are used, the same result can be achieved only at their preheating up to 100 °C. Therefore, it is rational to perform fillet welds with k = = 6–8 mm, using wires of 1.6–2.0 mm diamter. Welding heat input rises to 17.7–18.3 kJ / cm, HAZ cooling is delayed, and, as a result, its cold cracking resistance increases.

At evaluation of the influence of shielding gas on the cracking process in tee joints of high-strength steel, welding was performed with Sv-08G2S wire of 1.6 mm diameter in CO_2 and argon-based gas mixtures (Ar + 22 % CO_2). Investigation results are indicative of the fact that under the selected welding conditions prevention of cold cracking in the joints made in a gas mixture would require increasing the sample preheating temperature by 30–40 °C, compared to CO_2 welding (Figure 5, *a*). This is related to differences in the cooling rates of the HAZ metal of tee joints made in CO_2 and mixture (Figure 5, *b*, *c*). Despite the fact that during performance of these investigations, quite close welding modes were used (heat input Q_w = 17.5–17.7 kJ / cm), the intensity of cooling of the samples welded in a gas mixture, was higher. It is known that CO_2 welding is characterized by more intensive heating and cooling of the metal than in an argon-based gas mixture [14]. This circumstance, probably, was what determined the differences in the cooling rate and cold cracking resistance of tee joints made in CO_2 and Ar + 22 % CO_2 mixture. Therefore, at the change of the shielding medium composition the preheating temperature of the joints should be selected by the results of testing special technological samples.

On the whole, the results of the performed research are indicative of the fact that in welding of single-pass fillet welds with up to 8 mm leg, a minimum concentration of hydrogen ($[H]_{dif} \le 3.5$ ml / 100 g) in WM should be ensured, and such conditions of joint cooling should be selected under which the maximum cooling rate in the HAZ does not exceed the admissible value for specific grades of high-strength steels.

Thus, it becomes obvious that the resistance of tee joints on high-strength 13KhGMRB steel is influenced by the composition of the deposited metal, its concentration of diffusible hydrogen and preheating temperature.

1. Denis, A.E., Ivashchenko, G.A. (1985) *Increase of strength of welded structures*. Kiev: Naukova Dumka.
2. Mikhoduj, L.I., Poznyakov, V.D., Yushchenko, K.A. (2000) Resistance of 12KhN2MFDRA steel welded joints to a delayed fracture. *The Paton Welding J.*, **11**, 4–10.
3. Musiyachenko, V.F., Zhdanov, S.L. (1987) Application of acoustic emission method during investigation of cold crack formation process in high-strength steel welded joint. In: *Diagnostics and prediction of fracture in welded structures*, Issue 5, 73–77.
4. Kasatkin, O.G. (1994) Specifics of hydrogen embrittlement of high-strength steels during welding (Review). *Avtomatich. Svarka*, **1**, 3–7.
5. Musiyachenko, V.F. (1983) *Weldability and technology of welding high-strength steels*. Kiev: Naukova Dumka.
6. Makarov, E.L. (1981) *Cold cracks in welding of alloy steels*. Moscow: Mashinostroenie.
7. Hrivnyak, I. (1984) *Weldability of steels*. Moscow: Mashinostroenie.
8. Pokhodnya, I.K., Shvachko, V.I. (1997) Physical nature of hydrogen induced cold cracks in welded joints of structural steels. *Avtomatich. Svarka*, **5**, 3–10.
9. Hart, P.H.M. (1986) Resistance to hydrogen cracking in steel weld metals. *Welding J.*, **1**, 14–22.
10. Alexandrov, B., Theis, K., Streitenberger, M. et al. (2004) Cold cracking in weldments of steel S 690 QT. *IIW Doc. IX-2115–04*.
11. Nishimura, I., Chiba, N. (1984) Cracking in welded corner joints. *Metal Construction*, **1**, 30–34.
12. Pokhodnya, I.K., Paltsevich, A.P. (1980) Chromatographic method for determination of diffusion hydrogen content in welds. *Avtomatich. Svarka*, **1**, 37–39.
13. Mikhoduj, L.I., Poznyakov, V.D., Zhdanov, S.L. (1998) Delayed fracture of T-joints of high-strength steels. *Ibid.*, **10**, 14–19.
14. Potapievsky, A.G. (1974) *Consumable electrode shielded-gas welding*. Moscow: Mashinostroenie.

REVERSIBLE TEMPER BRITTLENESS OF WELDED JOINTS OF WWER REACTOR BODIES

O.G. KASATKIN
E.O. Paton Electric Welding Institute, NASU, Kiev, Ukraine

Reversible temper brittleness caused by an increased concentration of diffusible impurities, and phoshporus in particular, is the main reason of accelerated embrittlement of welded joints of a nuclear reactor body in the initial period of operation. Radiation defects of crystalline lattice caused by the neutron flux act as high-energy traps and decrease the concentration of the diffusible impurities. Increase in the fluence of fast neutrons leads to growth of the density of the crystalline lattice defects, which promote decrease in the concentration of impurities at grain boundaries, as well as decrease in temper brittleness.

Keywords: reactor body, welded joints, diffusion displacement of phosphorus, reversible temper brittleness, radiation defects, critical brittleness temperature

At present water-water power reactors of WWER-440 and WWER-1000 type of 440 and 1000 MW power make up the basis of nuclear power generation of Russia and Ukraine. One of the most critical parts of NPP equipment is the nuclear reactor body (RB) made of forged cylindrical shells and bottom which are welded by submerged-arc circumferential welding. Steel 15Kh3MFA is used for manufacturing WWER-440 RB, and steel 15Kh2NMFA ---- for WWER-1000 RB. WWER-1000 body has an inner austenitic coating.

In case of emergency stoppage of the reactor and its filling with cold water (at thermal shock) RB is exposed to considerable loads. Therefore, its metal should ensure a sufficiently high resistance to development of the possible (usually postulated) crack at thermal shock. RB metal state is evaluated chiefly by the critical brittleness temperature T_{cr}, at which the specified level of crack resistance is ensured.

As shown by investigations, RB service life is limited by the properties of welded joints, which are usually more prone to embrittlement than the base metal, in particular, due to an increased concentration of phosphorus (WWER-440) or nickel (WWER-1000) in the weld metal.

Characteristic features of RB core operation are presence of neutron irradiation and long-term heating (hundred thousand hours) up to 300 °C. The main embrittlement mechanism of RB and weld metal is determined by accumulation of radiation damage of the crystalline lattice under the impact of the neutron flow. Another serious factor promoting embrittlement is increase of the concentration of impurities, particularly phosphorus. The adverse influence of the impurities was found when studying the reference samples. Investigations showed that RB and, particularly, their welded joints, become embrittled much faster in the first years of operation than might have been anticipated, because of neutron irradiation.

The purpose of this study is evaluation of the influence of radiation effects forming in the metal of the body wall during reactor operation, on the nature of diffusion distribution of phospohorus.

RB working temperature, as well as additional energy evolved due to gamma-radiation, turn out to be sufficient for development of diffusion mobility of phosphorus, which is an interstitial element. Overall energy of Fe–P system decreases, when phosphorus atoms are in the crystalline lattice defects and on grain boundaries, which act as traps for these elements. Grain boundaries differ by a higher free energy than individual defects of the type of vacancies. The process of grain boundary enrichment in phosphorus under the isothermal conditions goes on until dynamic equilibrium sets in. Phosphorus concentration in a very thin zone (5–10 atomic layers) can be tens of times higher that the average value. Embrittling tempering does not cause any structural changes in the weld metal. The thickness of the adsorption layer is so small, that the change of plastic deformation resistance in it may not have any essential importance. More important, probably, is the lowering of surface energy at cracking along the grain boundaries. The fracture usually takes an intergranular nature, i.e. it occurs chiefly along the boundaries of the initial austenite grains. This results not only in T_{cr} increase, but also in lowering of fatigue fracture resistance, intercrystalline corrosion and cracking. Degree of embrittlement characterized by value ΔT_{cr} turns out to be proportional to impurity concentration on the boundaries.

At increase of metal temperature the energy of the bond of phosphorus atoms with the traps becomes smaller, and the equilibrium is established at lower levels of phosphorus segregation on the grain boundaries. At heating up to the temperature of high tempering, almost all the phosphorus goes into the crystalline lattice. At fast cooling this state is fixed and temper brittleness disappears, and at slow cooling it reappears. In metal science this phenomenon is called reversible temper brittleness [1]. Alloyed steels of conventional purity are the most prone to this type of brittleness.

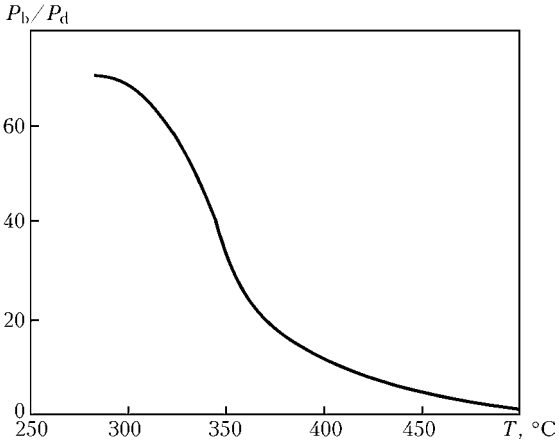

Figure 1. Dependence of the equilibrium phosphorus concentration on grain boundaries in the weld metal on temperature

Dependence of relative equilibrium concentration of phosphorus on grain boundaries P_b on temperature is given in Figure 1. Here P_d is the concentration of diffusion-mobile phosphorus in the crystalline lattice (part of it can be contained, for instance, in non-metallic inclusions, pores and other high-energy traps and not participate in the diffusion process). Ratio P_b / P_d increases with temperature lowering. At lower temperatures phosphorus mobility decreases and the segregation process stops.

Diffusion mobility of phosphorus atoms in the crystalline lattice at T ~ 300 °C is low. By the data of National Science Center «Kharkov Institute of Physics and Technology» and Russian Science Center «Kurchatovsky Institute» the process of «thermal ageing» of casing steels goes on for about 20,000 h [2]. Considering that the duration of RB operation is equal to hundred thousand hours, the process of phosphorus segregation along the grain boundaries can develop up to a practically equilibrium state.

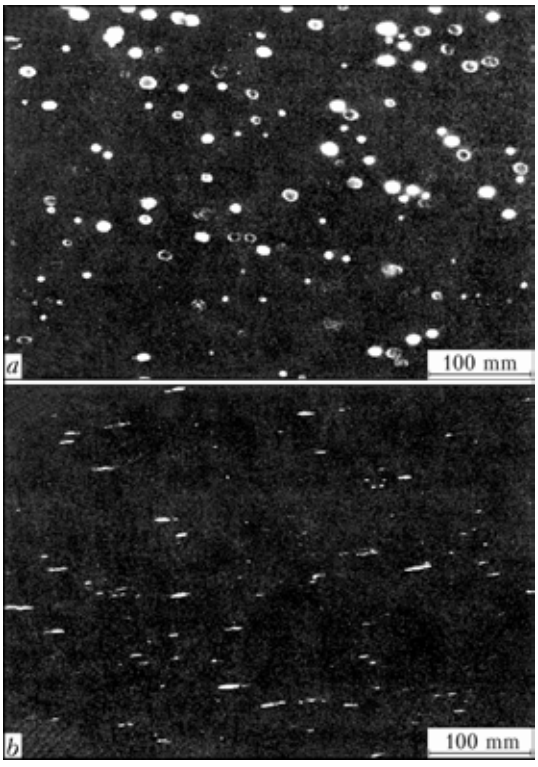

Figure 2. Front (*a*) and side (*b*) view of disc-shaped inclusions in the sample of irradiated casing steel [4]

Nickel is added to the weld to lower the critical brittleness temperature of the metal in the initial condition. However, nickel alloying increases the diffusion mobility of phosphorus in the crystalline lattice and to some extent increases P_d values. This is, possibly, related to a change of density of vacancy-type defects. As a result, at the specified temperature phosphorus concentration on grain boundaries increases.

At a low (up to 0.003 wt.%) phosphorus content, increase of nickel content from 1 up to 3 wt.% practically does not enhance the steel susceptibility to temper brittleness, whereas at 0.01 wt.% P the same change in nickel content ensures a quite intensive diffusion of phosphorus for running of the segregation process with an increase of the degree of embrittlement [1]. The equilibrium concentration of phosphorus on grain boundaries increases with the increase of phosphorus and nickel content. RB working temperature T = 300 °C promotes the maximum segregation of phosphorus (Figure 1).

Submerged-arc welding is used in RB manufacturing. The process of phosphorus segregation on grain boundaries in the weld metal develops more intensively than in the base metal. This is related, as a rule, to coarsening of austenite grains in the weld metal and use of insufficiently pure welding consumables. Phenomena of reversible temper brittleness were not taken into account to a sufficient degree when developing the technology of RB welding, particularly, of WWER-440 / 230 type. The weld metal of these RB contains 0.03–0.05 wt.% P, this leading to a fast growth of T_{cr}. It should be noted that in addition to phosphorus, other impurities are antimony, arsenic and tin.

In reactor operation the body core is irradiated by a strong neutron flux. Radiation defects developing in the crystalline lattice under the action of fast neutrons, can essentially change the kinetics of phosphorus segregation. The above defects are traps with a sufficiently high energy (for coarse defects the energy level can be close to free surface energy). Entrapping individual atoms, the traps lower the weight fraction of diffusible phosphorus [3].

Defect dimensions depend on energy spectrum of the neutron flux: the higher the neutron energy, the greater the size of the defect forming in the crystalline lattice. Investigations of weld metal of a trepan cut out of a body of WWER-440 reactor taken out of service in block #2 of Novo-Voronezhsky NPP showed that the defects have the form of discs about 1 nm thick and about 10 nm in diameter (Figure 2), their density being $\lambda \sim 7 \cdot 10^{16}$ cm^{-3} [4]. Composition of these inclusions was not determined unambiguously.

Based on the above dimensions of disc-shaped inclusions, it is possible to tentatively evaluate the relative value of defect volume to be about 0.0055, i.e. total volume of radiation defects is equal to approxi-

mately 0.5 % of that of the crystal. Proceeding from the same dimensions, it is possible to conditionally evaluate the total surface area of the inclusions per a unit of crystal volume:

$$S_{\text{incl}} \approx 11 \cdot 10^4 \text{ cm}^2 / \text{cm}^3,$$

which is much higher than the total area of grain boundaries.

On the whole, the kinetics of the diffusion process of phosphorus distribution at steel irradiation by the neutron flux looks as follows. Weight fraction of diffusible phosphorus and rate of steel embrittlement because of phosphorus segregation on grain boundaries are maximal at the initial stages of reactor operation and decrease with increase of the density of radiation defects in the crystalline lattice, which act as traps for phosphorus atoms. As the fluence of the neutron flux increases, the weight fraction of diffusion-mobile phosphorus decreases so much that by the conditions of dynamic equilibrium a reverse process can start, namely withdrawal of phosphorous from grain boundaries into the crystalline lattice. Metal sensitivity to temper brittleness decreases.

Analysis of samples of weld metal of Kozloduj NPP block #1 RB showed that phosphorus is non-uniformly distributed in the core metal across RB wall thickness [5]. The maximum phosphorus concentration was found in the metal of the wall inner surface, and the minimum one ---- near the outer wall. Similar phenomena were found near the above-mentioned trepan, cut out from Novo-Voronezhsky NPP RB. In addition, the impact toughness of weld metal on RB inner wall turned out to be higher than that of the outer one. This is in good agreement with the above phenomena of reversible temper brittleness. RB wall metal near its inner surface is exposed to the most intensive action of the neutron flux, phosphorus weight fraction in radiation defects of the crystalline lattice is maximum, and that of diffusible phosphorus is minimum. In this connection the phenomena of reversible temper brittleness near the RB inner wall are manifested to a lower degree.

Thus, the optimum reversible temper brittleness (particularly, the stage of fast growth of the critical brittleness temperature) develops at the initial stage of reactor operation and further on decreases in the core metal. Allowing for the processes of reversible temper brittleness, enables the most valid assessment of the current condition of RB metal and dynamics of its property degradation in the core.

1. Kurdyumov, G.V., Utevsky, L.M., Entin, R.I. (1983) Transformation of austenite during cooling and tempering of hardened steel. In: *Metals science and heat treatment of steel*. Moscow: Metallurgiya.
2. Zelensky, V.F., Neklyudov, I.M., Ozhigov, L.S. et al. (1997) Problem of radiation embrittlement of bodies of reactors WWER-440 and WWER-1000 and means of its solution. In: *Problems of nuclear science and engineering*. Series Physics of radiation damages and radiation materials science, Issue **1**(65) / **2**(66), 119–122.
3. Kasatkin, O.G. (1998) Mechanisms of embrittlement of welded joints in bodies of reactors of WWER type under the action of impurities. In: *Proc. of 5th Int. Conf. on Materials Science Problems in Design, Manufacturing and Service of NPP Equipment*. Vol. 2. St.-Petersburg: Prometej, 168–176.
4. Gurovich, B.A., Kuleshova, E.A., Nikolaev, Zu.A. et al. (1997) Assessment of relative contributions from different mechanisms to radiation embrittlement of reactor pressure vessel steels. *J. Nucl. Mater.*, **246**, 91–120.
5. Kamenova, T., Vodenicharov, S., Momchilova, E. et al. (1997) Phorphorous content and distribution in the metal of RPV weld 4. In: *Rep. of a Workshop on Kozloduy Unit 1 Reactor Pressure Vessel Integrity* (Sofia, Bulgaria, May 21–23, 1997). Sofia: Int. Atomic Energy Agency, 1–13.

TECHNOLOGY PECULIARITIES OF HIGH-FREQUENCY SEAM BRAZE-WELDING OF PIPES

A.S. PISMENNY, D.P. NOVIKOVA, R.V. YUKHIMENKO, A.S. PROKOFIEV, A.A. PISMENNY, V.V. POLUKHIN and **Vl.V. POLUKHIN**
E.O. Paton Electric Welding Institute, NASU, Kiev, Ukraine

Methodologies for investigating braze-welding processes of longitudinal pipe seams by the method of resistance heating and heating of the edges being connected by flowing along them electric current are presented. Results of metallographic investigations of pipe welds produced by mentioned methods are presented.

Keywords: high-frequency welding, induction heating, technology of braze-welding, activating substance, mechanical tests, pipes

In mass production of pipes high-frequency welding (HFW) is widely used, which is peculiar for high productivity and low production costs. However, this method ensures, as a rule, good quality of the weld formation only in welding of certain brands of structural and low-alloy steels, brass, copper and aluminium.

For using advantages of HFW and expanding assortment of materials welded a new method of welding is necessary, which would be characterized by reduction of welding temperature and gradient of temperatures in the edges being welded, and improvement of conditions of preparation of the edges to be welded. To achieve this it is necessary to change method of energy supply to the welding zone and the billet being formed in the said zone, and use substances that activate surfaces being welded.

The investigations were based on results of previous works, connected with development of the processes for forming strips into a tubular billet and development of the main equipment units for forming and welding of tubular items. Results of investigations of electro-thermal and thermo-mechanical welding processes, development of induction welding devices, solution of the issues, connected with stabilization of the processes of energy transfer into the welding zone in case of change of an item movement speed, and determination of technological parameters of welding conditions depending upon geometrical dimensions of the materials being welded were also used [1–4].

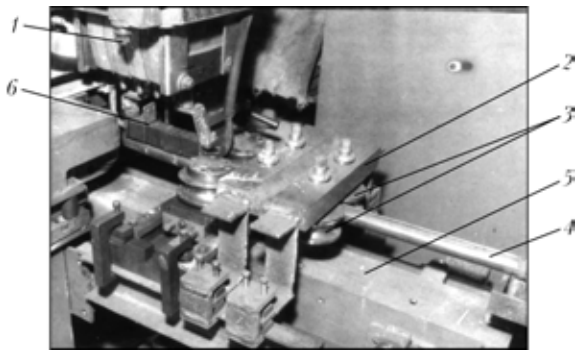

Figure 1. Laboratory equipment for carrying out experiments: *1* — high-frequency transformer; *2* — roll stand; *3* — two pairs of rolls; *4* — pipe being welded; *5* — bed; *6* — inductor

On basis of carried out investigations a new technology of the braze-welding process (DSTU 3761.2–98, i. 3.92) as well as elements of equipment for production of steel pipes by the induction heating method with introduction of activating substances into the zone, in which edges are connected, were developed. This method combined positive features of pressure welding and brazing, whereby it was taken into account that electrophysical properties of practically all structural and pipe steels in induction heating are similar, and heating conditions may apply both to one material and plurality of others.

Methodology for investigation of the process of braze-welding of pipe edges using method of their heating by flowing along them electric current (FCH). For carrying out the experiments, connected with braze-welding of straight seam pipes with induction supply of energy to the billet, a laboratory equipment was used (Figure 1), which consisted of the load-carrying metal structure, i.e. a bed with the guides, a mobile carriage with a rack, which is brought into motion by an electric drive and has a bracket for fixing front end of the pipes, a stationary roll stand for upset of edges, a drive for the carriage movement and for induction heating of edges being welded, a liquid cooling system, start-regulation and control equipment, power cables, and communications.

Movement of the pipes relative the inductor, roller guides and welding device (welding stand) in braze-welding is ensured by means of the drive with smooth adjustment of rotation speed of the drive electric motor, which has five-stage range of the speed adjustment of linear pipe movement ---- from 1.2 to 6.4 m / min.

Measurement and registration of the induction heating electric parameters of the edges being welded, heat parameters (temperature fields in cross section of the pipes) and deformations in the joint formation zone, were carried out. Voltage was measured using tube voltmeter of the VK7-9 type, and alternating current of 2.5 and 8.0 kHz frequency ---- using elec-

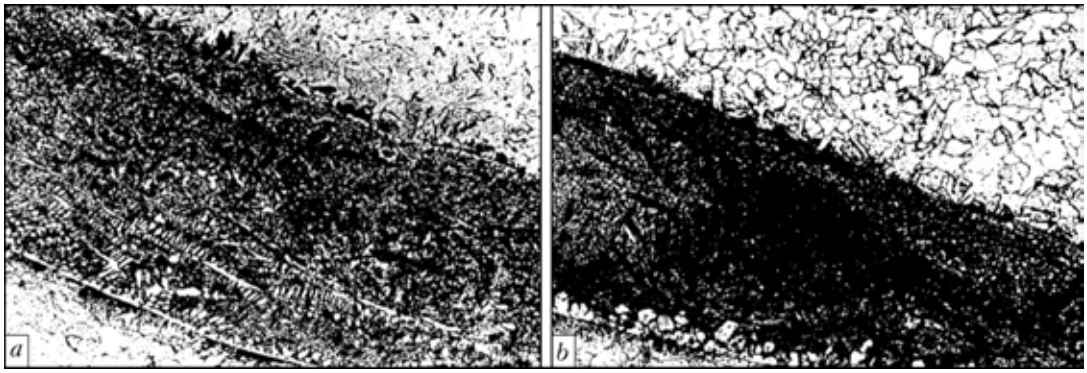

Figure 2. Microstructure of weld (*a* — ×400) and HAZ (*b* — ×800) metal

tromotive force of Rogowski loop by tube voltmeter of the VU-15 type with sensitivity factor of 834 and 260 A / V. Phase shift angle was determined using the F2-1 type instrument.

Temperature fields were registered by six-channel recorder of the N-3031-6 type. Chrome-nickel thermocouples were used as primary temperature converters. They were caulked into the holes, arranged over perimeter of the pipe being welded, which allowed evaluating temperature field both in walls and weld of the pipe both at the stage of its heating and cooling after welding. Experiments were carried out at different speeds of the pipe movement, power of heating and clearances between the inductor and zone of the pipe straight weld formation. Influence of the inductor location inaccuracy above the pipe was evaluated (general and parallel misalignment of installation of the inducting conductor of the inductor relative axis of the pipe). Measurements in five cross sections of the pipe, located along axis of the inductor, and registration of temperature fields were also made at constant power of heating and static position of the pipe under the inductor. For ensuring high accuracy of measurements readings taken from each thermocouple were calibrated using reference thermocouple with a respective channel of the recorder amplifier.

Results of metallographic investigations of pipe welds produced by FCH method. The experiments were carried using welding of longitudinal welds on steel pipes of 33.5 mm diameter with thickness of the walls 1.0–3.0 mm. Upset of edges of the pipes made of steel 20 (GOST 8737–78) of 33.5 × 3.0 mm size was selected experimentally. Standard brazing alloys of the PAN-3 and P-87 type and flux of the PV201 grade were used in the experiments.

Microstructure of the weld metal and HAZ, characteristic of this technological process, are presented in Figure 2.

It was found that mechanism of weld formation in pressure braze-welding consisted in the following. During heating of pipe edges an activating substance (brazing alloy and flux) melt, after which surface of the steel edge dissolves in molten brazing alloy and then enrichment of molten brazing alloy with iron occurs, whereby the brazing alloy is enriched with iron to such extent that the latter becomes main component of the molten metal pool.

The weld metal has a double-phase structure. It may be identified as a solid solution of copper in iron, formed in the course of dissolution-diffusion processes with addition of alloying elements of the brazing alloy — manganese, nickel and silicon (Figures 2 and 3).

The weld metal has dense fine dispersed dendrite structure (Figure 2). In some areas of the molten zone solidification is of the directed character. So, in Figure 2 aciculae of dendrites, oriented in direction of distribution of heat flow, are well seen [5].

Investigation of a group of the specimens showed that near the weld boundary on the side of the pipe base metal white ferrite strip α-Fe was located, which contained in solid solution alloying elements of the PAN-3 brazing alloy (Figure 3). It occurred due to segregation from the gap of low-melting components of the brazing alloy and acceleration of the diffusion processes under conditions of plastic deformation. Carried out metallographic investigations showed that increase of size of the grains in HAZ did not occur, and due to presence of fine grains in the weld metal high strength and plasticity of the brazed joints was ensured [5, 6].

In Figure 4 microstructure of the weld metal with good formation, produced at the degree of upset not less than 30 %, is shown.

There are specimens among investigated joints (Figure 4, *a*), in which liquid phase is absent and just clear separation line between butted surfaces exists, and specimens (Figure 4, *b*), in which liquid interlayer is not completely removed from the joint zone and the

Figure 3. Microstructure of joint zone with ferrite strip on interface between weld metal and HAZ (×800)

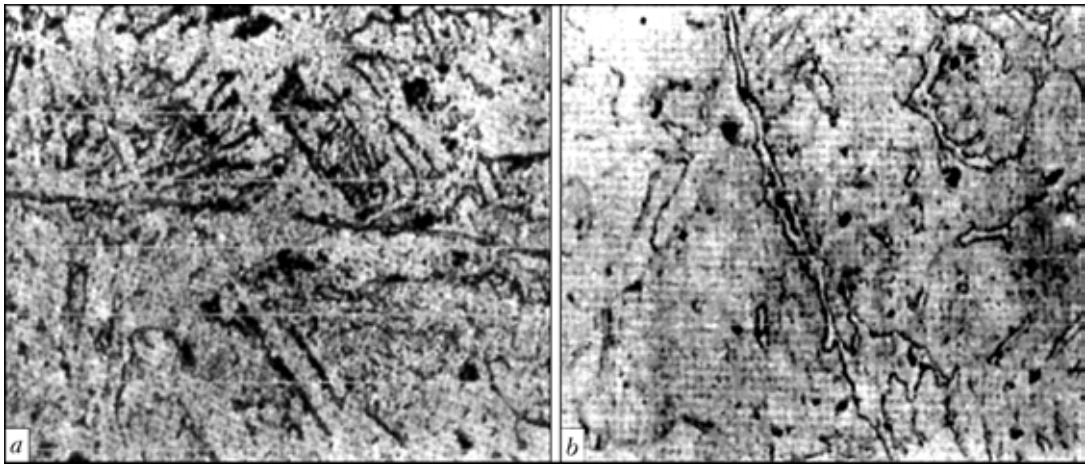

Figure 4. Microstructure of weld metal areas with complete (*a* — ×320) and incomplete (*b* — ×100) squeezing-out of liquid phase from joint zone

weld is produced due to solidification of the molten area.

On basis of investigation of microsections under microscope and obtained pictures one may draw conclusion that the weld has good formation. Not in a single specimen of the experimental lot defects in the form of cracks, pores and cavities were detected.

Results of mechanical tests of the specimens cut out from the pipes showed that their rupture strength is not lower than that of the base metal (BM) — 416 MPa for steel 20, and angle of curvature before fracture constituted 180°.

Results of investigation of the process of braze-welding of longitudinal pipe welds produced by the resistance heating (RH) method. Modeling of this process was performed with application of equipment of the production line for HFW of pipes of 20–76 mm diameter. In order to get initial data for development of a specialized assembly-welding unit experiments were carried out in braze-welding of pipes of 33.5 mm diameter, whereby steel strip (St3) 1.5 mm thick and 100 mm width was used. After the strip was formed into the tubular billet on its edges before the welding stand an activating substance — mixture of the PV201 flux and the PAN-3 brazing alloy, developed in the E.O. Paton EWI, was applied. Rubber dissolved in petrol was used as a binder.

Necessary thermal cycles of braze-welding are ensured by the installation for induction welding of pipes of 20–76 mm diameter.

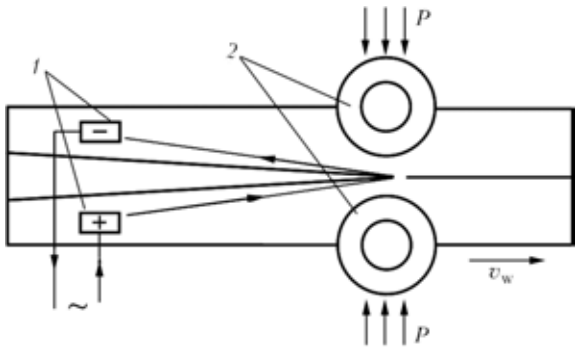

Figure 5. Scheme of HFW with contact supply of current to pipe edges: for designations see the text

In resistance braze-welding (Figure 5) current was fed to the pipe edges through sliding contacts *1* or located in this place inductor, which enveloped the pipe billet (it is not shown in the Figure).

During heating of the pipe billet edges by passing electric current, an activating substance, which was preliminary applied on the edges, is heated, and it interacts in molten state with metal of the edges.

Heating of the edges being welded continues up to the place of convergence of the edges, where process of braze-welding starts. Like in FCH method, a molten activating substance during contact with BM is significantly enriched with iron, whereby BM of the pipe billet is main component of the molten interlayer formed on the edges being welded before the place of their convergence. Here the weld is formed at maximum density of current, whereby under action of welding rolls *2* first contacting of the pipe billet edge surfaces, covered by the molten activating substance, and then upset of the edges, which are washed by the molten activating substance, take place.

Application of upset pressure *P* by the welding rolls causes squeezing-out of molten interlayer from the edges being welded into flash, whereby together with the molten interlayer into flash are also removed oxide films and activation products of the surfaces being welded. Squeezing-out of the molten interlayer occurs in the plane of convergence of the pipe billet edges in three directions — upwards, downwards and backwards.

In formation of the straight weld, which starts in the place of convergence of the edges, interlayers wetted by the melt and surfaces of the pipe billet, preliminarily cleaned from oxides and foreign matter, participate.

For experimental purpose braze-welding of pipes was performed under different conditions, which differed by certain ratios of electric power and rate of the process.

As a result four sections of the pipe were welded using different conditions (Table 1) with gradual reduction of specific input energy. Degree of deforma-

Table 1. Conditions of braze-welding of experimental specimens

Specimen No.	Speed of braze-welding, m / min	Degree of deformation, %
1	20	43
2	15	40
3	25	45
4	15	50

Table 2. Microhardness of joints produced using different conditions of braze-welding

Specimen No.	*HV* 005			
	BM	Weld	HAZ	Flash
1	169	205	192	184
2	169	194	186	206
3	177	181	169	227
4	172	199	176	182

tion of the connected edges within weld thickness constituted from 40 to 55 %.

Metallographic investigations of pipe welds produced by RH method. Four specimens of pipes were prepared for carrying out metallographic analysis. Metallographic investigations of sections of welded joints with polished surface showed that cracks in the weld metal were absent. After etching cracks in the weld metal were not detected either (Figure 6).

Measurements of microhardness were made on the LECO instrument M-400. Step between measurement points was 10 μm.

In Table 2 results of microhardness distribution over all zones of the joint are presented.

Degree of the joint deformation in the weld plane constituted 40–50 % (see Table 1). It is of the same value as in butt joints of pipes, produced by the braze-welding method [7–10]. Certain increase of hardness in some areas of the weld metal is connected with the fact that because of high (up to 25 m / min) speed of braze-welding intensive water cooling was used, whereby size of the weld metal grains was 1.5–2 times higher than of BM [5].

So, it was found that developed technology of seam induction welding in solid phase of pipes (braze-welding) may be implemented in two ways. The first one is performed by FCH method; second one ---- by combined FCH with RH of the pipe edge ends at final stage of the process before upset of the edges. Both methods of braze-welding ensure good quality of formation of the welds.

Activation substance as a physical-chemical agent, which enables connection of the edges, effects not just progress of long (for the considered technology) dissolution-diffusion processes, characteristic of conventional brazing, but also ensures cleaning of the edge surface. This allows expanding class of brazing alloys, which may be used for implementing technology of the seam braze-welding of items in solid phase.

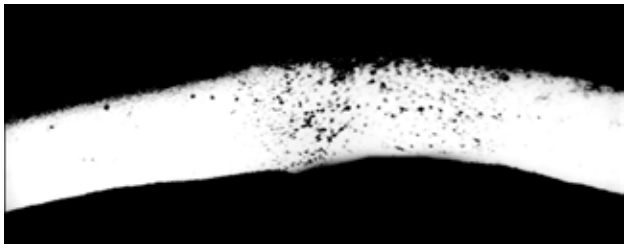

Figure 6. Macrosections of weld metal area and HAZ in specimen No. 1 (×25)

Process of braze-welding proceeds within temperature range, determined by melting point of used activation substances. In braze-welding of longitudinal welds of pipes the best results are achieved at heat input, which ensures temperature of this process that is by 150–200 °C higher than melting point of the brazing alloy and degree of plastic deformation of the edges (40 ± 10) %.

The investigations showed that as a rule in upset not less than 30 % of area of the formed weld metal represent formed common for both edges BM grains. During cooling and formation of a weld fine fragments (less than 10 μm) of non-squeezed out solidified interlayer, which is an alloy of used brazing alloy, enriched with BM of the edges, also occur.

Carried out static tensile strength tests of the specimens showed that it equaled that of BM. Values of angle of curvature of the specimens prove high plasticity of the joints. Using braze-welding method one may produce joints, which have high stable values of impact toughness.

It follows from mentioned above that method of braze-welding may be used as the basis of industrial technology for production of metal items not just from materials, which are usually connected by the HFW method, but also from new materials and grades of steels, especially those, which undergo negative changes in case of excess of certain critical temperatures of heating, and known methods of welding or brazing can not ensure necessary conditions for quality formation of welds.

1. Shamov, A.N., Bodazhkov, V.A. (1974) *Design and service of high-frequency units*. Leningrad: Mashinostroenie.
2. Slukhotsky, A.E., Nemkov, V.S., Pavlov, N.A. et al. (1981) *Induction heating units*. Leningrad: Energoizdat.
3. Shamov, A.N., Lunin, I.V., Ivanov, V.N. (1991) *High-frequency welding of metals*. Leningrad: Politekhnika.
4. Pismenny, A.S. (1997) High-frequency welding of metals. In: *Welding and Surfacing Rev.*, Vol. 7, Part 1. Amsterdam: Harwood AP.
5. Grabin, V.F. (1982) *Metals science of fusion welding*. Kiev: Naukova Dumka.
6. Shmykov, A.A. (1956) *Handbook of heat-treater*. Moscow: Mashgiz.
7. Lebedev, V.K., Tabelev, V.D., Pismenny, A.S. (1983) Pressure butt brazing of steel pipelines. *Avtomatich. Svarka*, **9**, 25–27.
8. Lebedev, V.K., Pismenny, A.S., Kasatkin, O.G. et al. (1993) Physical modeling of upset in butt welding or braze-welding of pipes. *Ibid.*, **8**, 17–20.
9. Lebedev, V.K., Tabelev, V.D., Pismenny, A.S. (1993) Impact toughness of butt joints brazed with plastic deformation of base metal. *Ibid.*, **8**, 29–31.
10. Pismenny, A.S., Shinlov, M.E., Buzhenetsky, A.I. (1995) Application of induction braze-welding for joining of oil assortment pipes. *Ibid.*, **12**, 35–38.

TECHNOLOGY OF SPOT ARC WELDING OF THREE-LAYER STEEL PANEL WITH CELLULAR FILLER

L.M. LOBANOV[1], **A.N. TIMOSHENKO**[1], **P.V. GONCHAROV**[1] and **V.I. ZAJTSEV**[2]
[1]E.O. Paton Electric Welding Institute, NASU, Kiev, Ukraine
[2]OJSC «VPK «NPO Mashinostroeniya», Reutov, RF

Considered are the features of arc spot welding application in manufacture of a three-layer panel with cellular filler of high-alloyed steel. A possibility is demonstrated of process implementation with one-sided access to the item and under constricted conditions without application of considerable forces for compression of the structural elements being joined, as well as at joining thin-walled metal 0.1–1.0 mm thick in the gravity position without a packing.

Keywords: argon-arc welding, arc spot welding, honeycomb structure, pulsed arc welding, three-layer panel, high-alloyed austenitic steel, thin-walled metal structures

Honeycomb structures are extensively applied in different industries, namely aircraft, rocket, mechanical engineering and shipbuilding and construction. Owing to a rational distribution of metal in the individual elements of honeycomb panels, they are an alternative for reducing the structure weight [1–4]. Such structures at their relatively low weight feature a high level of strength and rigidity, as well as good sound- and heat-insulating properties. A three-layer panel with cellular filler (Figure 1) is a variety of honeycomb structures. It is a component of a composite three-layer welded structure from sheet metal, consisting from two load-carrying layers, cellular filler located between them, and frame elements (trimming, end pieces and cover plates, etc). The load-carrying layers take up the loads (tension, compression, shear) and transverse bending moments. The filler monolithically connected to the load-carrying layers (skins) ensures joint work and stability of the entire three-layer structure and at its bending it is exposed to lateral forces [4]. Manufacturing of the honeycomb panel requires making a great number of spot welded joints, which it is more rational to produce by arc spot welding (ASW).

Resistance welding with current supply from one side has limited application because of a low rigidity of the produced joints, as well as impossibility of applying cover plates, counteracting electrode pressure. Another drawback of resistance welding is the fact that this process cannot be performed from the skin side.

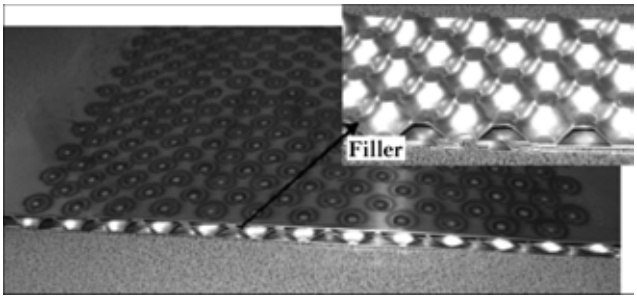

Figure 1. Three-layer panel with cellular filler

The purpose of this work is development and mastering of ASW technology of three-layer steel panel with cellular filler.

ASW technology was mastered on three-layer panel samples of $300 \times 300 \times 7.2$ mm size with cellular filler, the load-carrying layers of which are made of steel of the austenitic-ferritic class 03Kh11N10M2T 0.6 mm thick, and the cellular filler ---- from austenitic steel 12Kh18N10T 0.3 mm thick. ASW was performed from the skin side. ASW of samples and item mock-ups was conducted using tungsten electrode of 1.5–2.0 mm diameter with argon shielding of the welding arc and welding zone.

The laboratory unit for mastering ASW technology for welding a three-layer panel with a cellular filler (Figure 2) includes a welding current source *1*, welding bench *2*, welding cycle control module *4*, a set of connecting cables and hoses *3*. This unit allows an efficient performance of spot welded joints at 5–80 A currents in 0.05–0.50 s with protection of the joint zone by inert gas.

Welding bench *2* is designed for fastening the sample and its displacement to the point of ASW performance on the vertical plane. Control module *4* is used in the laboratory unit to perform coordinated control of all the actuators, providing the required welding cycle, switching the power source on and off, gas shielding and pressing the skin to the filler.

During optimization of the technology of AWS of three-layer panels with cellular filler, the following technological features were revealed.

In the unrestrained condition the three-layer panel blanks are characterized by a comparatively low rigidity and in order to eliminate gaps *B* forming in welding, it is necessary to apply local compressive forces *P* in the welded joint zone. To eliminate gaps between the outer skin and filler, a compressive force was applied, which is transmitted through a support nozzle of the welding torch directly to a circular platform on the filler top (Figure 3). In this case, an essential factor is the value of the applied compressive

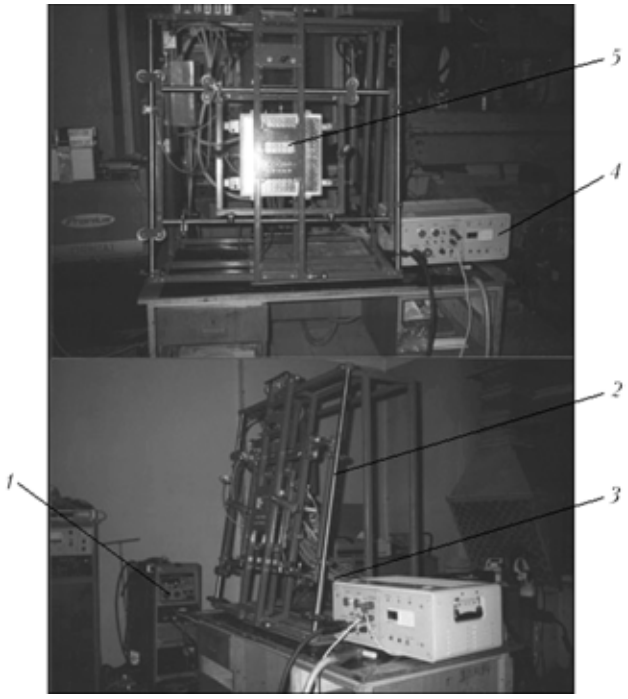

Figure 2. Laboratory unit for optimization of the technology of ASW of a three-layer panel with a cellular filler: *1* — welding current source; *2* — welding bench; *3* — connecting cables; *4* — welding cycle control module; *5* — frame with samples

force. In case of increased compressive forces a concavity develops on the flat platform of the welded top of the filler (Figure 4). The resulting formation of a gap between the filler and skin can lead to burns-through or lacks of fusion of the skin and filler.

In order to determine the admissible compressive force, measurements of the filler platform gap, depending on the applied force, were taken:

P, N	200	250	280	300	400	450
B, mm	–	0.09	0.10	0.12	0.15	0.20

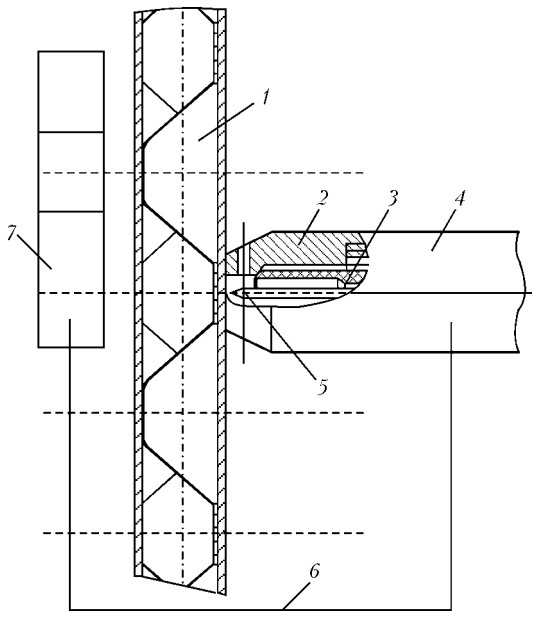

Figure 3. Schematic of ASW of a three-layer panel: *1* — three-layer panel; *2* — support nozzle; *3* — ceramic insert; *4* — welding torch; *5* — nonconsumable electrode; *6* — rigid tie; *7* — tracing system

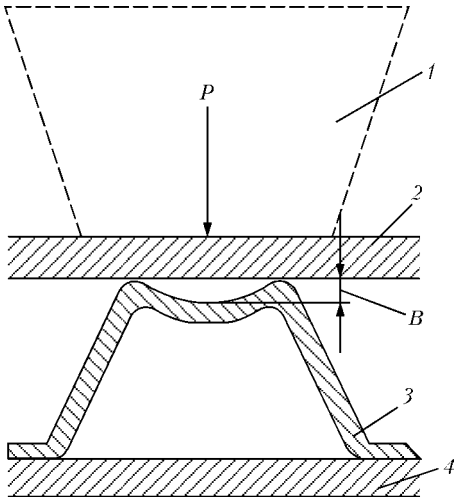

Figure 4. Schematic of formation of gap *B* in the location of ASW of a three-layer panel: *1* — welding torch; *2, 4* — panel skin; *3* — cellular filler

Gap measurement results are indicative of the fact that the compressive force, transferred through the supporting nozzle of the welding torch, should not exceed 200 N, as in this case no deformation of the flat platform on the filler top occurs. At compressive forces above 300 N gaps develop, leading to defects in the welded joint.

Technological modes of welding (duration of current pulse, pause, welding process, welding current, compressive force) are established experimentally on technological samples, using the control module and welding current source. Welded samples were made by pulsed ASW and arc welding with constant arc power. An inverter-type welding current source «Fronius MW 2600» was used.

Welded joints produced by a constant power arc had several defects, namely burns-through, hot cracks, increased level of its surface deformation. Use of pulsed ASW allowed elimination or reduction of a number of essential defects compared to constant power arc welding. As was noted in studies [5, 6], use of a pulsed welding mode reduces the process heat input at a specified penetration depth. Time of the HAZ metal staying in the high-temperature region is also much shorter than in direct current welding. Control of the frequency, duration of current pulses and

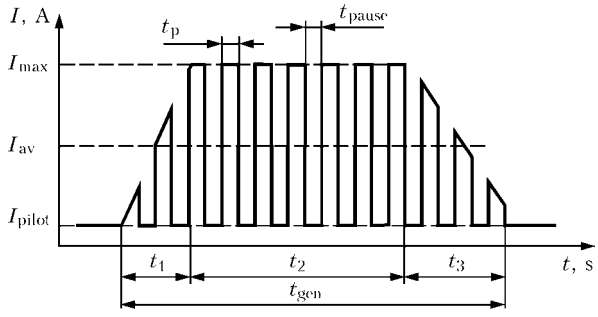

Figure 5. Cyclogram of welding current at pulsed ASW: I_{max}, I_{av}, I_{pilot} — welding current of maximum, average values and pilot arc, respectively; t_{gen} — total welding time; t_1 – t_3 — duration of rising of welding current, working welding current and its drop, respectively; t_p, t_{pause} — duration of welding current pulses and pause between them, respectively

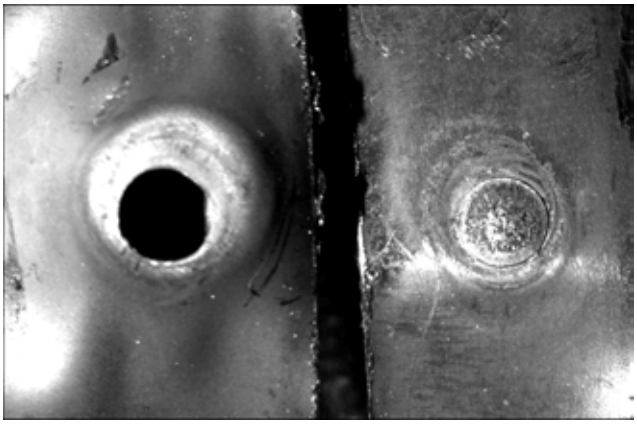

Figure 6. Appearance of weld spot with tearing of its nugget

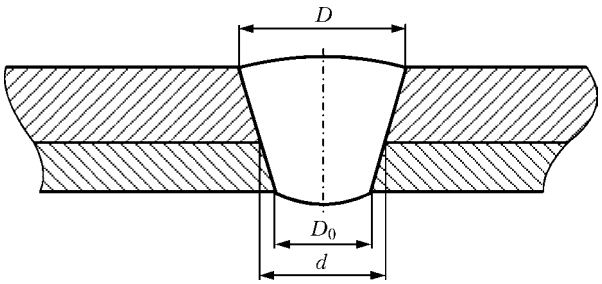

Figure 7. Cross-section of weld spot: D, D_0 — diameters of fusion zone from the face of weld spot and its reverse side, respectively

pause between them allows adjustment of the heat input into the welded joint.

Pulsed ASW of the samples was performed by a cyclogram given in Figure 5. Welding mode parameter ranges, in which the optimum welding mode was selected, are as follows: I_{max} = 40–80 A; I_{av} = 20–40 A; I_{pilot} = 6–20 A; t_1 = 0.05–0.45 s; t_2 = 0.5–4.0 s; t_3 = = 0.05–0.55 s; t_{gen} = 0.55–5 s.

Technological samples were tested to fracture in tensile testing machine RM-50, which was followed by measurement of the weld nugget diameter, using binocular microscope BM-1.

It is established that it is rational to select the geometrical parameters of the spot welded joint made by nonconsumable-electrode ASW so that sample fracture ran with tearing out of the weld spot nugget (Figure 6). Rupture force F applied to the welded joint depends on the weld spot diameter. For the accepted thickness ratio weld spot diameter d should be not less than 1.4 mm (Table). The diameters of the fusion zone from the welding side are equal to D = = 2.2–3.0 mm, D_0 = 1.4–2.0 mm (Figure 7).

Results of measurement of weld spot nugget diameter and rupture force

D, mm	d, mm	F. N
1.5	1.0	240
2.0	1.3	280
2.2	1.5	410
2.5	1.8	440
3.0	2.0	450

Deviation of the weld spot nugget diameter from the specified value caused by imperfection of welding technology (absence of a reliable mutual contact of the parts being welded, deviation of welding modes during welded joint performance, etc.) leads to considerable changes of the shear area, and, consequently, to instability of strength values of the spot joint.

The above-said leads to the conclusion that the developed technology of nonconsumable-electrode ASW of three-layer panels with a cellular filler has the following advantages: ability of welding with a one-sided access to the item and under confined conditions without application of considerable forces for compression of the structural elements being joined; ability of welding of a thin-walled structure 0.1–1.0 mm thick in the gravity position without a backing; simple and compact actuator (welding torch).

The developed technology and equipment for ASW can be the basis for development of automated units for welding large-sized three-layer items from structural elements. Small dimensions of the weld pool of spot joint allow ASW to be performed in all positions.

1. Kornienko, A.N., Zhadkevich, A.M. (2005) Development and application of brazed lattice and honeycomb structures in aircraft engineering (Retrospective review). *The Paton Welding J.*, **12**, 15–21.
2. Zharov, M.V. (2006) Technology of manufacturing of ribbed aircraft panels of complex shape. *Technologiya Mashinostroeniya*, **8**, 31–33.
3. Mosyagin, A.S. (2006) Technological process of assembling of honeycomb blocks. *Ibid.*, **5**, 36–37.
4. Panin, V.P., Gladkov, Yu.A. (1991) *Structures with filler material*: Refer. Book. Moscow: Mashinostroenie.
5. Karkhin, V.A., Khomich, P.N. (2006) Minimization of heat input in pulsed arc welding. *Svarochn. Proizvodstvo*, **10**, 3–6.
6. Vagner, V.A. (1980) Thermal cycling in tungsten electrode welding. *Ibid.*, **2**, 4–6.

STATE-OF-THE-ART AND PROSPECTS OF DEVELOPMENT OF LASER TECHNOLOGIES FOR DEPOSITION OF COATINGS AND SURFACE HARDENING (Review)

V.Yu. KHASKIN
E.O. Paton Electric Welding Institute, NASU, Kiev, Ukraine

Development of commercial technologies for laser hardening and coating is considered on the basis of the published data beginning from the 1980s up to now. The situation in this field in the CIS countries and Ukraine is analysed. Promising research areas in this fields are indicated.

Keywords: laser and hybrid technologies, cladding and alloying, heat treatment, commercial application, laser equipment, new materials

The range of the most promising research and technology areas for the application of lasers had been identified by the middle of the 1980s. These areas included electronics, mechanical engineering, instrument making, motor car construction, ship building, aircraft and space engineering, etc. [1]. The main directions for development of the laser technologies, which were distinguished and formed within the above areas, are as follows: cutting and piercing, welding, cladding, alloying, heat treatment, etc. (e.g. marking, refining of resistors, manufacture of capacitors and conducting elements, deposition of thin films [2]).

The volume of application of the main commercial domestic laser technologies by the end of the 1980s had been distributed as follows: cutting and piercing processes constituting about 75 %, welding ---- 15 %, other application fields (e.g. engraving, marking, holography, etc.) ---- 6 %, and surface modification and cladding ---- constituting only about 4 %. According to the data of 2006, proportion of the laser processes intended for a thermal surface effect (heat treatment, cladding, alloying and coating) decreased from 4 to less than 3 %, compared with other application fields [3], despite a continuous growth of absolute values of the volume of products manufactured by involving the above processes.

According to the current scientific-and-technical literature data, the laser technologies for surface hardening and coating can be subdivided into the following technological sub-areas: laser heat treatment with and without glazing (laser hardening), laser alloying, laser cladding, laser glazing of preliminarily deposited coatings, laser coating, and hybrid and combined processes for laser heat treatment, cladding and coating.

One of the first developments in the field of laser surface hardening is the technology for thermal hardening of various parts, i.e. from cutting edges of metal and wood working tools [4] to inside surfaces of cylinders of internal combustion engines [5]. Laser heat treatment usually involves hardening of the surface layer of metal to a depth of 0.1–2.0 mm. This treatment is normally employed to achieve the effect that cannot be provided by such methods as induction or plasma hardening, or thermochemical treatment [6]. Laser hardening is applied now in industrialized countries to harden drill rods and bits, cams of cast iron camshafts, and parts of ferrous and non-ferrous metals. Shock waves formed in laser treatment are used for increasing surface hardness of parts and their formation [7]. This effect is also employed for treatment of dielectric materials.

Along with investigations of the laser heat treatment process, technologies were developed for extending the service life of parts by surface alloying [8], where formation of the surface layer is accompanied by modification of its structure, which consists in formation of a matrix (e.g. austenitic) alloyed with individual elements (e.g. chromium) and reinforcing phases (e.g. carbides). Laser alloying is applied to tool and structural low-carbon steels, as well as to aluminium and titanium alloys [9].

One of the main difficulties in commercial application of the laser heat hardening and alloying processes is the need to substantiate addition of an extra technological operation to the existing process used for mass production of parts. This problem was solved much simpler with the development of technologies for restoration of machine parts and mechanisms subjected to wear (components of internal combustion engines, running gears of cars and agricultural machines) by using laser powder cladding or glazing of coatings deposited by thermal spraying methods [10]. Laser cladding is most often performed by using powder additives, which are fed by means of special feeders to the laser beam affected zone. At present, laser cladding is employed both for manufacture of new products [11] and for restoration of worn-out parts and tools (stamping tools in the first turn) [12]. With laser glazing of the preliminarily deposited coatings, the main problem is to melt a coating through its full thickness in order to provide a metallurgical contact

with the substrate metal and prevent its ingress into the coating. This method has gained wide acceptance owing to such an advantage as the absence of any need to feed an additive powder to the melting zone [13].

The demand for spare parts for automobile, railway and ship transport, as well as for machine building and instrument making equipment grew in the CIS countries in the 1990s. This fact contributed to a substantial progress in development of the repair technologies. The share of parts repaired by the arc, thermal spraying and laser methods increased. Many researchers (e.g. [14]) distinguish the laser technologies as very promising, allowing the strength of adhesion of the deposited layers characteristic of thermal spraying to be combined with the absence of residual thermal strains. The share of parts manufactured by laser welding was gradually decreased. At that time, in the field of laser cutting there was a transition from the manufacture of large lots of commercial products oriented to fulfilment of state orders, to the manufacture of small lots of such products oriented mostly to private customers (e.g. products of an advertisement or presentation character). These changes led to the development of the corresponding laser equipment, characterised by lower power consumption and compactness, and fitted with computer control systems [15].

The main peculiarity in the CIS countries in the field of development and application of the commercial technologies for laser cladding and modification was a smaller proportion of the laser hardening (heat treatment) and alloying processes. An example of application of the laser repair technologies that received acceptance in the 1990s is cladding of components of internal combustion engines (valve seats [16], journals of crank and distribution shafts [17], connecting rod pins, split cams, etc.), running gears of automobile [18] and railway transport, agricultural machines [19], machines for food processing and clothing industries, etc. Development of the corresponding technologies for rails was active as early as in the 1980s. The attempts were made to apply the laser repair processes in aircraft engineering (e.g. by the author of this review in 1995).

Actively developed in the last decade of the 20th century were such laser coating processes as spraying of heat-, corrosion- and wear-resistant metal coatings, glazing of preliminarily deposited ceramic coatings, deposition of composite coatings, deposition of evaporation products (ablation), vapour (gas) phase deposition [20], and chemical vapour deposition (CVD) by using the laser beam. The last three methods have the following application fields: production and repair of microcircuit masks, production of single-stage ohmic contacts, deposition of hard coatings on controlled surface areas, and production of non-equilibrium materials and materials with controlled grain sizes. However, application of the laser coating processes is hampered because of the necessity to eliminate the following drawbacks: cracking of ceramic and composite coatings in glazing or deposition with continuous-wave CO_2-lasers, low rates of growth of the coatings with the ablation and CVD methods, and the need to use an extra technological operation of preliminary surface preparation (e.g. shot blasting) for spraying.

Abroad, the active development of the laser technologies for surface treatment began as early as in the middle of the 1990s and continues up to now. In the first turn, this was caused by the emergence of a new

Table 1. Technical characteristics of some of the Rofin Sinar (Germany) modern laser units

Type of laser	Series	Model	Radiated wavelength, μm	Radiation generation mode	Power regulation ranges, W	Pulse frequency, Hz	Quality of radiation, mm·mrad	Minimal diameter / size of radiation focusing, mm	Notes
Slit-type CO_2-lasers	SC (sealed-off)	SC x60	10.6	Continuous-wave and pulsed	8–600	0–100,000	> 0.8	< 0.1	–
	DC (diffusion-cooled)	DC 040	10.6	Same	400–4000	0 or 2–5000	≥ 0.9	< 0.1	–
		DP 080 HP	10.6	Continuous-wave	800–8000	–	≥ 0.9	< 0.1	–
Solid-state diode-pumped lasers	DP (Nd:YAG-lasers)	DP 040 HP	1.06	Continuous-wave and pulsed	400–4000	–	25	0.6	Service life 10,000 h
	DS (disk Yb:YAG-lasers)	DS 030 HQ	1.06	Same	300–3000	–	≤ 10	0.2	Service life 10,000 h (efficiency up to 20 %)
Diode lasers	DL-Q	DL 031 Q	0.808 0.940	»	300–3100	–	–	0.8×1.3	Working distance at minimal focus — 66 mm (efficiency over 20 %)
	DL-R	DL 036 R	0.940	»	360–3600	–	–	1.2–3.0	Same at minimal focus 130 mm

generation of laser equipment (Table 1), which includes compact and, at the same time, high-power CO_2-lasers and computer-controlled technological systems based on the above lasers. Of special interest are the slit-type CO_2-lasers employed today mostly for cutting. They have an enormous potential for technological applications owing to sufficiently high (up to 8 kW) power of the generated radiation, absence of a pumping device, extremely low consumption of working gases (complete replacement of a working gas mixture has to be done once in half a year or once a year), and small dimensions. In addition to the new models of the CO_2-lasers, there appeared the Nd:YAG-lasers with an extended life and increased power, equipped with diode pumping, as well as the extremely compact and high-power diode and disc lasers (see Table 1). The fundamentally new optical fibre lasers [21] were developed, allowing a high power (up to 100 kW) of the continuously generated radiation to be combined with a super long (from 100,000 to 1,000,000 h) service life. Characteristic feature of the new generation of lasers is increase in their overall efficiency: from 5–10 to 8–15 % for the CO_2-lasers, from 1–2 to 5–8 % or more for the Nd:YAG-lasers, and up to 42–50 % for the diode lasers. An increased efficiency of the laser equipment combined with decreased production costs, smaller dimensions and higher effectiveness of utilisation of gas leads to a reduction of cost of the laser treatment processes, and makes this equipment more affordable for a customer.

Another important aspect that caused changes in the laser technologies considered is the development of the hybrid (or combined) cladding and coating processes, which has become active in the last decade [22]. These processes are aimed at widening of the capabilities of laser treatment due to a combined use of laser radiation and other heat sources, such as electric arc, plasma jet or high-frequency electromagnetic field. The hybrid processes are the processes where the laser beam, while interacting with the other energy source, forms a common energy source with new properties, and the combined processes are the processes where the laser beam and the second energy source, which do not interact with each other, exert a combined effect on a material treated.

The main goal of development of the hybrid and combined laser technologies is to maintain and, where possible, enhance advantages of each of the processes that make up a technology by avoiding, at the same time, their main drawbacks. Thus, the use of the arc component in laser cladding increases the overall heat input with a simultaneous decrease of the required laser power by replacing it with a power of the arc source [23]. This makes it possible not only to substantially reduce the costs of the equipment and the operating costs, but also decrease the risk of formation of one of the main defects, i.e. cracks in the deposited layers. The use of the laser beam for preheating and cleaning of the surface to be treated by thermal spraying methods allows avoidance of preliminary shot blasting of the workpiece surfaces [24].

Above peculiarities of advancements in the laser equipment and technology served as a basis for upgrading of the existing processes for laser coating and surface hardening, and development of the new ones. New methods for control of the laser cladding and auxiliary equipment used for this process are being developed [25], and new techniques are being worked out for overlaying of titanium [26] and aluminium alloys [27], as well as magnesium-based composite alloys [28]. At the same time, the existing technologies are being improved, e.g. cladding on heat-resistant nickel alloys [29] or steels [30]. Progress in the field of the laser restoration technologies allowed the development of the technologies for repair of stamping tools and jet engine turbine blades by using manual laser devices [31], reconditioning and hardening of tools [32], reconditioning of different types of aircraft engineering components, etc. [33]. Investigations are continued in the field of the processes of pulsed and continuous-wave laser treatment of coatings preliminarily deposited by thermal spraying methods [34]. For example, the use of the pulsed Nd:YAG-laser allowed glazing or deposition of crack-free ceramic coatings. Commercial application of such processes will make it possible to improve properties of thermal-barrier coatings on gas turbine engine blades, hydroxyapatite coatings on implants used in medicine, as well as to provide wear-resistant coatings of self-fluxing alloys.

Some technological developments (e.g. cladding by using filler wire) are initially oriented to application of new equipment (e.g. diode lasers) [35], which is related to peculiarities of formation of the beam and leads to qualitatively new results. Achievement of a high level in the already well-known processes of laser powder cladding is ensured also by using the metal-science and metal-physics approaches to solving the problems arising in the course of research [29, 30]. The stage of the manufacture of stationary laser systems has been passed, and mass production of mobile laser systems, including for restoration of the surfaces of parts (e.g. for repair cladding of casting moulds [36]), has been started. One of the promising directions in advancement of the laser cladding processes is development of the methods for 3D-forming of machine parts by the method of laser remelting of filler metal, as well as for restoration of gas turbine engine blades [31, 37]. The first direction is important for the manufacture of parts which cannot be produced by other methods. This is, for example, formation of cooling channels of complex configuration in the bulk of a steel part. Moreover, the walls of the channels should be made from copper to increase heat removal.

Surfaces of functional coatings produced by different cladding and coating methods often need to be subjected to finishing mechanical treatment. Meanwhile, increased requirements are imposed on tools employed for treatment of coatings produced by using the laser beam. For this, it is desirable to use, firstly, the tools with improved service characteristics, which

Table 2. Technical characteristics of some modern technological CO_2-lasers produced by Company «Technolaser» (Russia)

Type of lasers	Model	Radiation generation mode	Power regulation range, W	Pulse frequency, Hz	Aperture, mm	Beam divergence, mrad	Minimal diameter of focused beam, mm	Efficiency, %
Transverse-flow laser	TL-1.5	Continuous-wave and pulsed	100–1700	0–1000	∅ 25	1.4	< 0.10	5.0–6.0
	«Tandem»	Continuous-wave	100–7000	–	28 × 28	1.4	–	7.5
	TL-7.5	Same	400–10000	–	Ring 50 / 22	1.5	< 0.30	6.0–8.0
Tubular diffusion-cooled laser	TLV-700	Continuous-wave and pulsed	70–750	0–2000	∅ 5	–	< 0.05	7.0

Note. Here and in Table 3, radiation wavelength is 10.6 μm.

is related to increased hardness of the laser treated surfaces. Secondly, because of the trend to minimise machining allowances, which is characteristic of the laser technologies, the tools should provide a high accuracy of the finishing treatment. All these issues have become a subject of the recent research conducted in many countries, including Ukraine [38].

At present, Ukraine is active in research in the field of laser and hybrid technologies. However, the latter is still at an early stage of development, while the laser restoration technologies applied in Ukraine since the 1990s have lost to a considerable degree their topicality because of saturation of the market with comparatively inexpensive spare parts from manufacturers.

Unlike the above situation in Ukraine, in Russia the restoration of parts with a laser has gained a wider acceptance. One of the latest commercial applications is the technology for laser cladding of wagon axle necks, which was developed in Irkutsk and Nizhny Udinsk (East-Siberian Railroad) [39]. The hybrid technologies [40] using laser radiation in CVD processes [41], technologies for laser coating deposition [42] and other processes are being actively developed and applied. Such applications are based on the production of industrial laser units arranged in Russia (Tables 2 and 3). However, as shown by comparison of modern Russian equipment with the foreign one (see Tables 1–3), development of the latter is much ahead of that of the former. Thus, because of the technical solutions characteristic of the end of the 20th century, Russian lasers are inferior both in overall efficiency and individual technical characteristics, and in maintenance costs. In the future, it is planned to produce fast-flowing CO_2-lasers, which have a lower efficiency and consume several orders more helium than the diffusion-cooled slit lasers (Table 2). Solid-state lasers have an old lamp pumping (Table 3), instead of the advanced diode pumping. A marked progress is observed only in the field of development of fibre lasers [21]. However, for economic reasons the Russian customers prefer to use the domestic equipment instead of buying the foreign one.

To compare, consider the situation established in the field of laser restoration and modification in the Republic of Belarus. The technologies used there correspond primarily to the level of the 1980s–1990s. At the same time, they are characterised by substantial volumes of the commercial application. One of the reasons is that in Belarus the approach to addressing practical problems includes not only traditional technological developments, but also utilisation of mathematical (including thermal-physical) modelling and metal-science developments [43]. This concerns investigations both in the field of hardening and strengthening [43, 44], and in the field of coating and alloying [43, 45]. In addition, much attention is given to physical-mechanical properties (wear resistance in the first turn) of coatings produced with the laser beam both by cladding using a powder additive and by glazing of preliminarily sprayed coatings [46]. This integrated R&D approach makes it possible to compensate for the use of obsolete technological solutions and achieve the required practical results. Combined with meeting the industrial needs, it led to a substantial progress in the field of laser technologies in Belarus. Laser hardening is initially included into the manufacture of new products, rather than being used only for repair of worn-out parts.

The Ukrainian industry has been showing lately an increasingly high interest in application of surface heat hardening technologies also for the manufacture

Table 3. Technical characteristics of some modern pulsed-periodic Nd:YAG-lasers (DB «Bulat», Russia)

Model	Pulse energy, J	Mean / peak power, W	Pulse frequency, Hz	Stability of radiation energy, %	Diameter of focused beam, mm	Efficiency, %
LRS-200	≤ 80	200 / 8000	0.5–20	± 2	0.30–2.00	2.5–3.0
HTS-200	≤ 80	200 / 8000	0.5–100	± 2	0.30–2.00	2.5–3.0
HTF-150	≤ 60	150 / 6000	0.5–20	2	0.35–2.00	2.5

of new products. The laser hardening (heat treatment) and alloying technologies have again become topical [47]. In this case, the main Customers' requests include a 1.5–2 times increase in service life and no more than 10–30 % increase in costs of the process of production of a hardened part [48]. In a number of cases the laser technologies allow the service life of machine parts and mechanisms to be extended 2–3 times or more, but as far as the production costs are concerned, here the required values are not always achievable.

CONCLUSIONS

1. Of the highest interest for modern industry are such application fields for the laser technologies as synthesis of 3D objects, deposition of thin films and nanostructural coatings, production of coatings of new functional materials, and hybrid treatment processes, allowing the production costs to be reduced and quality of the deposited (modified) layers to be improved due to new technological effects.

2. The efforts are active in upgrading of the existing processes and development of the new processes for laser deposition of coatings and surface hardening. New methods are being developed to control the laser coating processes and corresponding auxiliary equipment, and new technological approaches are being elaborated, allowing the deposition of layers on titanium, aluminium and composite magnesium alloys. The known technologies, e.g. cladding on heat-resistant nickel alloys or steels, are being further developed.

3. To increase proportion of the surface treatment processes in a total volume of application of the laser technologies, and achieve progress in their further advancement, it seems expedient to develop methods for elimination of porosity and cracking in layers deposited or modified by means of the laser beam, and hybrid (combined) technological processes, where the laser beam energy is partially replaced by a cheaper plasma or arc energy.

4. The most advanced equipment for surface treatment includes slit-type CO_2-lasers with diffusion cooling, fibre and diode lasers, as well as diode-pumped Nd:YAG-laser. Worthy of special notice are mobile laser systems, which allow repair cladding to be performed on site, directly at the location of a failed part.

1. Diakova, Yu.G., Lunin, E.L., Stelmakh, M.F. (1981) State-of-the-art and prospects of application of lasers in national economy. *Elektron. Promyshlennost*, **5/6**, 3–9.
2. Boyakov, V.M., Epikhin, V.M., Kalin, B.A. et al. (1978) Spraying of chemical element films using the Nd-glass laser. *Kvant. Elektronika*, 5(**7**), 1582–1589.
3. Bernadsky, V.N., Shelyagin, V.D., Makovetskaya, O.K. (2007) Present market of laser equipment for welding and processing of materials. *The Paton Welding J.*, **10**, 44–49.
4. Kovalenko, V.S., Golovko, L.F., Merkulov, G.V. et al. (1981) *Hardening of parts by laser beam*. Ed. by V.S. Kovalenko. Kiev: Tekhnika.
5. Andriyakhin, V.M., Zverev S.E., Chekanova, N.T. (1980) On the problem of selection of parameters for laser hardening of ZIL-130 engine block sleeves. In: *Abstr. of 1st All-Union Sci. Conf. on Sci.-Techn. Cooperation «Enterprise–Higher Education Institution»* (Moscow, Dec. 9–11, 1980). Moscow: MGU.
6. Messer, K., Bergmann, H.W. (1997) Stand des Laserstrahlhartens. *Mitt.*, 52(**2**), 74–82.
7. Niehoff, H.Sc., Vollertsen, F. (2005) Laser induced shock waves in hardening and forming technologies. *J. Technol. Plast.*, 30(**1/2**), 37–50.
8. Mazumder, J., Singh, J. (1986) Laser surface alloying and cladding for corrosion and wear. *High Temp. Mater. and Proc.*, 7(**2/3**), 101–106.
9. Abboud, J.H., West, D.R.F. (1991) Processing aspects of laser surface alloying of titanium with aluminium. *Mater. Sci. and Technol.*, 7(**4**), 353–356.
10. Arkhipov, V.E., Birger, E.M., Smolonskaya, T.A. et al. (1985) Application of laser technology in repair production. *Svarochn. Proizvodstvo*, **1**, 7–8.
11. Jian, L.N., Wang, H.M. (2005) Microstructure and wear behaviours of laser-clad $Cr_{13}Ni_5Si_2$-based metal-silicide coatings on a titanium alloy. *Surface and Coat. Technol.*, 192(**2/3**), 305–310.
12. Frank, C. (2005) Laserstrahlschweissen von Hand mit dem Nd:YAG-Laser. Vol. 3: Notfallservice fuer Werkzeuge und Formen. *Praktiker*, 57(**10**), 293–295.
13. Pilipchuk, A.P., Devojno, O.G., Gribkov, Yu.A. et al. (2001) Examination of transition zone of coatings glazed by laser beam. In: *Theoretical and technological principles of hardening and restoration of machine-building parts*. Minsk: PolotskGU.
14. Kovalenko, V.S. (2001) Laser technology at a new stage of development. *The Paton Welding J.*, **12**, 3–8.
15. Bajko, I.Yu., Istomin, E.A., Pojzner, B.N. (1994) Leaders and outsiders of thirty-years marathon of gas discharge lasers. *Kvant. Elektronika*, **11**, 1103–1104.
16. Aihua, W., Zengyi, T., Beidi, Z. (1991) Laser beam cladding of seating surfaces on exhaust valves. *Welding J.*, 70(**4**), 1065–1095.
17. Backes, G. (1995) Beschichten von Kurbelzapfen mit CO_2-Laserstrahlung. *Maschinenmarkt*, 101(**12**), 42–45.
18. Khaskin, V.Yu., Velichko, O.A., Molchan, I.V. et al. (1995) Restoration of threads by laser cladding. *Avtomatich. Svarka*, **6**, 56–58.
19. Khaskin, V.Yu., Golego, N.N., Dmitrenko, V.N. et al. (1994) Equipment and technology for laser restoration of agricultural machine engine parts. In: *Proc. of Int. Sci.-Pract. Conf. on Modelling of Processes and Technological Equipment in Agriculture* (Melitopol, August 17–19, 1994), 31–32.
20. Hoking, M., Vasantasri, V., Sidki, P. (2000) *Metal and ceramic coatings: production, properties and applications*. Moscow: Mir.
21. Minaev, V.P. (2003) Company and its leader. In: *Laser-Inform*: Inform. Bul. of Laser Association, April, 8(263), 1–5.
22. Shelyagin, V.D., Khaskin, V.Yu. (2002) Tendencies in investigations of combined laser-arc processes. In: *Survey information of PWI*, No. 1. Preprint. Kiev: PWI.
23. Som, A.I., Krivtsun, I.V. (2000) Laser + plasma: search for new possibilities in cladding. *The Paton Welding J.*, **12**, 34–39.
24. Coddet, C., Montaron, C., Marchione, T. et al. (1998) Surface preparation and thermal spray in a single step: the PROTAL process. In: *Proc. of 15th Int. Thermal Spray Conf. on Meeting the Challenges of the 21st Century* (Nice, France, May 25–29, 1998), Vol. 2. Nice: ASM Int., 1321–1325.
25. Bayer, E., Steinwandel, J., Hoschele, J. et al. *Method for control of laser or plasma cladding process*. Appl. 10337149 Germany. Int. Cl. B 23 K 26/03, B 23 K 26/34. Filed 13.08.2003. Publ. 10.03.2005.
26. Liu, R.X., Lie, T.Q., Guo, L.X. (2004) Recent developments in the field of laser cladding on titanium surfaces. *Mater. Sci. and Technol.*, 12(**5**), 524–528.
27. Ma, N.H., Wang, H.W., Liang, G.Y. et al. (2004) Technology problems of laser cladding procedure for in-situ TiCp / Al composite layer on aluminium alloy. *J. Shanghai Jiaotong Univ. Sci.*, 9(**1**), 15–18.
28. Mei, Z., Guo, L.F., Yue, T.M.J. (2005) The effect of laser cladding on the corrosion resistance of magnesium ZK60 / SiC composite. *Mater. Proc. Technol.*, 161(**3**), 462–466.
29. Li, M., He, Y., Yuan, X. (2006) Effect of nano-Y_2O_3 on microstructure of laser cladding cobalt-based alloy coatings. *Appl. Surface Sci.*, 252(**8**), 2882–2887.
30. Zhang, D., Zhang, X. (2005) Laser cladding of stainless steel with Ni–Cr_3C_2 and Ni–WC for improving erosive-corrosive wear performance. *Surface and Coat. Technol.*, 190(**2/3**), 212–217.

31. Storch, W., Letsch, K., Jokiel, I. et al. (2006) Handgefuehrt mit dem Laserstrahl an Turbinenbauteilenschweissen. *Praktiker*, **6**, 170–175.
32. Lu, W., Hou, L.Q., Chen, K. et al. (2004) Microstructure and properties of coating deposited by laser cladding on cutter tip. *Transact. of China Welding Inst.*, 25(**6**), 51–53.
33. Yurkevich, S.N., Tomashevich, A.V., Yurkevich, A.S. (2006) Restoration of aircraft engineering parts by laser cladding method. *Remont, Vosstanovlenie i Modernizatsiya*, **3**, 31–32.
34. Iliushchenko, A.F., Okovity, V.A., Kundas, S.P. et al. (2002) *Formation of thermal spray coatings: theory and practice*. Ed. by A.F. Iliushchenko. Minsk: Bestprint.
35. Syed Waheed Ul Haq, Li Lin (2005) Effects of wire feeding direction and location in multiple layer diode laser direct metal deposition. *Appl. Surface Sci.*, 248(**1/4**), 518–524.
36. (2006) System zum Laserauftragsschweissen fuer 1400 Euro im Monat leasen: Carl Baasel La GmbH & Co KG. *Maschinenmarkt*, **13**, 56.
37. Grigoriants, A.G., Misyurov, A.I. (2005) Possibilities and prospects of laser cladding application. *Tekhnologiya Mashinostroeniya*, **10**, 52–56.
38. Kharlamov, Yu.A., Budagiants, N.A. (2003) *Principles of technology for restoration and hardening of machine parts*: Manual. Vol. 2. Lugansk: Vostochno-Ukr. Nats. Univ. im. V. Dalya.
39. Georgiev, V. (2003) With an old luggage into the new age? *Gudok*, 13 May, 4.
40. Melyukov, V.V., Kuzmin, V.A., Chastikov, A.V. et al. (2005) Laser-plasma hardening of high-speed steel surface layers. In: *Proc. of 7th Int. Pract. Conf.–Exhibition* (St.-Petersburg, April 13–16, 2005), 156–164.
41. Kononenko, V.V., Konov, V.I., Pimenov, S.M. et al. (2000) CVD diamond transmissive optics for CO_2-lasers. *New Diamond and Frontier Carbon Technol.*, 10(**2**), 97–107.
42. Zherikhin, A.N., Khudobenko, A.I., Villiams, R.T. et al. (2003) Laser spraying of ZnO films on silicon and sapphire substrates. *Kvant. Elektronika*, 11(**33**), 975–980.
43. Vityaz, P.A., Ivashko, V.S., Iliushchenko, A.F. et al. (1998) *Theory and practice of deposition of protective coatings*. Minsk: Belaruskaya Navuka.
44. Krajko, S.E. (2004) Effect of absorbing coating thickness on microhardness distribution in laser heat treatment. *Mashinostroenie*, Issue 20, 124–127.
45. Devojno, O.G., Kardapolova, M.A., Dorozhkin, N.N. et al. (2003) Formation of surface layer structure in repeated laser alloying. *Inzh.-Fizich. J.*, 76(**1**), 98–101.
46. Devojno, O.G., Kardapolova, M.A., Dyachenko, O.V. (2003) Effect of laser treatment parameters and alloying components on physical-mechanical properties of coatings. *Mashinostroenie*, Issue 19, 70–75.
47. Lyubchenko, A.P., Pashkova, G.I. (2005) Effect of laser treatment and rolling on fatigue strength of high-strength cast iron. *Novi Materialy i Tekhnologii v Metalurgii ta Mashynobuduvanni*, **1**, 90–93.
48. Kanarchuk, V.E., Chigrinets, A.D., Shaposhnikov, B.V. (1995) *Laser equipment and technology for hardening and restoration of parts and apparatuses*. Kyiv: Ukr. Transportn. Univ.

ADJUSTMENT OF THERMAL POWER OF HYDROGEN-OXYGEN FLAME AT FLAME TREATMENT

V.N. KORZH and **Yu.S. POPIL**
NTUU «Kiev Polytechnic Institute», Kiev, Ukraine

The effect of composition and character of flow of a combustible mixture on variation in thermal power of the flame is considered when using the hydrogen-oxygen flame formed as a result of combustion of a mixture produced by water-electrolysis generators. Thermal power of the flame produced in combustion of a pure hydrogen-oxygen mixture and mixture with additions of hydrocarbon compounds has been determined.

Keywords: flame treatment, hydrogen-oxygen flame, hydrocarbon compounds, jet, laminar flow, turbulent flow, flame thermal power

Flame treatment of metal is performed using the hydrogen-oxygen flame (HOF) produced at burning of hydrogen-oxygen mixture (HOM) generated by water-electrolysis generators (WEG). In technical literature [1–3] the thermo-physical characteristics of HOF obtained at burning of a combustible mixture with a different oxygen-hydrogen ratio in the mixture are quite broadly presented. There is practically no data on application of HOF generated by WEG.

The purpose of this work was determination of the possibility of controlling the thermal characteristics of HOF.

It is known [2, 4] that the total thermal power can be changed by changing the flow rate and composition of the gas mixture. Considering that HOM has a constant composition with hydrogen to oxygen ratio $\beta = V_{O_2} / V_{H_2} = 0.5$, adjustment of thermal power is only possible by changing the mixture flow rate. The flame is of an oxidizing nature.

Adjustment of the nature of burning from oxidizing to normal or carbonizing for HOM is possible only by its saturation by hydrocarbon vapours as a result of gas passing through liquid hydrocarbons (benzene, alcohol, etc.) through a special device ---- bubbler [5]. This leads to a change of the composition of combustion products and, accordingly, of the flame thermal power, as well as mixture flow rate. It is known that at the change of the combustion product composition the geometrical dimensions of the plume, flow nature and structure of combustion products are changed, as well as the maximum flame temperature and its distribution along the plume length [6].

Possibility of adjustment of the flame thermal power was determined using EURO-JET X S-7 torch with a standard set of replaceable nozzles of 1.6, 2.0 and 2.2 mm diameter and water electrolysis generator A1803. Investigations were performed for three mixtures the most widely applied at flame treatment using WEG, namely HOM, HOM with additives of 5.5 % of benzene vapours ($C_{7.07}H_{15}$) and HOM with additives of 16 % of ethyl alcohol vapours (C_2H_5OH).

Full thermal power of combustion products at combustion of 1 m^3 of HOM was determined as

$$q_{fl} = Q_{H_2} V_{H_2}, \quad (1)$$

where Q_{H_2} is the lower thermal value of hydrogen, MJ; V_{H_2} is the hydrogen consumption, m^3.

Total thermal power of the flame at combustion of 1 m^3 of HOM is equal to

$$q_{fl} = 0.67 \cdot 10.08 = 6.75 \text{ MJ} / m^3, \quad (2)$$

where 0.67 m^3 is the hydrogen volume at the proportion of $O_2 / H_2 = 0.5$ in 1 m^3 of HOM; 10.08 MJ is the thermal value of 1 m^3 of hydrogen.

Total thermal power of combustion products at combustion of 1 m^3 of HOM + 5.5 % of benzene vapours is equal to

$$q_{fl} = Q_{H_2} V_{H_2} + Q_{C_{7.07}H_{15}} V_{C_{7.07}H_{15}} = 17.1454 \text{ MJ} / m^3, \quad (3)$$

where $Q_{C_{7.07}H_{15}}$ is the lower thermal value of benzene; $V_{C_{7.07}H_{15}}$ is the volume of benzene in the mixture.

Total thermal power of combustion products at combustion of a mixture of 1 m^3 of HOM + 16 % of alcohol vapors is equal to

$$q_{fl} = Q_{H_2} V_{H_2} + Q_{C_2H_5OH} V_{C_2H_5OH} = 14.70 \text{ MJ} / m^3, \quad (4)$$

where $Q_{C_2H_5OH}$ is the lower thermal value of ethyl alcohol; $V_{C_2H_5OH}$ is the volume of ethyl alcohol in the mixture.

It is known [6] that for each torch nozzle, a laminar or turbulent nature of outflow of the flame combustion product jet is possible, depending on mixture flow rate. Distribution of temperatures and velocities of the gas flow along the plume length depends on the nature of outflow.

The Table gives the variation of thermal power, depending on the nature of flow of the combustion product jet and gas mixture flow rate, providing a stable burning of the flame.

Results of investigation of thermal power at HOF burning showed that addition of 5.5 % of benzene vapours to HOM increases the total thermal power of the flame within the laminar nature of the flow approximately by 2.6 times, at turbulent by 2.8 times

Thermal power of flame depending on the composition and nature of combustion product flow

Combustible mixture and nature of its flowing	Torch nozzle bore, mm	Gas mixture flow rate, m^3 / h		Total thermal power of flame q_{fl}, MJ / m^3	
		min	max	min	max
HOM, laminar	1.6	0.3	0.6	2.025	4.05
	2.0	0.4	0.62	2.7	4.185
	2.2	0.4	0.7	2.7	4.725
HOM, turbulent	1.6	0.6	0.76	4.05	5.13
	2.0	0.62	0.82	4.185	5.535
	2.2	0.7	1.1	4.725	7.425
HOM + benzene, laminar	1.6	0.2	0.4	3.428	6.856
	2.0	0.3	0.52	5.142	8.9128
	2.2	0.31	0.72	5.3134	12.3408
HOM + benzene, turbulent	1.6	0.4	0.78	6.856	13.3692
	2.0	0.52	0.9	8.9128	15.426
	2.2	0.72	1.22	12.3408	20.9108
HOM + alcohol, laminar	1.6	0.4	0.6	5.88	8.82
	2.0	0.42	0.78	6.174	11.466
	2.2	0.52	0.9	7.644	13.23
HOM + alcohol, turbulent	1.6	0.6	0.92	8.82	13.524
	2.0	0.78	1.18	11.466	17.346
	2.2	0.9	1.25	13.23	18.375

compared to the flame at burning of pure HOM. At addition of 16 % of ethyl alcohol vapours to HOM, the total thermal power of the flame is increased 2.7 and 2.4 times, respectively.

The above-derived regularities are confirmed by investigations of effective thermal power in the high-temperature zone of the plume (at the nugget end) at heating of samples, which simulates the processes of heating in welding, brazing and preheating at metal cutting, and effectiveness of heating of the samples placed at different sections along the length of the zone of delayed burning of the flame plume for the case of heating of the material (powders) at flame spraying of coatings.

Effective thermal power of flame q was determined by the quantity of heat applied by the flame to the metal in a unit of time. Effectiveness of metal heating by the gas flame was evaluated by effective efficiency η_i which was the ratio of effective flame power q determined by calorimetry, to the full thermal power of flame q_{fl} calculated by the lower thermal power of fuel [2, 7]:

$$\eta_i = \frac{q}{q_i}. \qquad (5)$$

Effective thermal power of the flame for different natures of flow and composition of HOM was determined using the method of calorimetry in an experimental unit with a water calorimeter.

Effectiveness of heating by the flame obtained at burning of a mixture produced by WEG at different flow rates and compositions of the gas mixture was determined at heating of a copper plate of 3 × 350 × × 150 mm size and 0.95 kg weight. Time of plate heating was recorded. Quantity of liquid in the calorimeter was 20 l (distilled water). Temperature in the calorimeter was measured by Beckman thermometer (measurement accuracy of ±0.01 °C).

Effectiveness of heating by gas flame was determined from the condition of thermal balance

$$q_{ef}t = Q_{cal} + Q_m + Q_{ch} + Q_v + Q_{at}, \qquad (6)$$

where q_{ef} is the effective thermal power of the flame plume, W; t is the heating time, s; Q_{cal} is the heat absorbed by the calorimetric liquid, J; Q_m is the heat absorbed by the metal parts of the calorimeter, J; Q_{ch} is the change of heat content of plate metal during heating by gas flame, J; Q_v is the heat lost with vapour formation at immersion of the heated plate into the calorimeter water, J; Q_{at} is the heat dissipated into the atmosphere as a result of convective and radiation heat transfer from the plate surface at heating and moving the plate into the calorimeter, J.

After substitution of values and transformation of equation (6) calculation was performed by the following formula:

$$q_{ef} = \frac{(c_w m_l + c_m m_m + c_{st} m)(T_{fin} - T_b + Q_v)}{t - \frac{\alpha}{c\rho}(t^2 + 2tt_{mov})}, \qquad (7)$$

where c_w is the heat capacity of calorimetric liquid (distilled water), J / (kg·K); m_l is the volume of calorimetric liquid, l; c_m is the heat capacity of metal (brass) parts of the calorimeter (384.9 J / (kg·K); m_m

is the weight of the metal parts of the calorimeter, kg; c_{st} is the heat capacity of the metal of the plate which interacted with the heat flow, J / (kg·K); m is the weight of the metal plate being heated, kg; T_{fin}, T_b is plate temperature after and before heating, respectively, °C; α is the coefficient of complete surface heat dissipation, W / (m_2·K); $c\rho$ is the volume fraction of plate metal, J / (kg·K); t_{mov} is the time of plate moving into the calorimeter, s.

Obtained experimental data of the effectiveness of sample heating depending on its position along the plume length are shown in the Figure. Time of fixed heating of the plate t = 15 s. Effectiveness of plate heating along the length of gas plume by combustion products of pure HOM practically does not change at a laminar nature of the flow. At a turbulent nature of the combustion product flow an abrupt reduction of the heating effectiveness is found.

Effectiveness of sample heating by a plume of flame obtained at combustion of HOM with additives of vapours of hydrocarbon compounds at different nature of the combustion product flow is higher than when pure HOM is used.

Increase of heating effectiveness at addition of vapours of hydrocarbon compounds to HOM is attributable to an increase of the amount of carbon in the flame plume. Transformation of carbon into carbon oxide occurs with evolution of an additional quantity of heat.

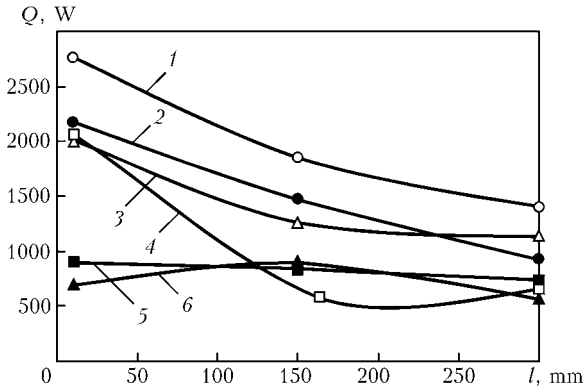

Effectiveness of sample heating by flame depending on its distance from torch nozzle tip (2.0 mm diameter), combustible mixture composition and nature of combustion product flow: *1, 2* — HOM + 5.5 % of benzene, turbulent and laminar flow, respectively; *3, 6* — HOM + 16 % of alcohol, turbulent and laminar flow, respectively; *4, 5* — HOM, turbulent and laminar flow, respectively.

CONCLUSIONS

1. Complete thermal power of hydrogen-oxygen flame at burning of a mixture of 1 m^3 volume is equal to 6.75 MJ. Adjustment of thermal power of HOF at constant flow rate of the gas mixture is possible by adding hydrocarbon compounds to the mixture. At addition of 5.5 % of benzene vapours to the mixture, the thermal power at burning of 1 m^3 of the mixture is equal to 17.1454 MJ, which is almost 2.7 times greater compared to the flame of pure HOM. At addition of 16 % of ethyl alcohol vapours to HOM, the thermal power of the mixture is equal to 14.70 MJ at combustion of the same volume of the combustible mixture.

2. In the zone of flame burning the effectiveness of plate heating by the combustion products of hydrogen-oxygen flame generated when burning a mixture produced by WEG is essentially increased at combustion of HOM + benzene vapour mixture and to a smaller degree of HOM + ethyl alcohol vapours compared to pure hydrogen-oxygen flame.

1. Nekrasov, Yu.I. (1974) *Gases-substitutes of acetylene*. Moscow: Mashinostroenie.
2. Glizmanenko, D.L., Evseev, G.B. (1954) *Gas welding and cutting of metals*. Moscow: Mashgiz.
3. (1964) *Application of gases-substitutes of acetylene in gas flame treatment of metals*. Ed. by I.A. Antonov. Moscow: Mashinostroenie.
4. Donik, G.A. (1974) Investigation of heat source power in natural gas cutting of low-carbon steel. *Svarochn. Proizvodstvo*, **11**, 10–11.
5. Korzh, V.N. (1983) Control of nature of gas mixture burning by addition of liquid carbon-hydrogen compounds. *Avtomatich. Svarka*, **11**, 65–66, 69.
6. Korzh, V.N., Popil, Yu.S. (2004) Influence of hydrocarbon additives on the structure of hydrogen-oxygen flame and temperature distribution along the plume length. *The Paton Welding J.*, **11**, 32–36.
7. Rykalin, N.N. (1951) *Calculations of thermal processes in welding*. Moscow: Mashgiz.
8. Vargaftik, N.B. (1972) *Handbook on thermophysical gases and liquids*. Moscow: Nauka.

INFLUENCE OF NETWORK VOLTAGE FLUCTUATION ON PROCESS OF PULSED ARC WELDING

A.M. ZHERNOSEKOV
E.O. Paton Electric Welding Institute, NASU, Kiev, Ukraine

Influence of reduction of the power supply network voltage on sputtering and characteristics of the deposited metal in the consumable-electrode gas-shielded pulsed-arc welding of carbon steels is experimentally determined. It is shown that at mentioned disturbance it is efficient to use the two-channel automatic stabilization system.

K e y w o r d s : pulsed arc welding, consumable electrode, network voltage, disturbance, sputtering, stabilization of parameters

Nowadays consumable electrode gas-shielded pulsed-arc welding (CEPAW) is rather widely used in different branches of industry. It was further developed in a number of new technologies, such as double-arc pulsed welding or combination of pulsed and laser welding. As far as CEPAW is connected with production of items at big industrial enterprises, where other methods of welding, for example, resistance butt welding and powerful consumers of electric energy are used (motors, transformers, etc.), the issue of action on the CEPAW process of the power supply network fluctuations remains rather actual. Available on the market pulsed sources of the arc power supply ensure welding within the range of the network voltage change ±10 %. In addition, the arc length stabilization conditions are envisaged in them. However, as far as the CEPAW process occurs without short circuits of the arc gap, the most hazardous are disturbances in direction of reduction of the power supply network voltage, which may cause short-term violation of the CEPAW principle «1 pulse – 1 drop» and worsen quality of the weld metal.

Purpose of this work is experimental investigation of influence of the network voltage reduction on the CEPAW of steels and efficiency of application of developed systems for automatic stabilization of the process parameters.

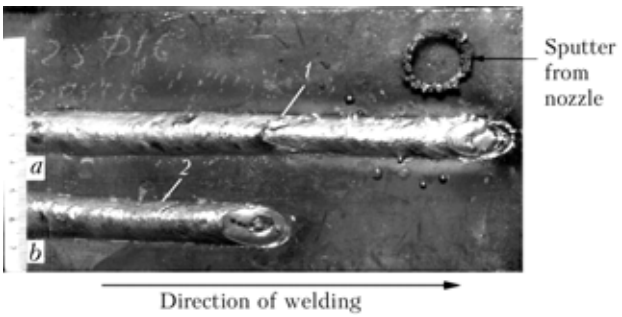

Figure 1. Appearance of weld metal in CEPAW of steel St3sp using Sv-08G2S wire of 1.6 mm diameter in mixture of gases Ar + + 18 % CO_2 (welding speed is 16 m / h, pulse duration is 3.4 ms): *I* — U_n = 376–380 V (first half of weld), 342–354 V (second one); K_s = 6.5–7.0 %; *2* — U_n = 376–380 V, I_{mean} = 250 A, U_{mean} = = 25 V; frequency of pulses is 82 Hz, K_s = 1.0–1.5 %

The experiments were carried out with application of the thyristor arc supply source (with smooth adjustment of duration, amplitude and frequency of pulses), connected via the voltage «potential–regulator» to the power supply network, and welding automatic machine and developed automatic systems for stabilization (ASS) of the CEPAW process parameters [1]. Gas mixture Ar + 18 % CO_2 and the Sv-08G2S wire of 1.2 and 1.6 mm diameter were used.

In Figure 1 appearance of the weld metal in case of CEPAW of steel St3sp (killed) without disturbances in the network with nominal voltage 380 V and reduction of the network voltage U_n from nominal down to 342–354 V is shown. In case of CEPAW of steels in mixture of gases using nominal conditions, sputtering of the metal constituted 1.0–1.5 %, which is confirmed by other authors as well [2, 3]. Reduction of voltage in the power supply network causes reduction of mean value of the arc voltage (power supply source with gently dipping volt-ampere characteristics) and occurrence of short circuits of the arc gap that cause increase of the metal sputtering (K_s = = 6.5–7.0 %) with sticking of spatter to the nozzle, which also worsens gas shielding (Figure 1).

For determining influence of the network voltage reduction on the weld metal characteristics steel 25 was surfaced using the Sv-08G2S wire of 1.2 mm diameter and nominal conditions of pulsed arc welding with reduction of the power supply network voltage and application of the developed ASS. In CEPAW of steels a single-channel ASS of mean welding voltage values U_{mean} was used with governing action on parameters of the arc power supply source and the double-channel one. In second case stabilization of mean values of welding current I_{mean} was carried out with governing action on welding wire feed rate, and stabilization of U_{mean} — by action on parameters of the arc power supply source. Application of both single- and double-channel ASS allows removing short circuits in case of lowering of the network voltage and reducing metal sputtering down to the level of undisturbed network. In Figure 2 macrosections of longitudinal cuts (along the axis) of the weld metal are shown. In case of operation of the double-channel ASS

depth of penetration and height of the convexity are most stable (Figure 2, *c*).

For investigation of the microstructure components of the weld metal the specimens were cut across. On basis of the metallographic investigations one may draw conclusion that when voltage of the power supply network is 376–380 V, cast microstructure in center of the weld metal of steel 25 consists of pro-eutectoid ferrite precipitated over boundaries of cast crystallites, separate grains of structure-free ferrite sometimes oriented similar to the Widmanstaetten structure, and small areas of pearlite. In body of the crystallites structure of upper and lower bainite is observed. Hardness is *HV*50-2100–2210 MPa (five measurements in center of the weld metal). In case of reduction of the power supply network voltage down to 342–354 V appear more areas of pearlite and ferrite, oriented similar to the Widmanstaetten structure (*HV*50-2320–2370 MPa). In case of application of ASS of the arc voltage mean values, structure of a specimen also contains more areas of pearlite and more areas of ferrite, oriented similar to the Widmanstaetten structure (*HV*50-2290–2379 MPa). Application of the double-channel ASS of the arc voltage and welding current mean values allows getting more uniform structural components than in case of a single-channel ASS of U_{mean}, whereby hardness did not change and equaled *HV*50-2340 MPa.

It is known than formation of Widmanstaetten structure depends upon content in the metal of carbon, size of the austenite grain, and rate of the metal cooling [4]. Appearance of higher amount of this structure in the weld metal in case of occurrence of voltage disturbances in the power supply network and in case of application of ASS of U_{mean} is, evidently, connected with change of the metal cooling rate.

So, reduction of the power supply network voltage in CEPAW may cause increased sputtering of metal, fouling of a nozzle, and fluctuations of the penetration depth. Application of a single-channel ASS does not completely compensate influence of the network disturbances. More efficient are double-channel systems.

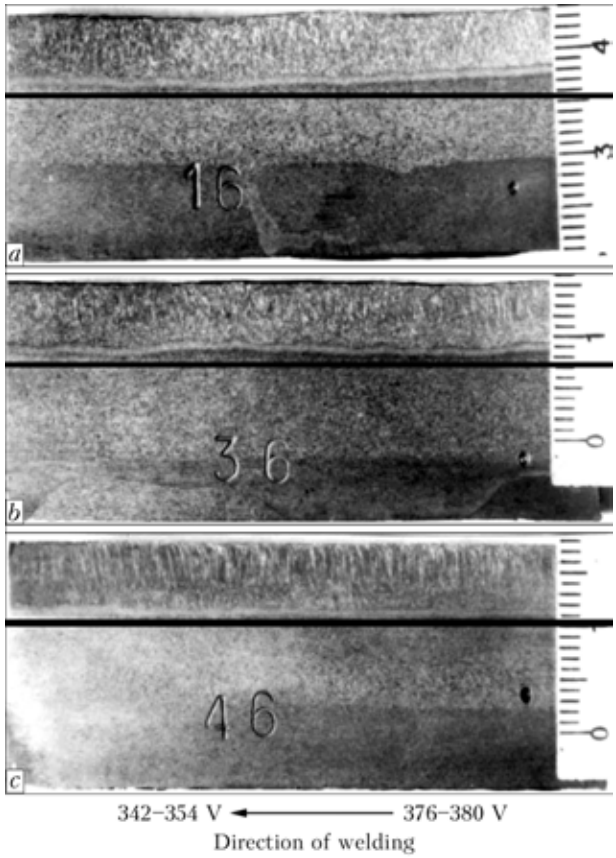

Figure 2. Macrosections (along axis of deposit) of metal deposited on steel 25 in case of smooth reduction of U_n down to 342–354 V (CEPAW in mixture of Ar + 18 % CO_2 using Sv-08G2S wire of 1.2 mm diameter; welding speed is 23 m / h, pulse duration is 3.2 ms): *a* — without ASS; *b* — ASS of arc voltage U_{mean}; *c* — ASS of U_{mean} and I_{mean}

1. Shejko, P.P., Zhernosekov, A.M., Shimanovsky, Yu.O. (2004) Consumable-electrode pulsed-arc welding with automatic stabilization of mode parameters. *The Paton Welding J.*, **1**, 7–10.
2. Rimsky, S.T., Svetsinsky, V.G., Shejko, P.P. et al. (1993) Consumable-electrode argon-CO_2 mixture pulsed-arc welding of low-alloy steels. *Avtomatich. Svarka*, **2**, 38–41.
3. Killing, R. (1993) Schutzgase zum Lichtbogenschweissen — schweisstechnische Eigenschaften. *Praktiker*, **8**, 448–455.
4. (1974) *Technology of fusion electric welding of metals and alloys.* Ed. by B.E. Paton. Moscow: Mashinostroenie.

THESIS FOR SCIENTIFIC DEGREE

Kharkov National Road-Transport University

V.V. Dmitruk (Ukrainian Engineering-Pedagogical Academy) defended on 13 December 2007 his thesis for a Doctor's degree on subject «Theoretical and Practical Principles of Extending Service Life of Welded Joints in Heat-Resistant Pearlitic Steels».

The thesis is dedicated to the issues of optimisation of formation of structure and properties of welded joints in heat-resistant pearlitic Cr–Mo–V steels for power generation equipment operating at heat power stations. Relationships between the initial structure of the above welded joints and its physical-chemical properties under creep conditions, as well as porosity formation, were derived. The principles of formation of the optimised initial structure characterised by the improved physical-chemical properties under creep conditions were elaborated, which allowed the intensity of initiation and propagation of pores in structure of the welded joints to be decreased. The concept of formation of pores in the welded joints, and ways of improving the structure to decrease the intensity of their formation were offered. Physical conditions of formation of the optimal initial structure of the welded joints were determined on the basis of results of solving the proposed conjugate problem realised under conditions of the Navier–Stokes and Fourier laws.

Relationships between the structure, properties and intensity of its damageability by pores were established on the basis of the data of modelling the initial structure of welded joints and investigation of their physical-chemical and mechanical properties, as well as damageability of the structure by pores under creep conditions.

A new research area providing development of new functional and structural materials for welding equipment to decrease structural heterogeneity and initial rate of defects in the weld metal was substantiated and put forward.

The initial structure of the welded joints in pearlitic Cr–Mo–V steels, characterised by a lower degree of initial structural heterogeneity, was theoretically substantiated and practically provided. The structure is characterised by improved physical-chemical and mechanical properties of the welded joints under creep conditions, which allows their service life to be extended to 300,000–350,000 h.

NEWS

NEW INSTALLATIONS FOR AIR-PLASMA CUTTING

OJSC «Electric Machine Works SELMA Company» mastered production of air-plasma cutting installations both for semi-automatic (with manual plasmatron movement) ---- UVPR-200 model, and automatic (as part of automatic machines) ---- UVPR-400 model.

Compared to manual gas cutting, the installations provide the following:

- higher cutting speed (by 3–5 times) and high quality of the cut at minimum cost;
- cutting of polluted and painted surfaces without preparatory operations;
- absence of deformations and need for straightening after cutting;
- minimum material losses at cutting;
- small amount of subsequent treatment for welding-assembling operations after cutting.

The main advantages of UVPR-200 and UVPR-400 installations are:

- smooth regulation of cutting current;
- plasmatron connection through euro-connector;
- connection of remote control panel for regulation of cutting current;
- plasmatron connection at a distance from installation (the distance is agreed with manufacturer) through a remote oscillator that provides stable pilot arc ignition;

- contactless system of arc ignition;
- possibility of non-ferrous and high-alloyed metal cutting;
- availability of compressed air parameter control devices;
- protection from inadequate parameters of compressed air;
- availability of filter and moisture separator for air cleaning;
- availability of water flow meter for plasmatron cooling;
- small maintenance expenses;
- insulation class N;
- higher reliability and service life.

«ARIADNA» — PACKING OF COPPER-PLATED WELDING WIRE

«Ariadna» is a new type of packing of Sv-08G2S and Sv-08G1S copper-plated welding wires, designed by OJSC «Mezhgosmetiz» (Russia) on the basis of European experience of welding consumable supply.

Copper-plated welding wire is packed into «Ariadna» barrels by a special technology of winding that guarantees layer-by-layer placing by the container height and straightness of the wire. Rectilinear welding wire easily moves along the guiding hose, providing high contact accuracy in the joint. This property allows using guiding hoses of up to 12 m length. Wire straightness with the effect of turn-by-turn pushing out at unwinding, decreases the load on welding equipment feeding device and correspondingly lowers the need for technological maintenance of welding machine. «Ariadna» packing provides a high stability and reliability of the welding process.

The number of interruptions of the welding process for changing the cassettes and reels decreases, thus providing a saving of the wire; the probability of defect formation in the weld metal decreases due to welding wire protection from the dust and other contaminations; wear of welding equipment feeding device components decreases; maintenance of robotic complexes and stationary semi-automatic welding stations is simplified, and conditions of transportation and storage are improved.

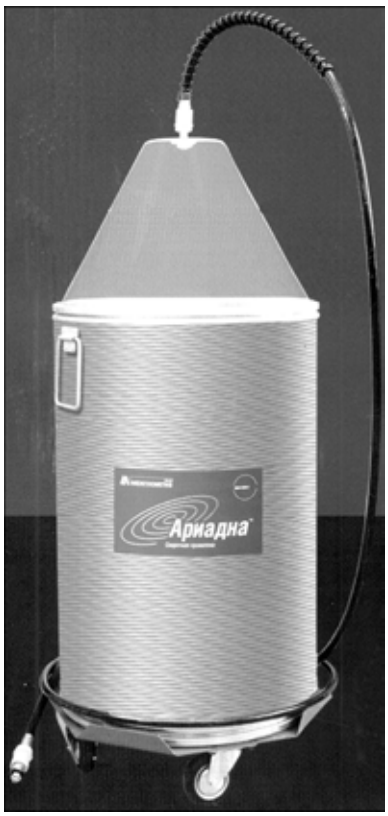

THE FIRST INTERNATIONAL CONFERENCE «JOINING ALUMINIUM STRUCTURES»

The First International Conference and Exhibition «Joining Aluminium Structures» took place in Moscow at «Holiday Inn Moskva Lesnaya» on December 3–5, 2007. The Conference was organized by ALUSIL-MViT Company. The Conference was officially supported by APRAL Association (Russia), the E.O. Paton Electric Welding Institute (Ukraine), Russian Scientific and Technical Welding Society, Aluminium Association (USA), European Institute of Industrial Fastening (Great Britain), National Association of Car Components Manufacturers (Russia). 65 delegates from 51 companies, representing 12 countries (Russia, Ukraine, Belarus, Austria, Belgium, Great Britain, Germany, Italy, Poland, USA, France, Switzerland) participated in the Conference. A wide range of issues dedicated to achievements in the sphere of technologies and equipment practically for all types of joining aluminium structures (welding, soldering, mechanical joints) was studied at the Conference. 33 reports of Russian and foreign specialists were made during the plenary session and meetings of the 5 sessions. In the opinion of the Conference participants the following reports attracted the greatest interest:

Tomasz Siwowski (Rzeszow University of Technology, Poland) «*Joining structure in aluminium bridges*». Review of aluminium bridges, beginning from the first one built in the USA in 1993, was made in the report. More than 100 aluminium bridges were built in the whole world for more than 70 years;

Giorgio Destefani (Alcan Aluminium Valais SA, LP Rail & Bus, Switzerland) «*Innovation aluminium frames for railway carriages*». Different technologies of joining aluminium structures used in manufacturing the railway carriages, taking into account the operation duration about 30 years, were considered in the report;

Michael J. Skinner (MTS Systems Corporation, Friction Stir Welding Group, USA) «*Application of friction stir welding in civil aircraft construction*». It was noted in the report that in aircraft construction the friction stir welding method is used to join aluminium sheets of 4–25 mm thickness. It was noted that at present the airframe of Eclipse 500 plane (for 7 persons) is welded completely by friction stir welding;

Gedopt Jan (VITO Laser Centre Flanders (LCV), Belgium) «*Hybrid welding: laser + friction stir welding used for EN AW 6065 alloy*». The possibilities of one more hybrid technology are shown in the report;

N. Kudryashov (TC «Tena», Russia) «*Development of equipment and new technology of aluminium alloys welding by dynamic plasma*». The results of experimental works, carried out at OJSC «Criogenmash» and TC «Tena» on applying a new process of welding by dynamic plasma, providing a differentiated supply of shielding gas;

A.D. Konyukhov (VNIIZhT, Russia) «*Russian experience of manufacturing and operation of carriages from aluminium alloys*». The information about passenger cars from aluminium alloys of Russian production is given in the report. Investigation results of base metal and welded joints of carriage body carrying elements of ER200 electric train after 30 years of operation, as well as information about cargo carriages from aluminium alloys of Russian production were given. Special attention was paid to VA 2005 experimental gondola wagon, which was manufactured using hollow extruded profiles;

A.Ya. Ishchenko (PWI, NASU, Ukraine) «*Welded structures from aluminium alloys*». It was noted in the report that aluminium alloys of different alloying systems are widely used in different branches of industrial production. Many of the high-strength alloys can

be welded as by fusion processes, as well as in solid-state processes, for example, by friction stir welding, by high pressure pulses including explosion and diffusion welding. The most widely spread fusion welding processes are arc welding, electron and laser beam welding. They are being continuously improved to comply with the new higher demands of modern mechanical engineering, especially as applied to advanced structures. At the same time alloys and welding consumables proper are improved in view of the need for their application in production of welded structures;

Herbert Staufer (Fronius, Austria) «*Laser-hybrid welding: state-of-the-art of technology development and examples of practical application in motor industry*»;

N.A. Steshenkova (FSUE CSRI of Shipbuilding Technologies, Russia) «*Technology and equipment for semi-automatic plasma welding of aluminium alloy structures*». The advantages of semi-automatic non-consumable electrode plasma welding of aluminium alloy ship hull structures with reverse polarity are shown in the report, and semiautomatic machine PPN-200 is presented;

V.I. Pavlova (FSUE CSRI of Structural Materials «Prometej», Russia) «*Aluminium–steel bimetal joints for steel-aluminium hull structures in shipbuilding*». New ship-building bimetal of KBM-1 grade on basis of low-alloy steel of 10KhSND (D40S) grade and aluminium alloy of 1561 grade was designed and put into production at «Prometej». The bimetal is designed for joining the aluminium superstructure to the steel hull body. Technology of welding the butt, overlap and tee joints using the bimetal was designed on the basis of new engineering solutions for the design and technological aspects of steel-aluminium joints, that allowed creating reliable ship hull structures, increasing the fatigue strength of steel-aluminium components by 15–20 %, eliminating the use of deficit austenitic welding consumables, providing the impermeability of the bimetal butt joints and corrosion resistance of steel-aluminium joints on the level of the requirements made of ship hull materials.

The most recent technologies in the sphere of aluminium structures joints were presented at the exhibition, organized in the framework of the Conference, namely a wide range of mechanical fasteners of CJSC «Vyurt Rus», the advanced friction stir welding technology of MTS Systems Corporation, technology of manufacturing heat-exchangers of braze-welded structure of «Gazkholodtekhnika» Ltd., car disks of CJSC «Disk BB».










During the Conference work, its participants were given the possibility to visit Technological Center «Tena» (Moscow) and «Gazkholodtekhnika» Ltd. (Moscow).

The previous conference, organized at high scientific and technical level, in the opinion of its participants, was of great interest from the point of view of exchange of new technology achievements and results of their practical application.

A.T. Zelnichenko,
Cand. of PhMath Sci., PWI

MECHANIZED SITE WELDING OF A LARGE-SIZED VACUUM CHAMBER MADE FROM HIGH-ALLOY STEELS

The casing of a vacuum chamber represents a cylindrical vessel with a bottom and a removable roof. Dimensions of the casing: diameter — 17500 mm, height — 39500 mm, total volume — 8500 m^3, vacuum — $1 \cdot 10^{-6}$ mm Hg, service temperature — 77 K. Chamber casing is manufactured from high-alloy stainless steels 12Kh18N10T and 03Kh13AG19 of 20–70 mm thickness, load-carrying elements (ring frames, stringers) are made from structural carbon steel of VSt3sp (killed), St20 or 09G2S grades.

Technology of assembly, welding and erection of casing of the chamber for vacuum tests has been developed. To conduct the mechanized works, the specialized automatic machines allowing producing welds in all spatial positions were developed at the E.O. Paton Electric Welding Institute. Bottom, cylindrical part and casing roof are assembled from transportable elements manufactured in the shop conditions. Welding of elements into large sub-assemblies is performed on an intermediate platform near the erection site.

Pre-fabrications of transportable chamber elements are welded in the shop conditions in carts, made from sheet metal, using submerged arc welding. Transportable elements of the bottom pass the petal-by-petal check assembly at the plant-manufacturer. Bottom petals are welded by the automatic shielded-gas welding on an intermediate platform from the external (convex) side. Then, the bottom is tilted and welded by the same method from the internal (concave) side. Neck (roof) of the chamber casing is manufactured similar to the bottom; cylindrical part of the chamber casing is manufactured by assembly of a girth from four transportable elements of a shop manufacture into a single block. All operations of assembly, welding and inspection of girths (rings) are made on an intermediate platform in a special assembly-welding rig, providing a preset geometry. Tack welding of the next girth of the chamber is performed after welding, erection and mounting of the next girth on it. To join the shells between themselves (horizontal welds), the automatic welding with a consumable electrode in argon or mixture of gases is used. Neck (roof) is erected as a single block, after a comprehensive inspection it is mounted into a design position and welded to the casing. Welding-in of hatches and windows is made from external and internal side of the chamber casing and welded by a manual argon-arc welding using a filler wire. Load-carrying structures (ring frames, stringers) are manufactured in the shop conditions, mounted and tack welded to transportable elements at the plant-manufacturer. The final welding of the load-carrying structures is realized in site after assembly, erection and welding of the chamber casing as a whole.

The developed technology of welding, assembly and erection made it possible to decrease the metal consumption, to strengthen its design and to improve special characteristics of cryogenic systems as a whole.

Purpose and application. Technology is used in manufacture of large-sized cryogenic and vacuum chambers of a special purpose, used in cryogenic and aerospace engineering.

Status and level of development. Ready for realization.

Proposals for co-operation. Signing contract for the technology of welding and author's supervision.

Main developers and performers: Prof. Yushchenlo K.A., Dr. Monko G.G., Lead. Eng. Shulzhenko G.S.

WELDING OF LARGE-SIZED SIMULATORS OF SPACE ENVIRONMENT

Technology has been developed for fabrication of a chamber for vertical tests, which is a cylindrical vessel of 16000 mm diameter, ≈ 50000 mm length and ≈ 10000 m^3 volume. The chamber is designed for simulation of space environment and testing of various items in the vertical position under these conditions. Space simulator consists of a cylindrical part made of steel 03Kh13AG19 (ChS-46) 20 mm thick, two bottoms of steel 12Kh18N10T 24 mm thick and force frame of steel 09G2S up to 30 mm thick.

Billets of the cylindrical part of the chamber (shell of 1 / 4 diameter) were made in the shop together with the load-carrying structures, and were delivered to the site. In site the vertical welds of shells up to 4000 mm long were made by ESW with Sv-05Kh15N9AG6 (ChS-31) wire using AN-45 flux. Electrodes ANV-24 were used for welding horizontal welds on the vertical plane, when joining the shells.

Bottom blanks of steel 12Kh18N10T were welded in the shop. Shields, through which liquid helium flows for simulation of space temperatures, were made of Invar alloy and welded by the argon-arc process. Weld quality was controlled by X-ray, and the vacuum plane ---- by helium leak detector.

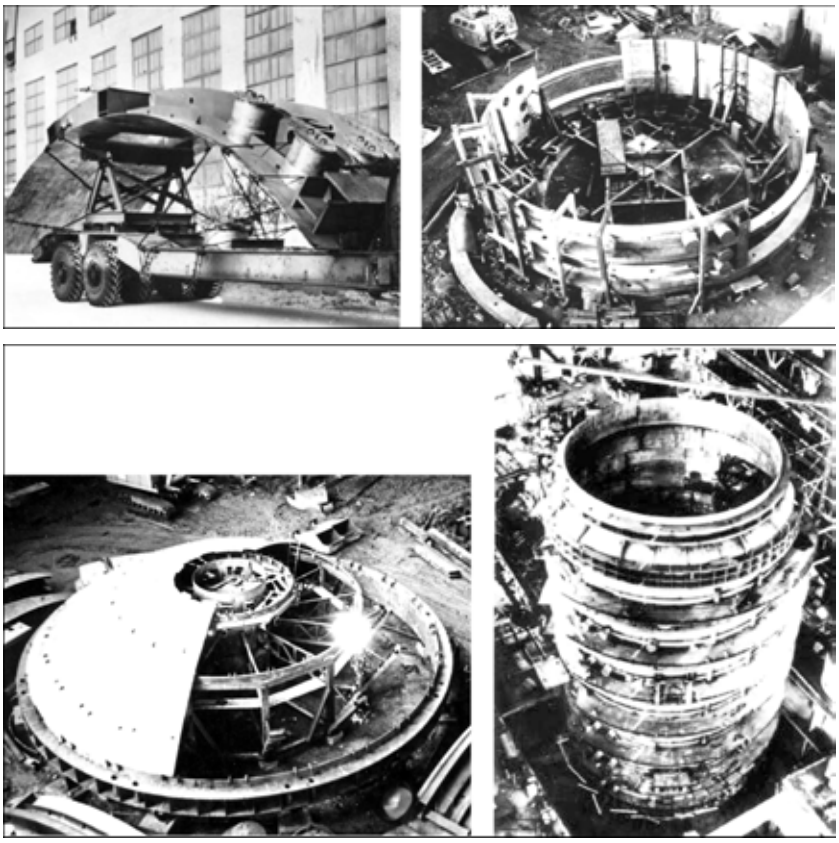

Purpose and application. Vertical testing chamber is designed for simulation of space conditions (temperature, vacuum, lighting) and rocket testing. Developed technology has been used in fabrication of a vertical testing chamber in Russia.

Status and level of development. Welding technology has been verified by pilot production trials, when making the commercial unit.

Proposals for co-operation. Contract for development of welding technology and large-sized chamber construction.

Main developers and performers: Prof. Yushchenko K.A., Dr. Monko G.G., Lead. Eng. Shulzhenko G.S.

ASSEMBLY, WELDING AND ERECTION OF SPHERICAL ISOTHERMAL CRYOGENIC TANKS WITH A CAPACITY OF 1400 m^3

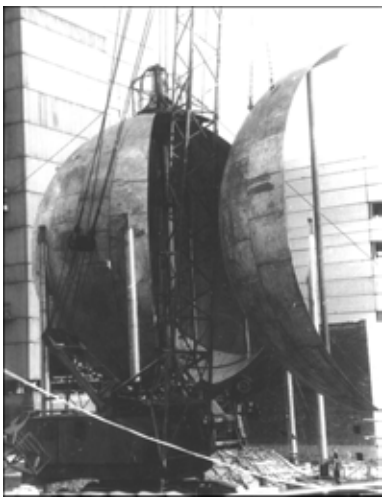

Spherical isothermal cryogenic tanks consist of two spheres: internal vessel, made from high-alloy steel of the 03Kh20N16AG6 grade, and external vessel, made from steel 09G2S. The tanks are intended for storage of liquefied gases –– nitrogen (at a temperature of 77 K), hydrogen (20 K) and helium (4.2 K). The volume of a tank is 1400 m^3, pressure is 6 atm, wall thickness of the internal vessel is 20 mm and that of the external vessel is 24 mm.

The technology was developed for assembly, welding and erection of spherical isothermal tanks. The internal vessels are assembled from lobes, the roots of which are welded to each other by manual argon-arc welding, followed by automatic submerged-arc welding using manipulator for rotation. The technology for manufacture of the external vessels provides for assembly of a lower hemisphere of the vessel, tack welding and welding of the root pass manually using covered electrodes, and automatic self-shielding wire welding in all spatial positions up to closing of the weld. After that an internal vessel is installed into the lower hemisphere. The upper hemisphere of the external vessel is made similarly to the lower one. Then the upper hemisphere is put on the lower one, and they are welded together by a closing circumferential weld.

The developed technology reduces time and costs needed to manufacture spherical isothermal tanks, and improves their quality and reliability.

The isothermal tank design reduces losses of cryogenic products stored in them.

The stock of tanks for storage of liquid oxygen, nitrogen, hydrogen and helium for aerospace application was made using the developed technology.

Application. The technology is applied for manufacture of spherical isothermal tanks for storage of liquefied gases used and cryogenic and rocket engineering.

Status and level of development. Ready for application.

Proposals for co-operation. Contract for the welding technology and author's supervision.

Main developers and performers: Prof. Yushchenko K.A., Dr. Monko G.G., Lead. Eng. Shulzhenko G.S.

TECHNOLOGY OF WELDING ISOTHERMAL TANKS OF STEELS ON6 AND ON9 FOR LIQUEFIED GAS STORAGE

A technology has been developed for fabrication of isothermal tanks of 10–60 ths m^3 capacity by a modular method. The modules are assembled and welded of transportable elements in a jig in site. Transportable elements are made under the shop conditions, this allowing complete automation of the welding process. In this case the scope of erection welding is up to 15–20 % of the total volume of welding operations. Residual magnetization of the base metal is not higher than 80–100 Gs.

Technology eliminates formation of solidification cracks, this allowing making X- and T-shaped butt joints. Selection of the system of steel alloying and filler material ensures high service properties of the vessels, in particular, equivalent strength of the welds at operating temperatures.

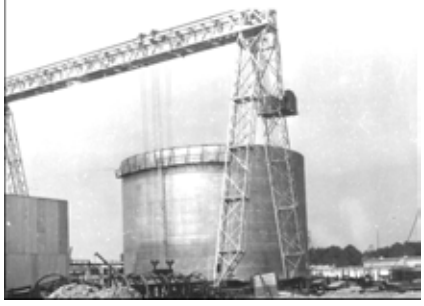

Purpose and application. Technology is designed for fabrication of cryogenic engineering equipment.

Status and level of development. Technology of fabrication of 10 ths m^3 tanks of steel ON6 has been mastered in Zaporozhie Metallurgical Works and Kaluga PA «Khlorvinil» (two tanks for liquefied gas storage have been made); those of steel ON9 in the Sumgait PA «Sintezkauchuk» (Azerbaijan) (technological tank for liquid ethylene has been made). Pilot production verification and welding of samples for tanks of 60 ths m^3 capacity of steel ON9 has been performed in «Armtransgaz» (Erevan, Armenia), where construction of a liquid natural gas storage has begun.

Proposals for co-operation. Making a contract for technology application.

Main developers and performers: Prof. Yushchenko K.A., Dr. Starushchenko T.M., Lead. Eng. Peskov V.A.

TECHNOLOGY, MATERIALS AND METHODS OF CONSTRUCTION OF INTRICATE MONUMENTAL SCULPTURES

Technology has been developed for manufacture of monumental sculptures from stainless steel. In 1981 on the Dnieper river bank in Kiev an all-welded sculpture «Motherland» of 115 m total height was constructed. The more than 15-year experience of service showed the high reliability and serviceability of the structure.

Technology and taken technological solutions allow creation of monumental structures of any sizes, including the art masterpieces of intricate three-dimensional shape.

Purpose and application. Civil engineering.

Status and level of development. Technology and structures were tested in practice.

Proposals for co-operation. Any forms of cooperation, contracts on use of technology and assistance in construction of monumental sculptures.

Main developers and performers: Prof. Yushchenko K.A., Lead. Eng. Fomin V.V.

Sculpture «Motherland», the museum of the Great Patriotic War of 1941–1945, Kiev

ELECTRON BEAM WELDING OF HEAT-RESISTANT ALLOYS ON NICKEL AND TITANIUM BASE

Technology is based on producing complete penetration of elements being joined with the formation of a smooth weld root bead at a definite margin of electron beam power and increased speed of welding.

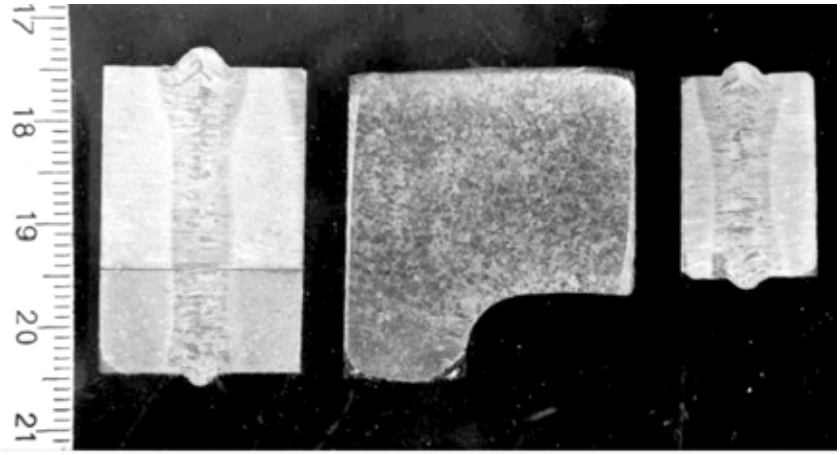

Transverse (*a*, *c*) and longitudinal (*b*) welds of a variable-section welded joint made for one pass

Technology is realized easily in industrial conditions without use of additional expenses. It guarantees the stabilization of formation and optimization of weld geometry, improvement of structural-phase composition and stress-strain state of welded joints.

Specifics of heat input makes it possible to improve the structure at reduction (1.5–2 times) of residual stresses and to increase (1.3–2 times) the mechanical properties and service characteristics. The significant metal saving (2–3 times) is attained, typical weld defects (pores, cracks, undercuts, etc.) are eliminated.

Purpose and application. Technology can be used successfully in welding of variable-section parts, T-joints and joints of different thicknesses. Its application is especially effective in welding of high-precision complex-loaded sub-assemblies and parts of aircraft gas turbine engines and on-land units made of structure-sensitive heat-resistant alloys of nickel and titanium.

Main developers and performers: Prof. Yushchenko K.A., Dr. Zadery V.A., Dr. Polishchuk E.P.

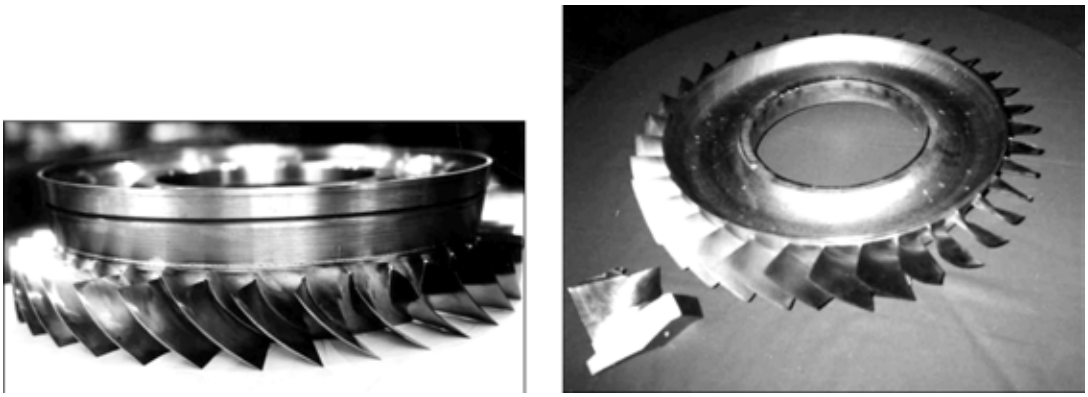

All-welded running wheel of gas turbine engine

EBW OF SINGLE-CRYSTAL TUBULAR MONOFACED SURFACE BILLETS MADE FROM POLYCRYSTALLINE INITIAL MATERIAL

The technology of producing single-crystal monofaced surface billets from polycrystalline refractory metals using electron beam methods of welding.

Technology is based on a successive local remelting of initial material with an allowance for inheritance of different crystallographic orientation depending on the parameters and conditions of remelting.

Characteristics of billets produced

Size of subgrains, μm	10–20
Disorientation of structural fragments, mrad	15–17
Mean density of dislocations, cm^{-2}	~ 10^7
Diameter of billets produced, mm	10 and more
Wall thickness, mm	0.6–2.0

Stable microstructure of the produced metal provides the high quality and properties of the billets.

Creep rate of the material of billets made using the proposed method is 3 times lower than that in initial polycrystalline material, and the duration of a steady stage of creep is increased by more than twice. The thermionic properties are improved. Effectiveness of the method is stipulated by the increase in physical-mechanical characteristics and use of single-crystals as initial polycrystalline materials, which are almost 10 times less expensive, and by the 2–10 times increase in labor productivity.

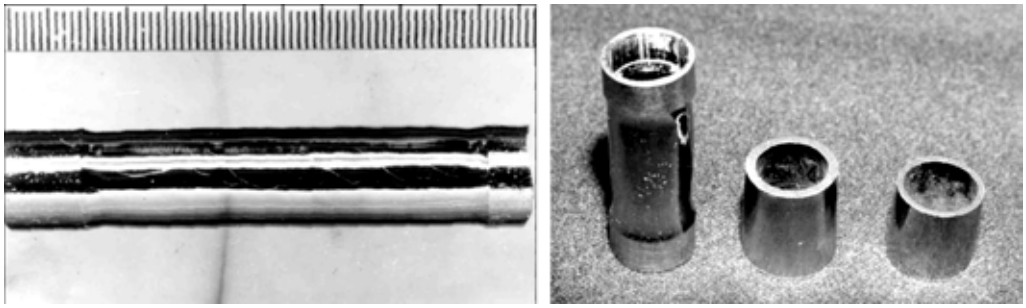

Single-crystal tubular billets produced from polycrystalline initial material

Purpose and application. Production of single-crystals and their semi-products, converters of different kinds of energy into electric energy (including TECs), parts and sub-assemblies of instruments of nuclear, space and electronic industry, blades of gas-turbine engines.

Main developers and performers: Prof. Yushchenko K.A., Dr. Zadery V.A., Dr. Polishchuk E.P.

Contacts: Prof. Yushchenko K.A.
Tel. / fax: (38044) 289 2202

SUBSCRIPTION
FOR «THE PATON WELDING JOURNAL»

If You are interested in making subscription directly via Editorial Board, fill, please, the coupon and send application by fax or e-mail.

The cost of annual subscription via Editorial Board is $324.

Telephones and faxes of Editorial Board of «The Paton Welding Journal»:

Tel.: (38044) 287 6302, 271 2403, 529 2623

Fax: (38044) 528 3484, 528 0486, 529 2623.

«The Paton Welding Journal» can be also subscribed worldwide from catalogues of subscription agency EBSO.

SUBSCRIPTION COUPON

Address for journal delivery _____

Term of subscription since _____ **200** **till** _____ **200**

Name, initials _____

Affiliation _____

Position _____

Tel., Fax, E-mail _____

ADVERTISEMENT
IN «THE PATON WELDING JOURNAL»

External cover, fully-colored:
First page of cover (190×190 mm) – $500
Second page of cover (200×290 mm) – $350
Third page of cover (200×290 mm) – $350
Fourth page of cover (200×290 mm) – $400

Internal cover, fully-colored:
First page of cover (200×290 mm) – $350
Second page of cover (200×290 mm) – $350
Third page of cover (200×290 mm) – $350
Fourth page of cover (200×290 mm) – $350

Internal insert:
Fully-colored (200×290 mm) – $300
Fully-colored (double page A3) (400×290 mm) – $500
Fully-colored (200×145 mm) – $150
Black-and-white (170×250 mm) – $80
Black-and-white (170×125 mm) – $50
Black-and-white (80×80 mm) – $15

- Article in the form of advertising is 50 % of the cost of advertising area
- When the sum of advertising contracts exceeds $1000, a flexible system of discounts is envisaged

Technical requirement for the advertising materials:
- Size of journal after cutting is 200×290 mm
- In advertising layouts, the texts, logotypes and other elements should be located 5 mm from the module edge to prevent the loss of a part of information

All files in format IBM PC:
- Corell Draw, version up to 10.0
- Adobe Photoshop, version up to 7.0
- Quark, version up to 5.0
- Representations in format TIFF, color model CMYK, resolution 300 dpi
- Files should be added with a printed copy (makeups in WORD for are not accepted)